Electronic Supporting Information

[2.2]Paracyclophane–Dicyanorhodanine Conjugates as Planar Chiral Molecular Photoswitches

Parag Das,[a] Cole D. Stearns,[a] Ion Ghiviriga,[a] Łukasz Dobrzycki,[a] and Ronald K. Castellano[a]*

[a]Department of Chemistry, University of Florida, PO Box 117200, Gainesville, FL, 32611, USA

Email: castellano@chem.ufl.edu

*indicates corresponding author

TABLE OF CONTENTS

COMPOUND SYNTHESIS

General Information

Reagents and solvents were purchased from commercial sources and used without further purification unless otherwise specified. DCM and DMF were degassed in a 20 L drum and passed through activated alumina under a positive argon atmosphere. Thin layer chromatography (TLC) was performed on SiO_2-60 F_{254} aluminum plates with visualization by UV light. Column chromatography was performed using Silica gel technical grade, pore size 60 Å, 230–400 mesh particle size, 40–63 μm particle size from Sigma-Aldrich.

Note: Due to the photosensitivity of the RCN-functionalized products, the reaction vessels were covered with aluminum foil during the synthesis of compounds **(±)-1-*Z***, **(±)-2-*Z***, **(±)-3-*Z***, and **(R_p)-2-*Z***. In an effort to minimize unintentional photoisomerization, aluminum foil was used to cover all glassware during purification processes such that any source of excessive light exposure was eliminated while samples were dissolved in solution.

Synthesis Schemes

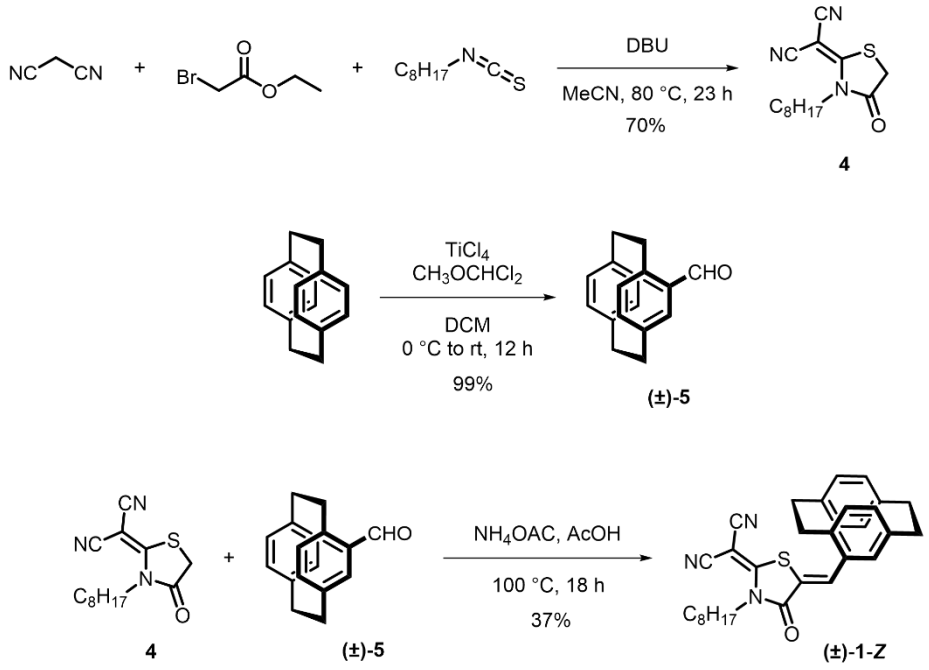

Scheme S1. Synthesis of compound **(±)-1-*Z***.

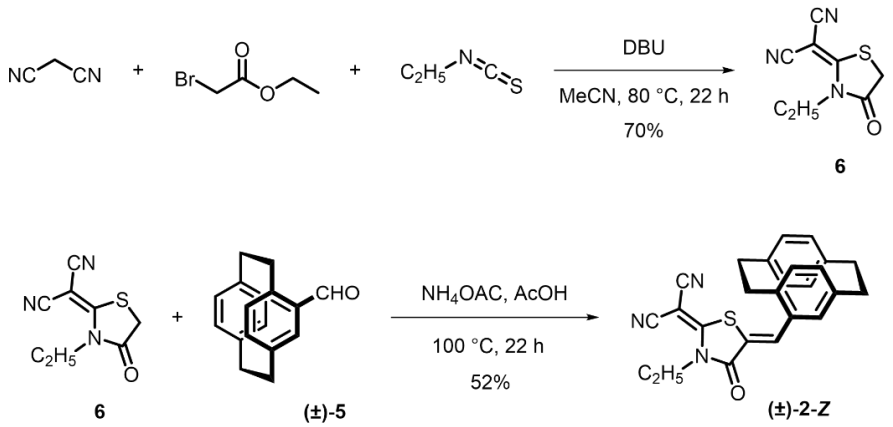

Scheme S2. Synthesis of compound **(±)-2-*Z***.

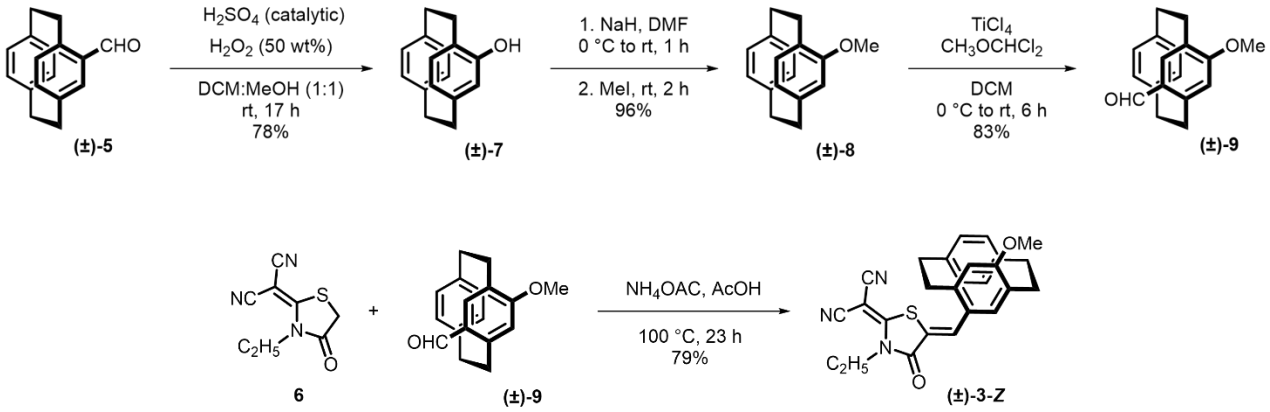

Scheme S3. Synthesis of compound **(±)-3-*Z***.

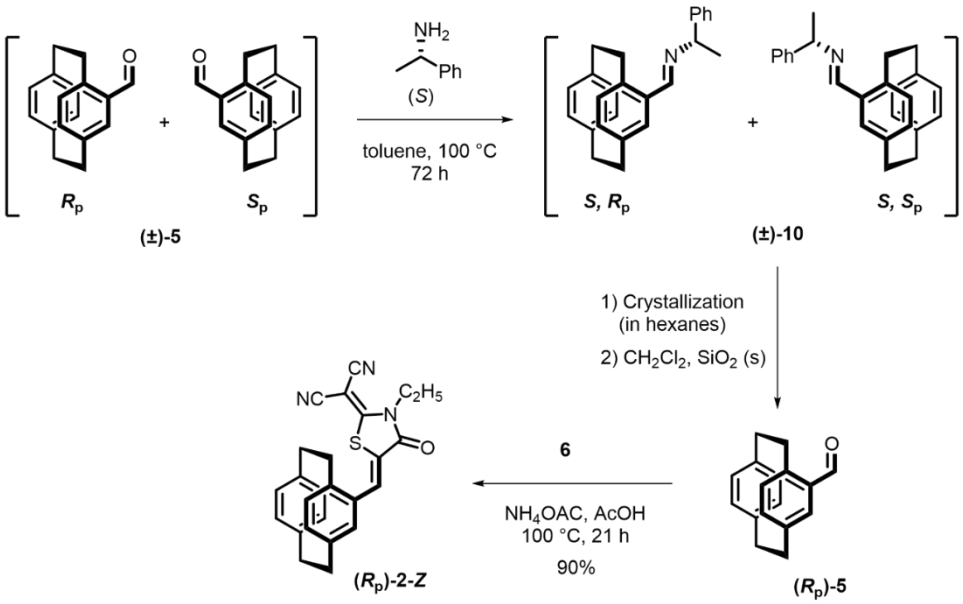

Scheme S4. Synthesis of compound **(R_p)-2-*Z***.

STRUCTURAL CHARACTERIZATION

General Information

^{1}H (^{13}C) NMR spectra were recorded on a Bruker 600 MHz spectrometer (^{1}H at 600 MHz; ^{13}C at 150 MHz) and an INOVA-500 (^{1}H at 500 MHz; ^{13}C at 125 MHz) spectrometer. Chemical shifts (δ) are given in parts per million (ppm) referenced to residual deuterated solvent purchased from Cambridge Isotope Laboratories, Inc. ($CDCl_3$: δ H 7.26 ppm, δ C 77.16 ppm). Abbreviations used are s (singlet), d (doublet), t (triplet), q (quartet), quin (quintet), and m (multiplet). Abbreviations used for complex splitting patterns are dd (doublet of doublets), dt (doublet of triplets), ddd (doublet of doublet of doublets), and td (triplet of doublets). High resolution mass spectra (HRMS) were recorded using the Direct Analysis in Real Time (DART, analyzed in positive mode) ionization technique on an Agilent 6220 Time-of-Flight (TOF) spectrometer with MassHunter software.

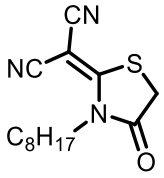

4

2-(3-Octyl-4-oxothiazolidin-2-ylidene)malononitrile (4): A three-necked round-bottom flask (RBF) containing malononitrile (0.60 g, 9.1 mmol) was equipped with a stir bar, two septa, and a reflux condenser. The flask was flushed with argon three times. Octyl isothiocyanate (1.7 g, 9.9 mmol) and acetonitrile (12 mL) were added to the flask. 1,8-Diazabicyclo[5.4.0]undec-7-ene (1.92 g, 12.6 mmol) was added dropwise to the mixture. The reaction mixture was stirred at 25 °C for 1 h. Ethyl bromoacetate (2.67 g, 15.9 mmol) was added to the mixture. The reaction mixture was heated to reflux (80 °C) and was allowed to stir overnight (23 h). The solvent was removed after cooling to room temperature. The resulting concentrate was purified by silica column chromatography using 1:2:5 (EtOAc:DCM:hexanes) as the eluent to yield an off-white solid (1.8 g, 6.4 mmol, 70%).

^{1}H NMR ($CDCl_3$, 600 MHz) of **4**: δ 4.08 – 4.06 (m, 2H), 3.99 (s, 2H), 1.70 – 1.65 (m, 2H), 1.39 – 1.22 (m, 10H), 0.88 – 0.86 (m, 3H) ppm.

^{13}C NMR ($CDCl_3$, 150 MHz) of **4**: δ 171.7, 113.0, 111.8, 56.8, 45.5, 32.4, 31.8, 29.1, 28.7, 26.0, 22.7, 14.2 ppm.

The NMR spectra match the literature.[1, 2]

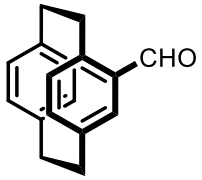

(±)-5

(±)-4-Formyl-[2.2]paracyclophane ((±)-5): To a flame-dried 200 mL three-necked RBF with stir bar, [2.2]paracyclophane (5.0 g, 24 mmol) was added and purged with N_2, dissolved in 100 mL anhydrous DCM, and cooled to 0 °C. Titanium tetrachloride (5.26 mL, 48.0 mmol) was added. Dichloromethyl methyl ether (2.28 mL, 25.2 mmol) was slowly added dropwise. The reaction was then stirred at 25 °C for 12 h, monitoring via TLC. The reaction was then poured into ice water and stirred for 1 h. After separating the biphasic mixture, the aqueous phase was extracted 3× with DCM. The combined organic phases were washed with saturated aqueous $NaHCO_3$ and brine, dried over $MgSO_4$, filtered, and evaporated to give the product as pale-yellow solid (5.60 g, 23.7 mmol, 99%).

^{1}H NMR ($CDCl_3$, 500 MHz) of **(±)-5**: δ 9.95 (s, 1H), 7.02 (d, J = 2.0 Hz, 1H), 6.73 (dd, J = 7.7, 2.0 Hz, 1H) 6.60 – 6.55 (m, 2H), 6.50 (dd, J = 7.9, 1.9 Hz, 1H), 6.42 (dd, J = 7.9, 1.9 Hz, 1H), 6.38 (dd, J = 7.9, 1.9 Hz, 1H), 4.10 (ddd, J = 13.2, 10.1, 1.8 Hz, 1H), 3.26 (ddd, J = 12.7, 10.3, 2.0 Hz, 1H), 3.20 (s, 2H), 3.07 (s, 3H), 2.95 (ddd, J = 13.2, 10.2, 6.7 Hz, 1H) ppm.

^{13}C NMR ($CDCl_3$, 126 MHz) of **(±)-5**: δ 192.1, 143.4, 140.8, 139.6, 138.2, 136.7, 136.5, 136.3, 133.4, 133.1, 132.5, 132.3, 35.4, 35.3, 35.1, 33.8 ppm.

The NMR spectra match the literature.[3]

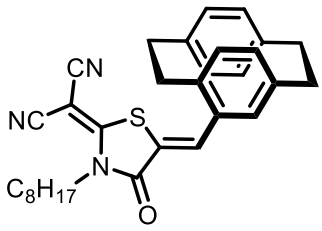

(±)-1-*Z*

(±)-(*Z*)-2-(5-([2.2]Paracyclophane)-3-octyl-4-oxothiazolidin-2-ylidene)malononitrile ((±)-1-*Z*): A three-necked round-bottom flask containing 2-(3-octyl-4-oxothiazolidin-2-ylidene)malononitrile (0.10 g, 0.36 mmol) and ammonium acetate (34 mg, 0.43 mmol) was equipped with a stir bar, two septa, and a reflux condenser. The flask was flushed with argon three times. (±)-4-Formyl-[2.2]paracyclophane (93 mg, 0.39 mmol) and glacial acetic acid (7 mL) were added to the flask and the reaction apparatus was covered in aluminum foil. The mixture was heated to 100 °C and allowed to reflux overnight (19 h) with stirring. After cooling to room temperature, the reaction mixture was neutralized with a saturated $NaHCO_3$ solution. The aqueous phase was extracted three times with DCM and the combined organic extracts were dried over anhydrous Na_2SO_4. The solvent was removed under reduced pressure and the resulting concentrate was purified by silica column chromatography using a gradient of 3:1 to 7:1 DCM:hexanes as the eluent to yield a pale-yellow solid (66 mg, 0.13 mmol, 37%).

^{1}H NMR ($CDCl_3$, 600 MHz) of **(±)-1-*Z***: δ 8.01 (s, 1H), 6.66 (d, J = 7.8 Hz, 1H), 6.61 (s, 1H), 6.59 (d, J = 7.9 Hz, 1H), 6.57 (s, 2H), 6.40 (s, 2H), 4.27 – 4.21 (m, 2H), 3.64 – 3.57 (m, 1H), 3.29 – 3.15 (m, 4H), 3.12 – 2.95 (m, 5H), 1.80 – 1.75 (m, 2H), 1.47 – 1.42 (m, 2H), 1.41 – 1.26 (m, 10H), 0.89 (t, J = 7.0 Hz, 3H) ppm.

^{13}C NMR ($CDCl_3$, 150 MHz) of **(±)-1-*Z***: δ 166.7, 166.5, 143.2, 141.6, 139.7, 138.9, 136.5, 136.0, 134.6, 133.5, 133.4, 133.0, 132.9, 132.1, 131.9, 116.6, 113.3, 112.3, 56.0, 45.4, 35.4, 35.3, 35.3, 34.0, 31.8, 29.2, 29.2, 28.9, 26.1, 22.7, 14.2 ppm.

HRMS-DART of **(±)-1-*Z***: m/z $[M+H]^+$ calculated for $[C_{31}H_{34}N_3OS]^+$: 496.2417, found 496.2437 (4.0 ppm); m/z $[M+NH_4]^+$ calculated for $[C_{31}H_{37}N_4OS]^+$: 513.2683, found 513.2683 (<0.1 ppm).

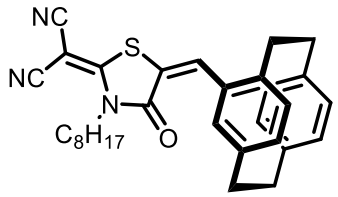

(±)-1-*E*

(±)-(*E*)-2-(5-([2.2]Paracyclophane)-3-octyl-4-oxothiazolidin-2-ylidene)malononitrile ((±)-1-*E*): An NMR sample of **(±)-1-*Z*** (30 mg, in chloroform-*d*) was irradiated using a 404 nm LED (irradiance: 1.9 mW/cm^2) for 3 h to obtain a *Z*/*E* mixture. The solvent was removed under reduced pressure, and the resulting concentrate was subjected to silica column chromatography to separate the *Z* and *E* isomers using a gradient of 3:1 to 1:1 hexanes:DCM as the eluent. The highest possible *E*-isomer rich fraction was obtained as 94/6 of **(±)-1-*E*:(±)-1-*Z***. This fraction was used for further structural characterization of compound **(±)-1-*E*** using 1D- and 2D-NMR spectroscopy (*vide infra*, page S32–S38).

^{1}H NMR ($CDCl_3$, 600 MHz) of **(±)-1-*E***: δ 7.34 (s, 1H), 7.11 (s, 1H), 6.62 (d, J = 7.9 Hz, 1H), 6.58 (s, 2H), 6.53 (d, J = 7.8 Hz, 1H), 6.47 (d, J = 8.1 Hz, 1H), 6.43 (d, J = 8.0 Hz, 1H), 4.09 (t, J = 8.0 Hz, 2H), 3.43 – 3.35 (m, 1H), 3.24 – 3.12 (m, 4H), 3.09 – 2.92 (m, 5H), 1.74 – 1.64 (m, 2H), 1.39 – 1.20 (m, 12H), 0.87 (t, J = 7.0 Hz, 3H) ppm.

^{13}C NMR ($CDCl_3$, 150 MHz) of **(±)-1-*E***: δ 166.4, 162.7, 141.6, 139.9, 139.8, 139.5, 138.8, 136.7, 136.1, 135.1, 133.2, 133.1, 132.4, 132.0, 131.3, 118.2, 113.4, 112.5, 54.7, 45.4, 35.4, 35.1, 35.1, 33.9, 31.8, 29.2, 29.2, 28.8, 26.1, 22.7, 14.2 ppm.

HRMS-DART of **(±)-1-*E***: m/z $[M+H]^+$ calculated for $[C_{31}H_{34}N_3OS]^+$: 496.2417, found 496.2433 (3.2 ppm); m/z $[M+NH_4]^+$ calculated for $[C_{31}H_{37}N_4OS]^+$: 513.2683, found 513.2700 (3.3 ppm).

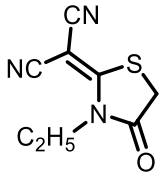

6

2-(3-Ethyl-4-oxothiazolidin-2-ylidene)malononitrile (6): A three-necked round-bottom flask containing malononitrile (0.74 g, 11 mmol) was equipped with a stir bar, two septa, and a reflux condenser. The flask was flushed with argon three times. Ethyl isothiocyanate (1.17 g, 13.4 mmol) and acetonitrile (30 mL) were added to the flask. 1,8-Diazabicyclo[5.4.0]undec-7-ene (2.22 g, 14.6 mmol) was added dropwise to the mixture. The reaction mixture was stirred at 25 °C for 1 h. Ethyl bromoacetate (3.19 g, 19.1 mmol) was added to the mixture. The reaction mixture was heated to reflux (80 °C) and allowed to stir overnight (22 h). The solvent was removed after cooling to room temperature. The resulting concentrate was purified by silica column chromatography using 1:2:5 (EtOAc:DCM:hexanes) as the eluent to yield an off-white solid (1.5 g, 7.8 mmol, 70%).

^{1}H NMR ($CDCl_3$, 600 MHz) of **6**: δ 4.17 (q, J = 7.2 Hz, 2H), 3.99 (s, 2H), 1.34 (t, J = 7.2 Hz, 3H) ppm.

^{13}C NMR ($CDCl_3$, 150 MHz) of **6**: δ 171.8, 171.6, 113.0, 111.8, 56.4, 40.7, 32.5, 14.0 ppm.

The NMR spectra match the literature.[4]

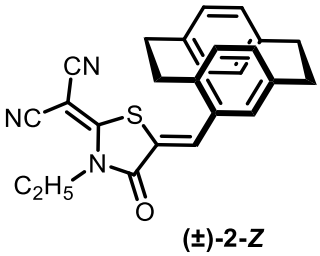

(±)-2-*Z*

(±)-(*Z*)-2-(5-([2.2]Paracyclophane)-3-ethyl-4-oxothiazolidin-2-ylidene)malononitrile ((±)-2-*Z*): A three-necked round-bottom flask containing 2-(3-ethyl-4-oxothiazolidin-2-ylidene)malononitrile (0.19 g, 1.0 mmol) and ammonium acetate (93 mg, 1.2 mmol) was equipped with a stir bar, two septa, and a reflux condenser. The flask was flushed with argon three times. (±)-4-Formyl-[2.2]paracyclophane (0.25 g, 1.1 mmol) and glacial acetic acid (10 mL) were added to the flask and the reaction apparatus was covered in aluminum foil. The mixture was heated to 100 °C and allowed to reflux overnight (22 h) with stirring. After cooling to room temperature, the reaction mixture was neutralized with a saturated $NaHCO_3$ solution. The aqueous phase was extracted three times with DCM and the combined organic extracts were dried over anhydrous Na_2SO_4. The solvent was removed under reduced pressure and the resulting concentrate was purified by silica column chromatography using 10:1 DCM:hexanes as the eluent to yield a bright yellow solid (0.21 g, 0.52 mmol, 52%).

^{1}H NMR ($CDCl_3$, 600 MHz) of **(±)-2-*Z***: δ 8.02 (s, 1H), 6.66 (d, J = 6.0 Hz, 1H), 6.63 – 6.55 (m, 4H), 6.40 (s, 2H), 4.36 (q, J = 7.2 Hz, 2H), 3.65 – 3.57 (m, 1H), 3.30 – 3.16 (m, 3H), 3.12 – 2.96 (m, 4H), 1.45 (t, J = 7.2 Hz, 3H) ppm.

^{13}C NMR ($CDCl_3$, 150 MHz) of **(±)-2-*Z***: δ 166.6, 166.3, 143.2, 141.6, 139.6, 138.8, 136.5, 136.0, 134.5, 133.4, 133.0, 132.9, 132.1, 131.8, 116.6, 113.2, 112.3, 55.8, 40.6, 35.4, 35.3, 35.2, 34.0, 14.3 ppm.

HRMS-DART of **(±)-2-*Z***: *m*/*z* $[M+H]^+$ calculated for $[C_{25}H_{22}N_3OS]^+$: 412.1478, found 412.1470 (1.9 ppm).

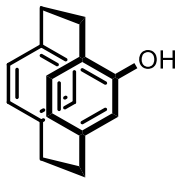

(±)-7

(±)-4-Hydroxy[2.2]paracyclophane ((±)-7): A three-necked round-bottom flask containing (±)-4-formyl-[2.2]paracyclophane (0.47 g, 2.0 mmol) was equipped with a stir bar and two septa. The flask was flushed with argon three times. A 1:1 mixture of DCM/methanol (16 mL) was added. To this solution, conc. H_2SO_4 (12 drops) and H_2O_2 (50 wt% in water, 0.19 mL, 2.8 mmol) were added subsequently, and the reaction mixture was allowed to stir overnight (17 h) at 25 °C. The solvent was removed under reduced pressure, and the residue was taken up in DCM and water. The aqueous phase was extracted three times with DCM and the combined organic extracts were dried over anhydrous Na_2SO_4. The solvent was removed under reduced pressure and the resulting concentrate was purified by silica column chromatography using a gradient of 10:1 to 7:1 hexanes:ethyl acetate as the eluent to yield a yellow solid (0.35 g, 1.6 mmol, 78%).

^{1}H NMR ($CDCl_3$, 600 MHz) of **(±)-7**: δ 7.01 (d, J = 7.8 Hz, 1H), 6.56 (d, J = 7.8 Hz, 1H), 6.45 (d, J = 7.8 Hz, 1H), 6.40 (t, J = 7.7 Hz, 2H), 6.27 (d, J = 7.7 Hz, 1H), 5.54 (s, 1H), 4.54 (s, 1H), 3.38 – 3.31 (m, 1H), 3.13 – 2.96 (m, 6H), 2.94 – 2.88 (m, 1H), 2.70 – 2.63 (m, 1H) ppm.

^{13}C NMR ($CDCl_3$, 150 MHz) of **(±)-7**: δ 153.8, 142.1, 139.8, 138.9, 135.6, 133.7, 132.9, 132.0, 128.1, 125.6, 125.1, 122.7, 35.4, 34.9, 33.9, 31.2 ppm.

The NMR spectra match the literature.[5]

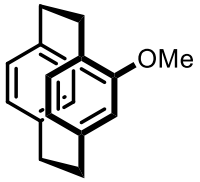

(±)-8

(±)-4-Methoxy[2.2]paracyclophane ((±)-8): A three-necked round-bottom flask containing (±)-4-hydroxy[2.2]paracyclophane (0.1 g, 0.5 mmol) was equipped with a stir bar, and two septa. The flask was flushed with argon three times. The solid was dissolved in DMF (7 mL) and the solution was cooled to 0 °C. Sodium hydride (60% dispersion in mineral oil, 22 mg, 0.55 mmol) was added, and the reaction mixture was stirred at 25 °C for 1 h. Iodomethane (47 µL, 0.75 mmol) was added to the mixture, and the solution was allowed to stir for additional 2 h. The reaction mixture was diluted with water, and the aqueous phase was extracted three times with Et_2O and the combined organic extracts were dried over anhydrous Na_2SO_4. The solvent was removed under reduced pressure and the resulting concentrate was purified by silica column chromatography using a gradient of 10:1 to 9:1 hexanes:ethyl acetate as the eluent to yield a white solid (0.12 g, 0.48 mmol, 96%).

^{1}H NMR ($CDCl_3$, 600 MHz) of **(±)-8**: δ 6.85 (d, J = 7.8 Hz, 1H), 6.60 (d, J = 5.8 Hz, 1H), 6.54 – 6.49 (m, 2H), 6.46 (d, J = 5.8 Hz, 1H), 6.35 (d, J = 7.5 Hz, 1H), 5.73 (s, 1H), 3.76 (s, 3H), 3.58 – 3.50 (m, 1H), 3.21 – 3.04 (m, 7H), 2.74 – 2.65 (m, 1H) ppm.

^{13}C NMR ($CDCl_3$, 150 MHz) of **(±)-8**: δ 157.5, 142.0, 140.1, 138.7, 134.9, 133.5, 133.0, 131.4, 128.2, 127.4, 124.3, 116.6, 54.1, 35.4, 35.3, 34.0, 31.6 ppm.

The NMR spectra match the literature.[6]

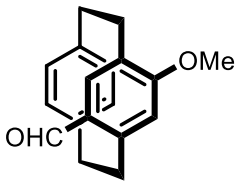

(±)-9

(±)-7-Methoxy[2.2]paracyclophane-4-carbaldehyde ((±)-9): A three-necked round-bottom flask containing (±)-4-methoxy[2.2]paracyclophane (0.11 g, 0.48 mmol) was equipped with a stir bar, and two septa. The flask was flushed with argon three times. The solid was dissolved in DCM (5 mL) and the solution was cooled to 0 °C. $TiCl_4$ (60 µL, 0.57 mmol) was added, followed by dichloromethyl methyl ether (40 µL, 0.49 mmol), and the solution was allowed to stir at 25 °C for 6 h. The reaction mixture was diluted with DCM, cooled to 0 °C, and then deionized water and 2N HCl were added successively. The organic phase was extracted three times with water and saturated $NaHCO_3$ solution. The combined organic extracts were dried over anhydrous Na_2SO_4. The solvent was removed under reduced pressure and the resulting concentrate was purified by silica column chromatography using a gradient of 7:1 to 5:1 hexanes:ethyl acetate as the eluent to yield a white solid (0.11 g, 0.40 mmol, 83%).

^{1}H NMR ($CDCl_3$, 600 MHz) of **(±)-9**: δ 9.88 (s, 1H), 6.98 (s, 1H), 6.71 (d, J = 7.8 Hz, 1H), 6.51 (d, J = 7.9 Hz, 1H), 6.42 (d, J = 5.8 Hz, 1H), 6.37 (d, J = 7.9 Hz, 1H), 5.71 (s, 1H), 4.12 – 4.04 (m, 1H), 3.77 (s, 3H), 3.44 – 3.37 (m, 1H), 3.23 – 3.16 (m, 1H), 3.16 – 3.09 (m, 1H), 3.03 (dd, J = 14.5, 8.3 Hz, 2H), 2.80 (dd, J = 18.5, 11.7 Hz, 1H), 2.62 (dd, J = 21.9, 8.7 Hz, 1H) ppm.

^{13}C NMR ($CDCl_3$, 150 MHz) of **(±)-9**: δ 190.3, 162.0, 147.3, 140.0, 138.5, 132.8, 132.7, 131.2, 130.2, 128.6, 128.3, 119.0, 54.9, 35.3, 33.6, 33.1, 31.3 ppm.

HRMS-DART of **(±)-9**: m/z $[M+H]^+$ calculated for $[C_{18}H_{19}O_2]^+$: 267.1380, found 267.1382 (0.7 ppm).

The compound was previously synthesized by Sergeeva, et al.[7]

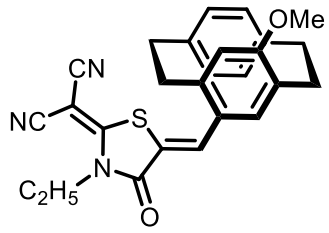

(±)-3-*Z*

(±)-(*Z*)-2-(5-(7-Methoxy[2.2]paracyclophane)-3-ethyl-4-oxothiazolidin-2-ylidene)malononitrile ((±)-3-*Z*): A three-necked round-bottom flask containing 2-(3-ethyl-4-oxothiazolidin-2-ylidene)malononitrile (72 mg, 0.37 mmol) and ammonium acetate (35 mg, 0.45 mmol) was equipped with a stir bar, two septa, and a reflux condenser. The flask was flushed with argon three times. (±)-7-Methoxy[2.2]paracyclophane-4-carbaldehyde (0.10 g, 0.39 mmol) and glacial acetic acid (7 mL) were added to the flask and the reaction apparatus was covered in aluminum foil. The mixture was heated to 100 °C and allowed to reflux overnight (23 h) with stirring. After cooling to room temperature, the reaction mixture was neutralized with a saturated $NaHCO_3$ solution. The aqueous phase was extracted three times with DCM and the combined organic extracts were dried over anhydrous Na_2SO_4. The solvent was removed under reduced pressure and the resulting concentrate was purified by silica chromatography using a gradient of 3:1 to 10:1 DCM:hexanes as the eluent to yield a yellow-orange solid (0.13 g, 0.29 mmol, 79%).

^{1}H NMR ($CDCl_3$, 600 MHz) of **(±)-3-*Z***: δ 8.01 (s, 1H), 6.75 (d, J = 7.8 Hz, 1H), 6.60 (s, 1H), 6.52 (d, J = 7.9 Hz, 1H), 6.39 (d, J = 5.8 Hz, 1H), 6.33 (d, J = 7.9 Hz, 1H), 5.77 (s, 1H), 4.30 (q, J = 7.2, 6.7 Hz, 2H), 3.78 (s, 3H), 3.61 – 3.53 (m, 1H), 3.46 – 3.39 (m, 1H), 3.23 – 3.12 (m, 2H), 3.10 – 2.97 (m, 2H), 2.92 – 2.83 (m, 1H), 2.68 – 2.58 (m, 1H), 1.42 (t, J = 7.2 Hz, 3H) ppm.

^{13}C NMR ($CDCl_3$, 150 MHz) of **(±)-3-*Z***: δ 166.7, 166.5, 161.0, 147.5, 140.1, 137.8, 135.7, 134.4, 132.8, 132.2, 131.3, 129.7, 129.0, 125.5, 119.0, 113.5, 112.7, 112.6, 55.0, 54.7, 40.4, 35.3, 33.7, 33.6, 31.6, 14.3 ppm.

HRMS-DART of **(±)-3-*Z***: m/z $[M+H]^+$ calculated for $[C_{26}H_{24}N_3O_2S]^+$: 442.1584, found 442.1583 (0.2 ppm); m/z $[M+NH_4]^+$ calculated for $[C_{26}H_{27}N_4O_2S]^+$: 459.1849, found 459.1853 (0.9 ppm).

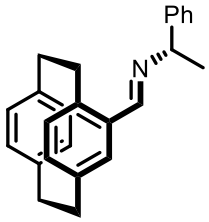

(*S*, R_p)-10

(*S*, R_p)-[*N*-(1-Phenylethyl)]-4-[2.2]paracyclophanemethanimine ((*S*, R_p)-10): A 100 mL RBF was charged with **(±)-5** (0.500 g, 2.12 mmol), equipped with stir bar and condenser, and flushed with argon three times. Degassed toluene (30 mL) was added, followed by (*S*)-(−)-α-phenylethylamine (297 µL, 2.32 mmol). The reaction was heated to reflux under argon atmosphere for 72 h. Volatiles were removed under reduced pressure, yielding a mixture of diastereomers. Repeated recrystallization from hexanes (4×) yielded 145 mg of **(*S*, R_p)-10** (0.43 mmol, 20%).

^{1}H NMR ($CDCl_3$, 600 MHz): δ 8.36 (s, 1H), 7.52 (d, J = 7.6 Hz, 2H), 7.40 (t, J = 7.6 Hz, 2H, 7.30 – 7.26 (m, 1H), 6.59 – 6.57 (m, 1H), 6.52 – 6.48 (m, 3H), 6.40 – 6.37 (m, 1H), 6.30 – 6.27 (m, 1H), 4.57 (s, 1H), 3.94 – 3.86 (m, 1H), 3.22 – 3.00 (m, 6H), 2.92 – 2.82 (m, 2H), 1.66 (d, J = 6.8 Hz, 3H) ppm.

The compound was previously synthesized by Cakici, et al.[8]

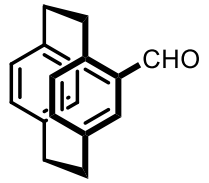

(R_p)-5

(*S*, R_p)-10 was passed through a short silica gel plug using 100% DCM, yielding **(R_p)-5** (100 mg, 0.43 mmol, 99%).

^{1}H NMR ($CDCl_3$, 600 MHz) of **(R_p)-5**: δ 9.95 (s, 1H), 7.02 (s, 1H), 6.73 (d, J = 5.6 Hz, 1H), 6.59 (d, J = 7.8 Hz, 1H), 6.56 (d, J = 7.9 Hz, 1H), 6.50 (d, J = 7.8 Hz, 1H), 6.43 (d, J = 5.8 Hz, 1H), 6.38 (d, J = 7.8 Hz, 1H), 4.14 – 4.07 (m, 1H), 3.26 (t, J = 10.7 Hz, 1H), 3.23 – 3.15 (m, 3H), 3.13 – 3.00 (m, 4H), 2.99 – 2.92 (m, 1H) ppm.

^{13}C NMR ($CDCl_3$, 151 MHz) of **(R_p)-5**: δ 192.1, 143.4, 140.8 139.7, 139.6, 138.2, 136.8, 136.5, 136.3, 133.4, 133.1, 132.5, 132.3, 35.4, 35.3, 35.1, 33.8 ppm.

The compound was previously synthesized by Cakici, et al.[8]

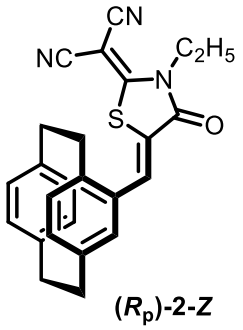

(R_p)-2-*Z*

(R_p)-(*Z*)-2-(5-([2.2]Paracyclophane)-3-ethyl-4-oxothiazolidin-2-ylidene)malononitrile ((R_p)-2-*Z*): A three-necked round-bottom flask containing 2-(3-ethyl-4-oxothiazolidin-2-ylidene)malononitrile (60 mg, 0.31 mmol) and ammonium acetate (29 mg, 0.37 mmol) was equipped with a stir bar, two septa, and a reflux condenser. The flask was flushed with argon three times. (R_p)-4-Formyl-[2.2]paracyclophane (77 mg, 0.33 mmol) and glacial acetic acid (5 mL) were added to the flask and the reaction apparatus was covered in aluminum foil. The mixture was heated to 100 °C and allowed to reflux overnight (21 h) with stirring. After cooling to room temperature, the reaction mixture was neutralized with a saturated $NaHCO_3$ solution. The aqueous phase was extracted three times with DCM and the combined organic extracts were dried over anhydrous Na_2SO_4. The solvent was removed under reduced pressure and the resulting concentrate was purified by silica column chromatography using a gradient of 5:1 to 9:1 DCM:hexanes as the eluent to yield a yellow solid (0.11 g, 0.28 mmol, 90%).

^{1}H NMR ($CDCl_3$, 600 MHz) of **(R_p)-2-*Z***: δ 8.00 (s, 1H), 6.65 (d, J = 7.9 Hz, 1H), 6.61 – 6.55 (m, 4H), 6.39 (s, 2H), 4.31 (q, J = 7.2 Hz, 2H), 3.64 – 3.55 (m, 1H), 3.29 – 3.14 (m, 3H), 3.11 – 2.94 (m, 4H), 1.43 (t, J = 7.2 Hz, 3H) ppm.

^{13}C NMR ($CDCl_3$, 151 MHz) of **(R_p)-2-*Z***: δ 166.5, 166.2, 143.2, 141.5, 139.6, 138.8, 136.5, 135.9, 134.4, 133.3, 132.9, 132.8, 132.0, 131.8, 116.6, 113.2, 112.2, 55.8, 40.6, 35.3, 35.3, 35.2, 33.9, 14.2 ppm.

HRMS-DART of **(R_p)-2-*Z***: *m*/*z* $[M+H]^+$ calculated for $[C_{25}H_{22}N_3OS]^+$: 412.1478, found 412.1463 (3.6 ppm).

[1]H NMR SPECTRA

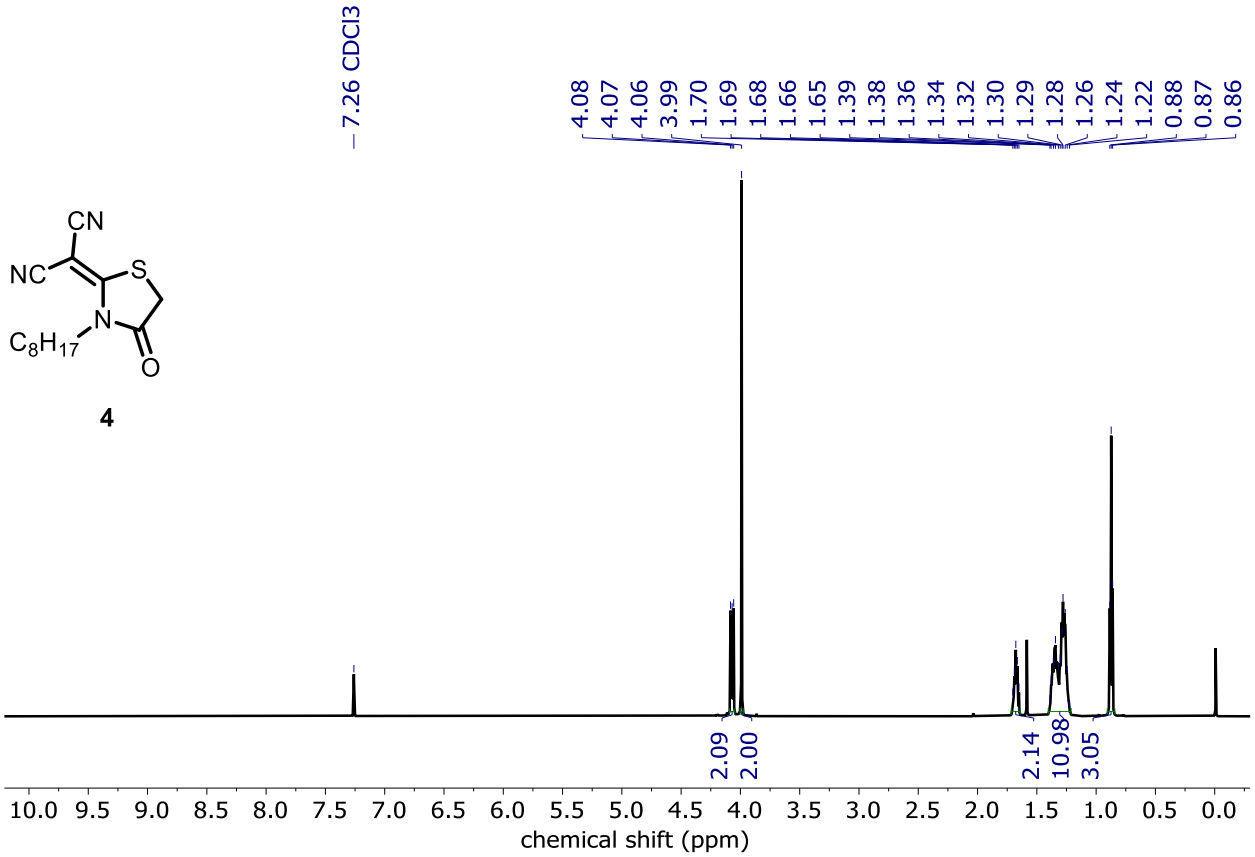

Figure S1. [1]H NMR (600 MHz) of **4** in chloroform-*d*.

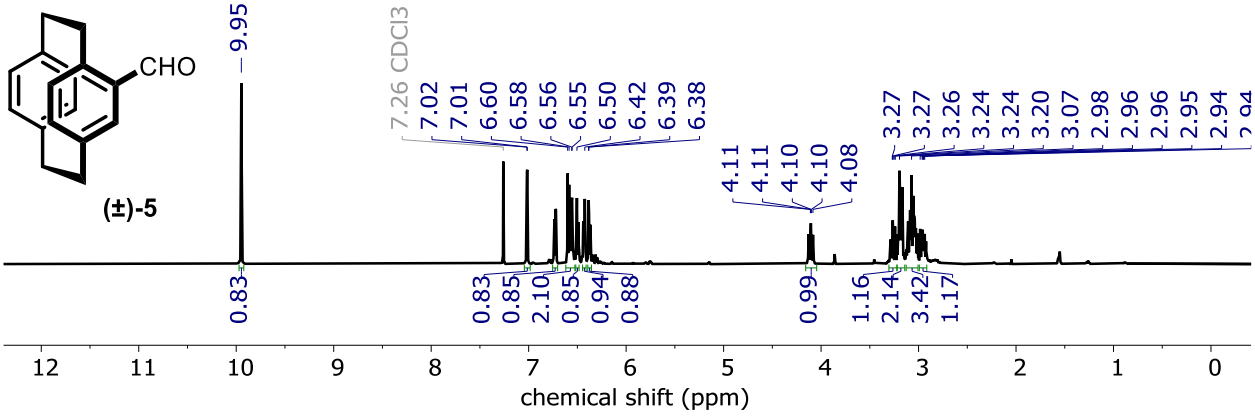

Figure S2. [1]H NMR (500 MHz) of **(±)-5** in chloroform-*d*.

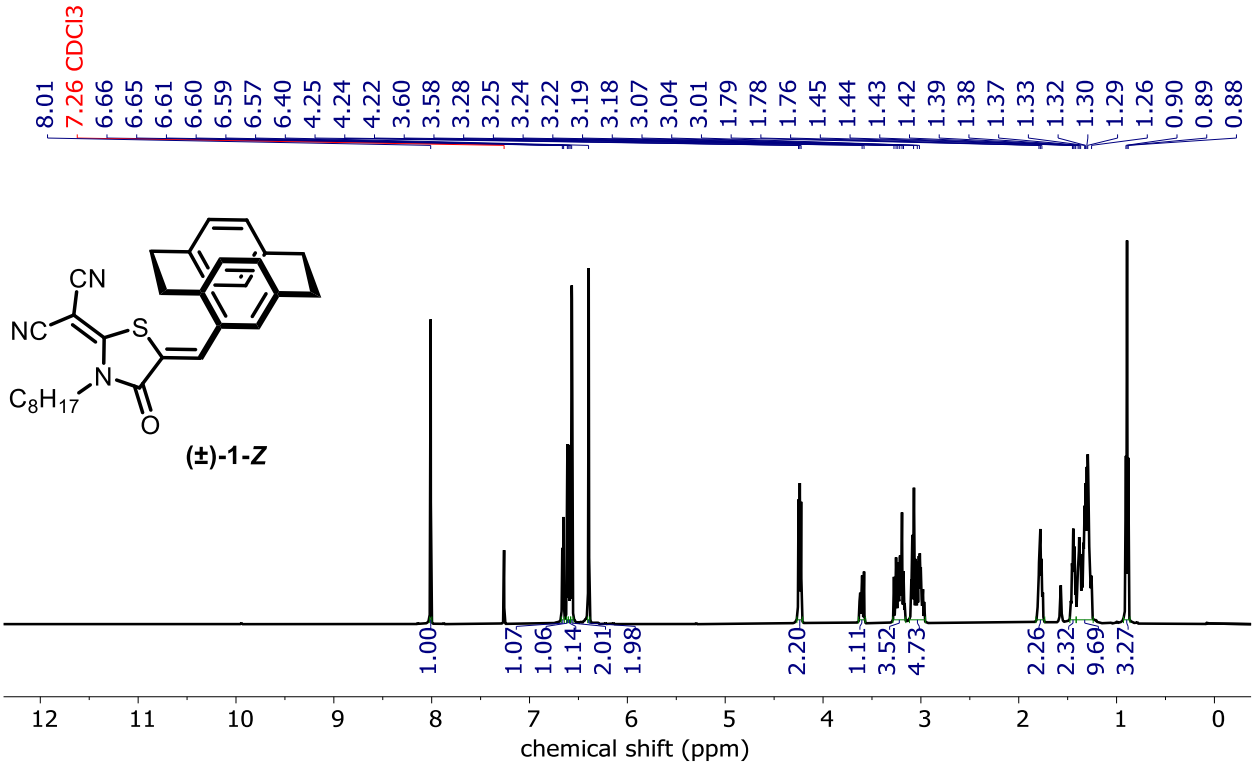

Figure S3. [1]H NMR (600 MHz) of **(±)-1-*Z*** in chloroform-*d*.

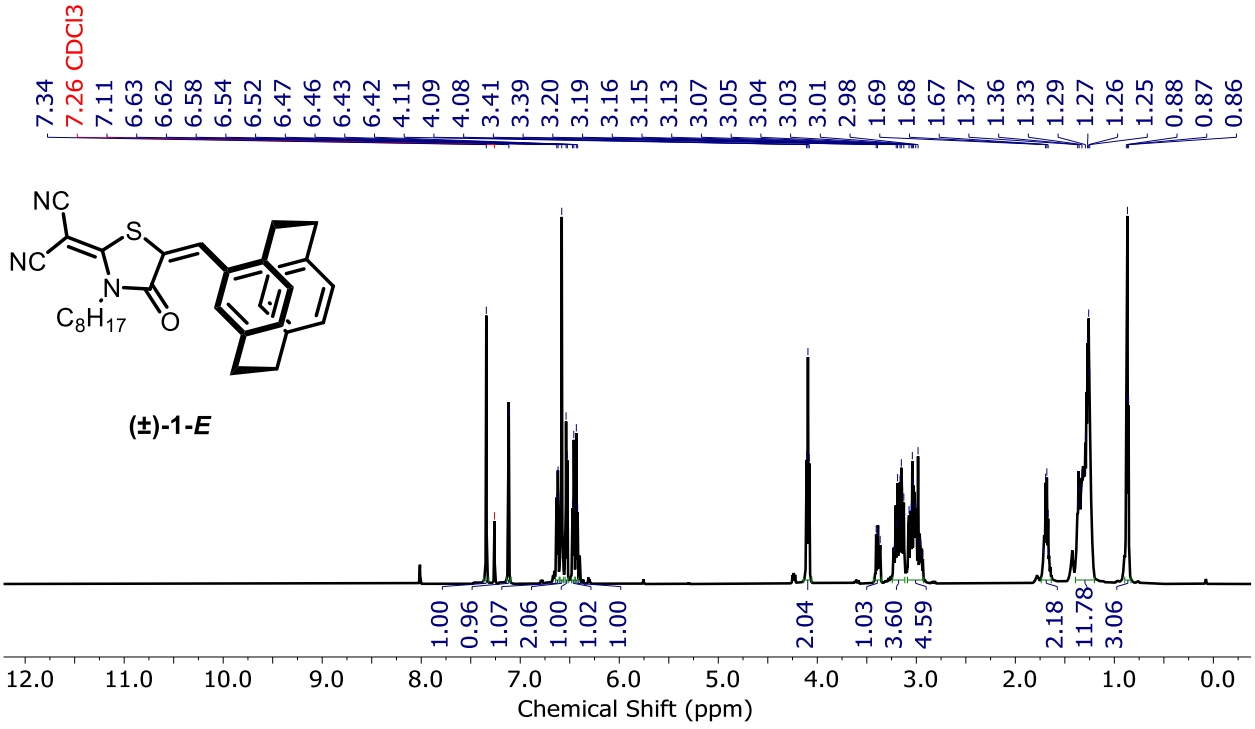

Figure S4. [1]H NMR (600 MHz) of **(±)-1-*E*** (94%) in chloroform-*d*.

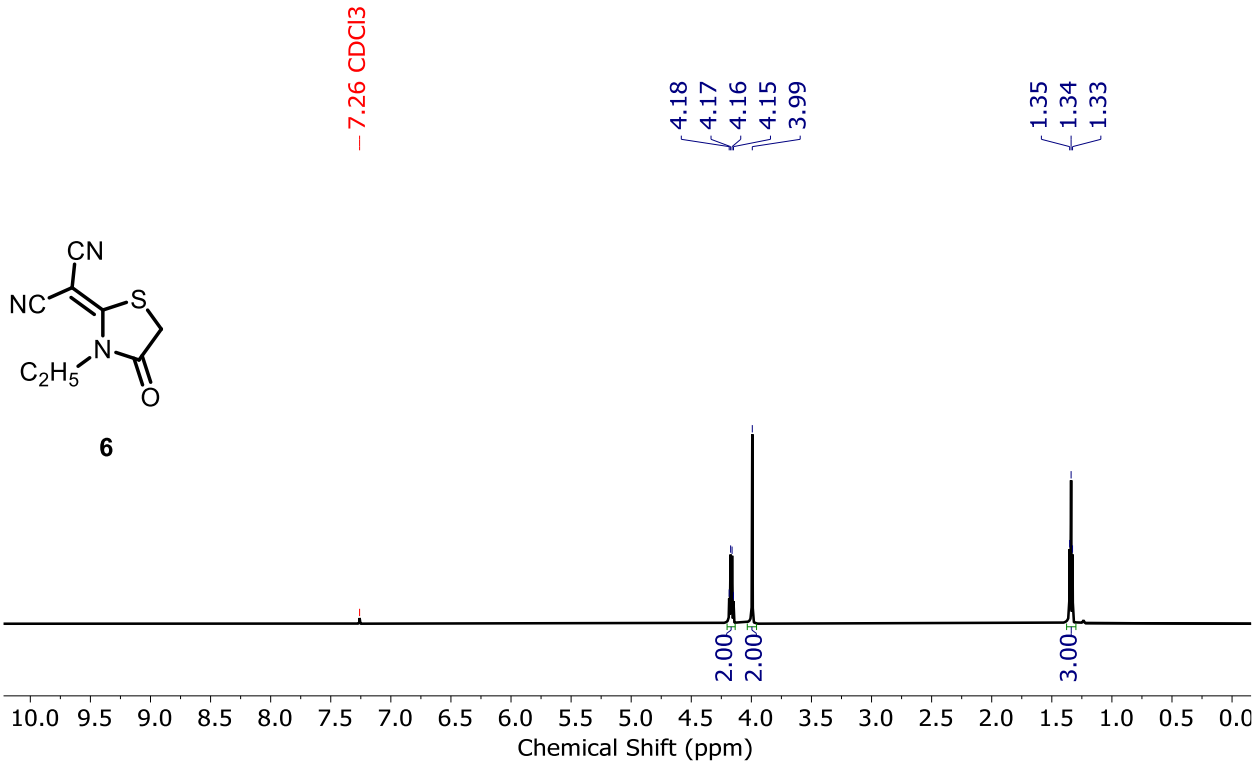

Figure S5. ^{1}H NMR (600 MHz) of **6** in chloroform-*d*.

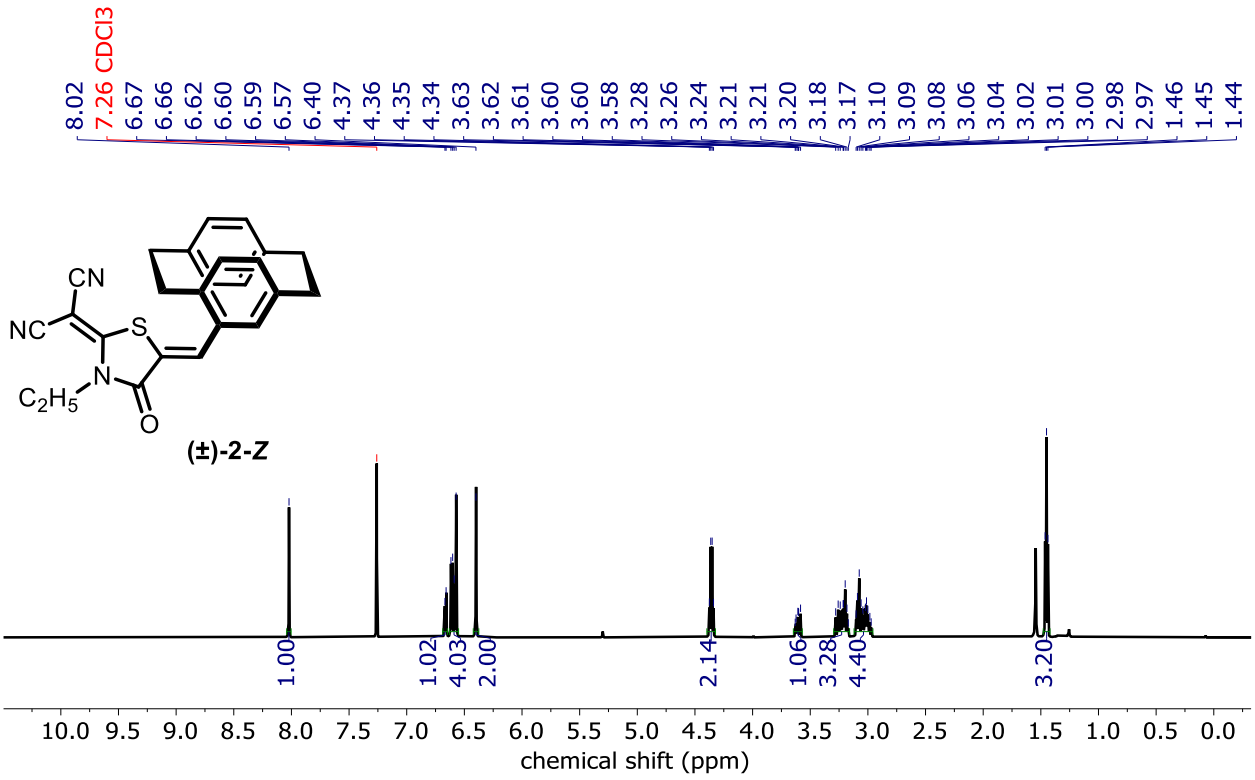

Figure S6. ^{1}H NMR (600 MHz) of **(±)-2-*Z*** in chloroform-*d*.

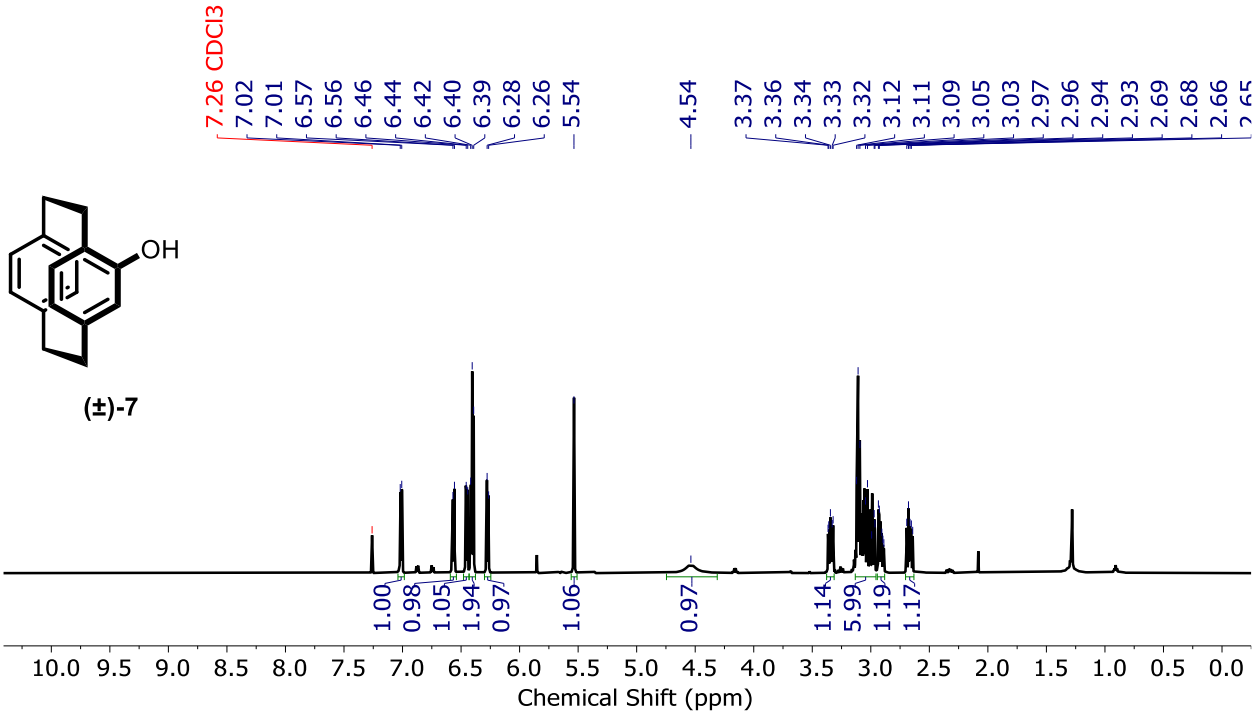

Figure S7. ^{1}H NMR (600 MHz) of **(±)-7** in chloroform-*d*.

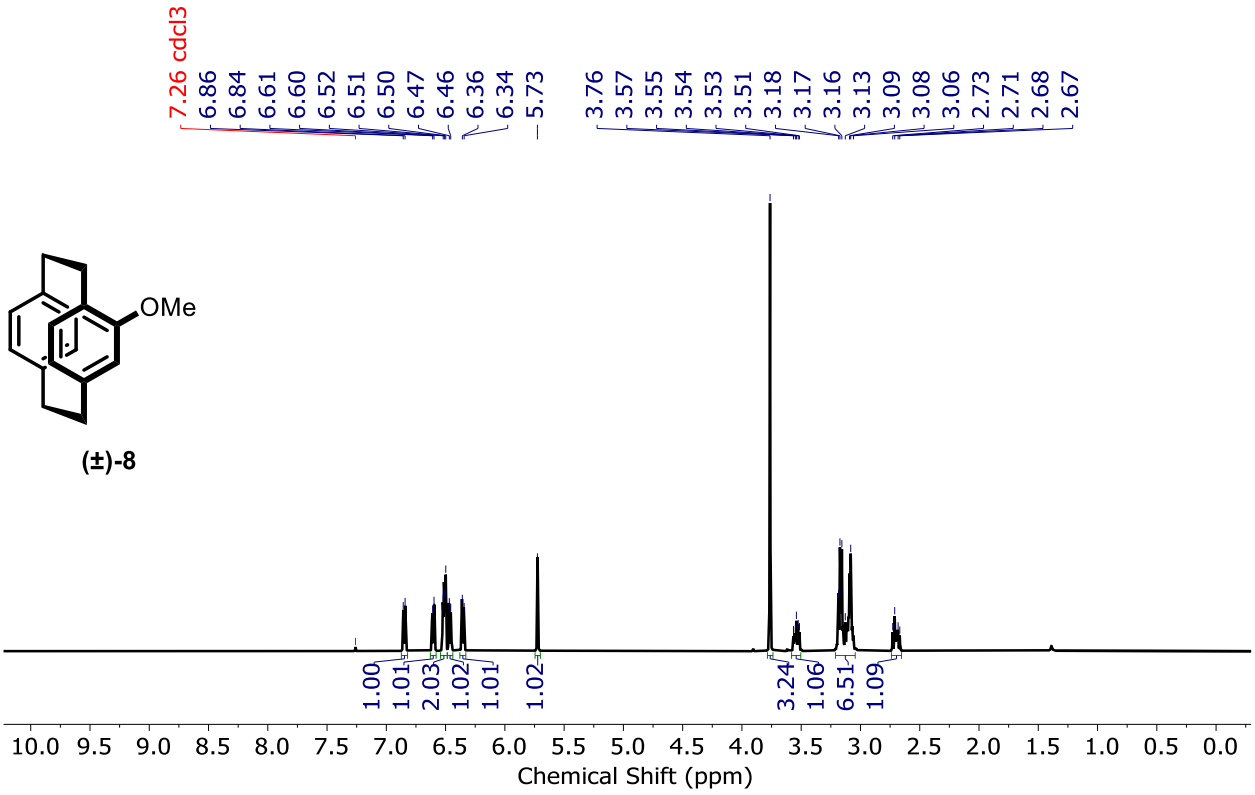

Figure S8. ^{1}H NMR (600 MHz) of **(±)-8** in chloroform-*d*.

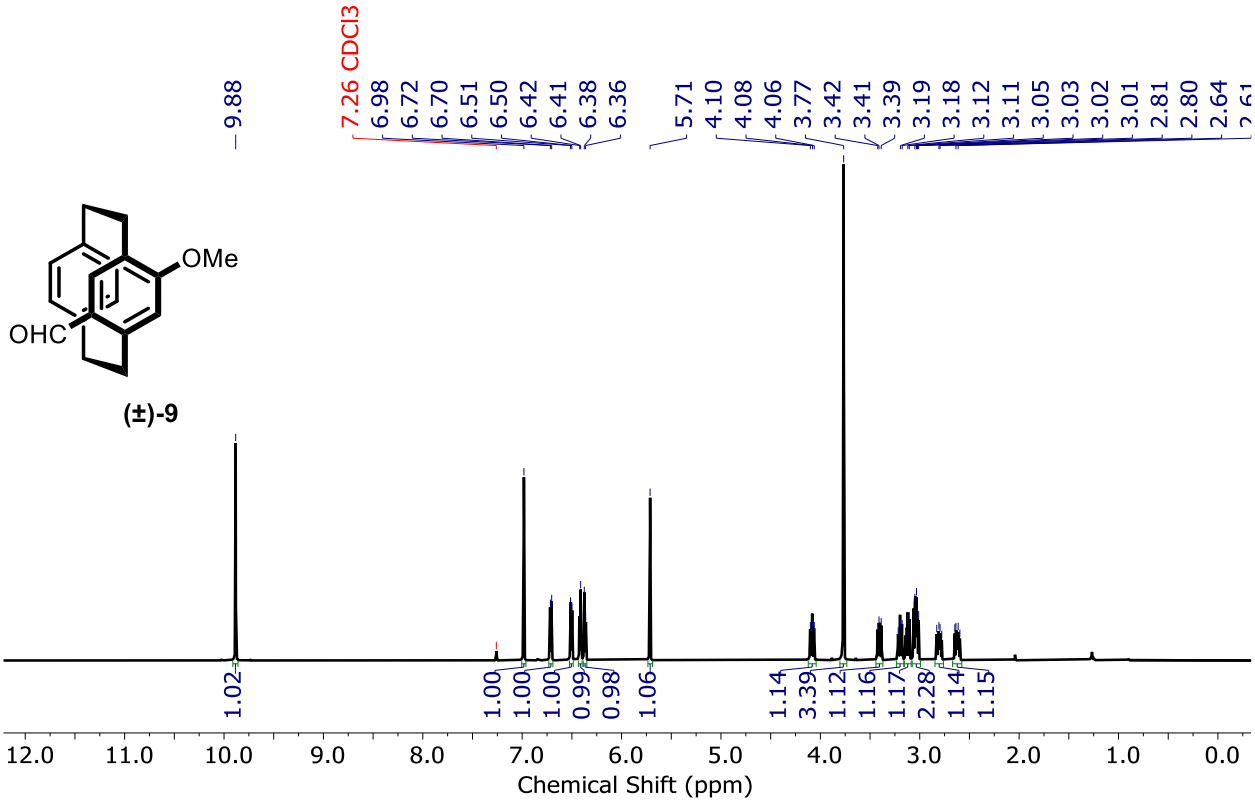

Figure S9. ^{1}H NMR (600 MHz) of **(±)-9** in chloroform-*d*.

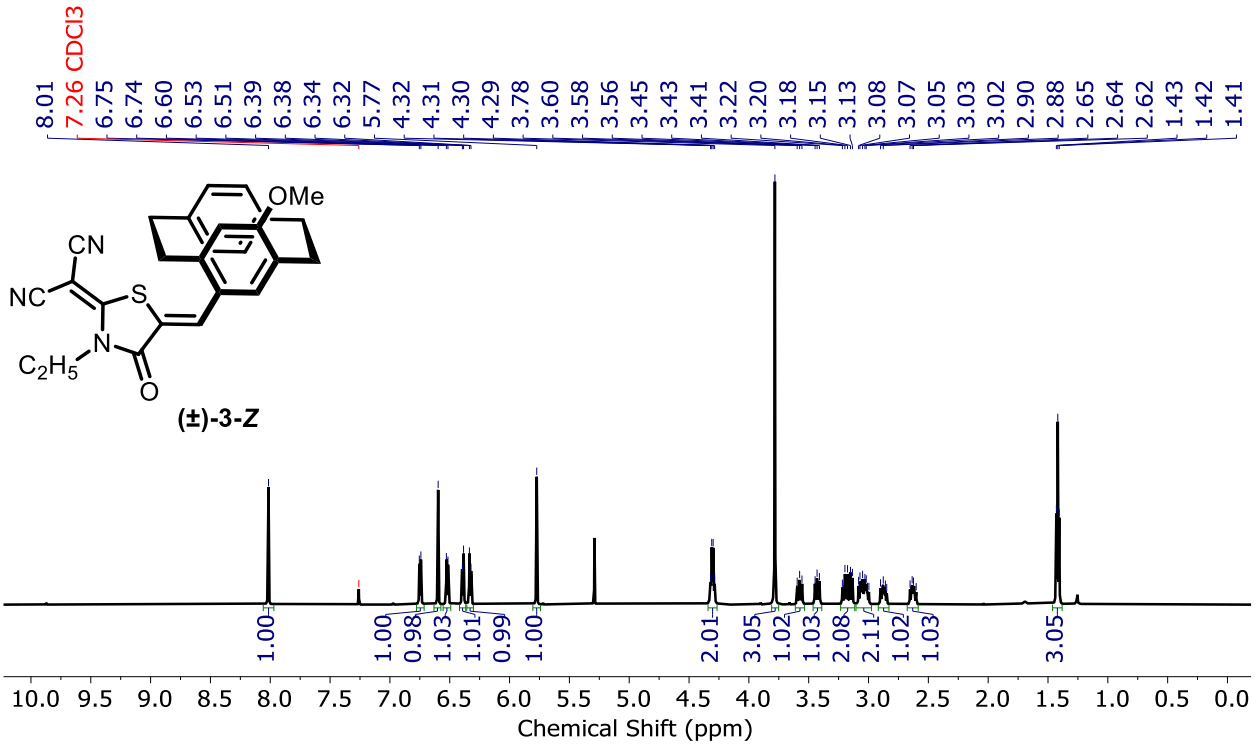

Figure S10. ^{1}H NMR (600 MHz) of **(±)-3-*Z*** in chloroform-*d*.

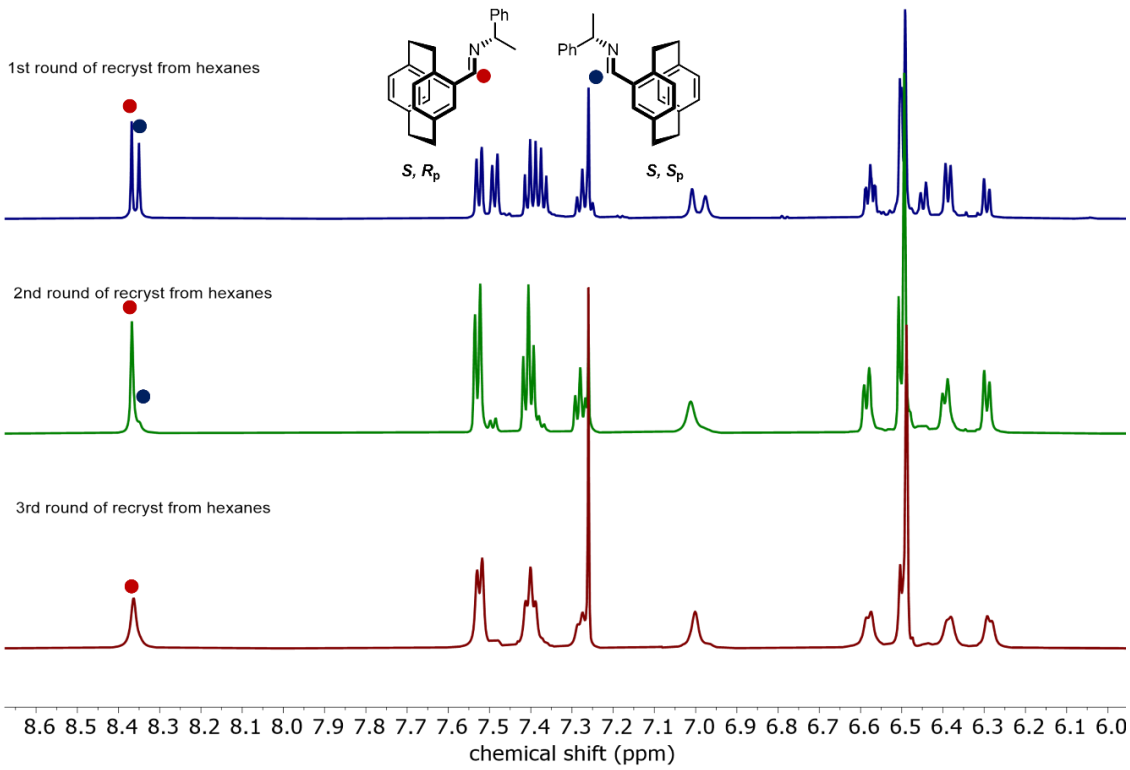

Figure S11. Stacked ^{1}H NMR (500 MHz, chloroform-*d*) of **(±)-10** (blue, top spectrum) after successive recrystallization steps in hexanes to form enantioenriched **(R_p)-10** (maroon, bottom spectrum).

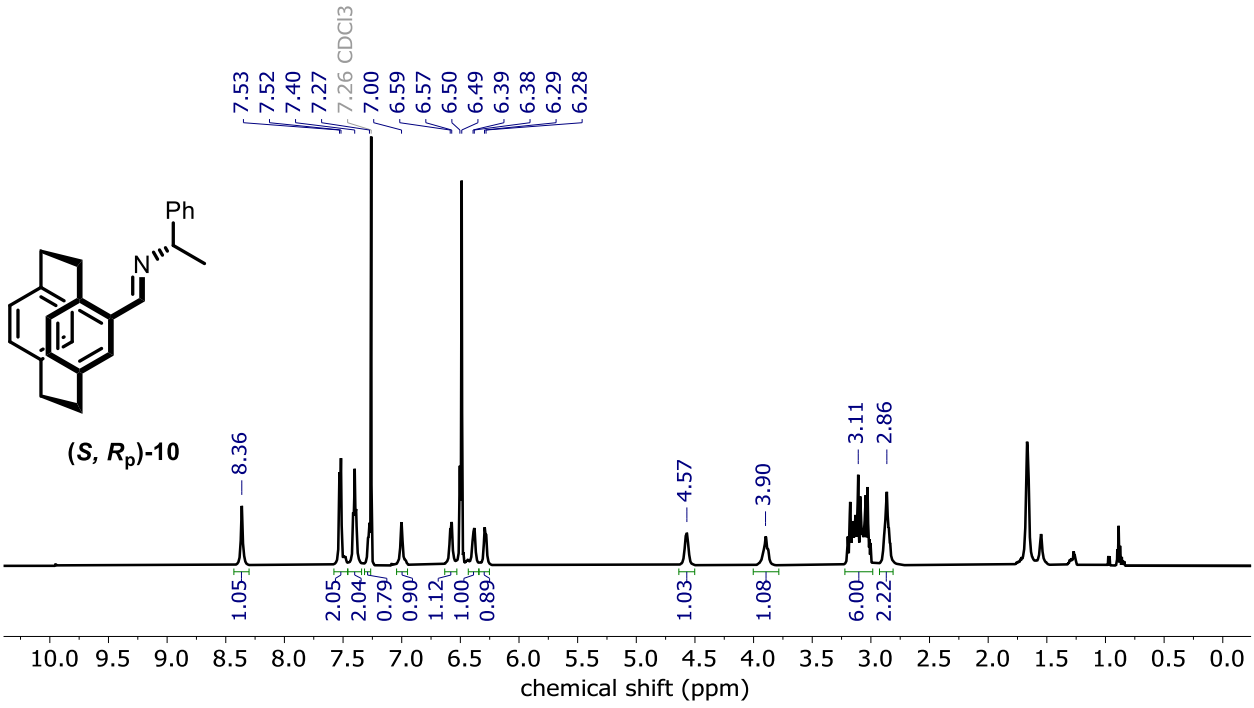

Figure S12. ^{1}H NMR (600 MHz) of **(S, R_p)-10** in chloroform-*d*.

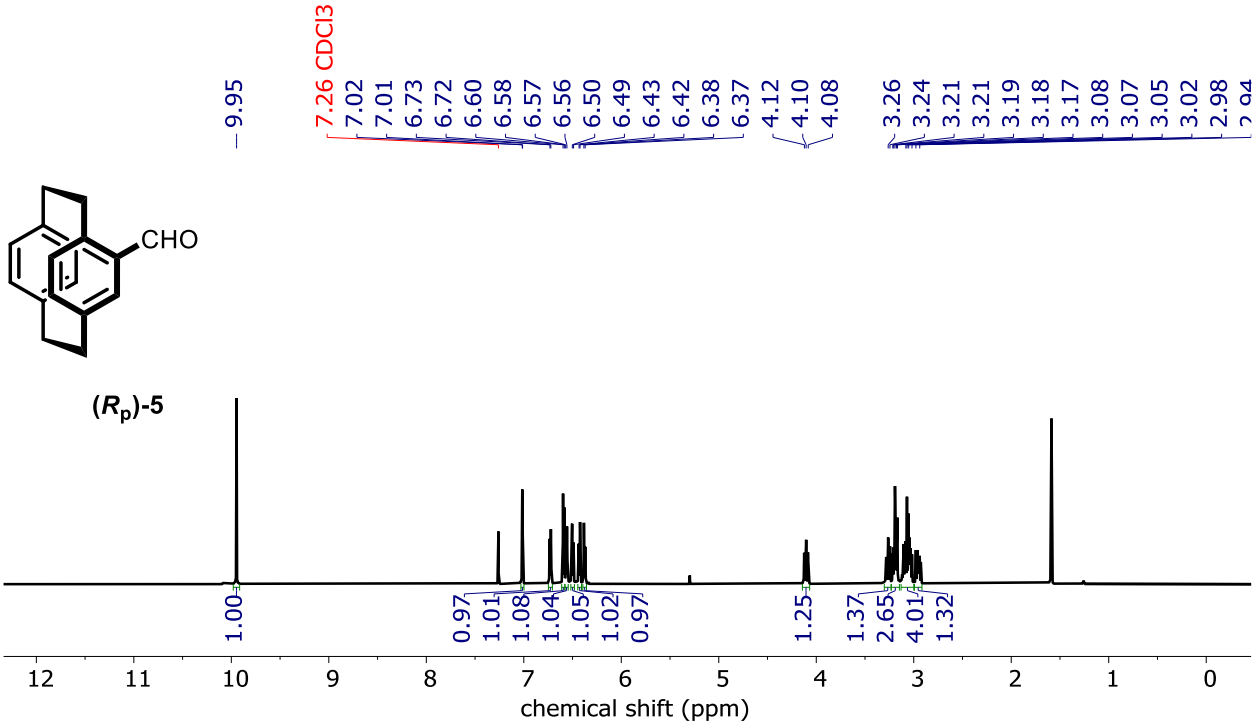

Figure S13. ^{1}H NMR (600 MHz) of **(R_p)-5** in chloroform-*d*.

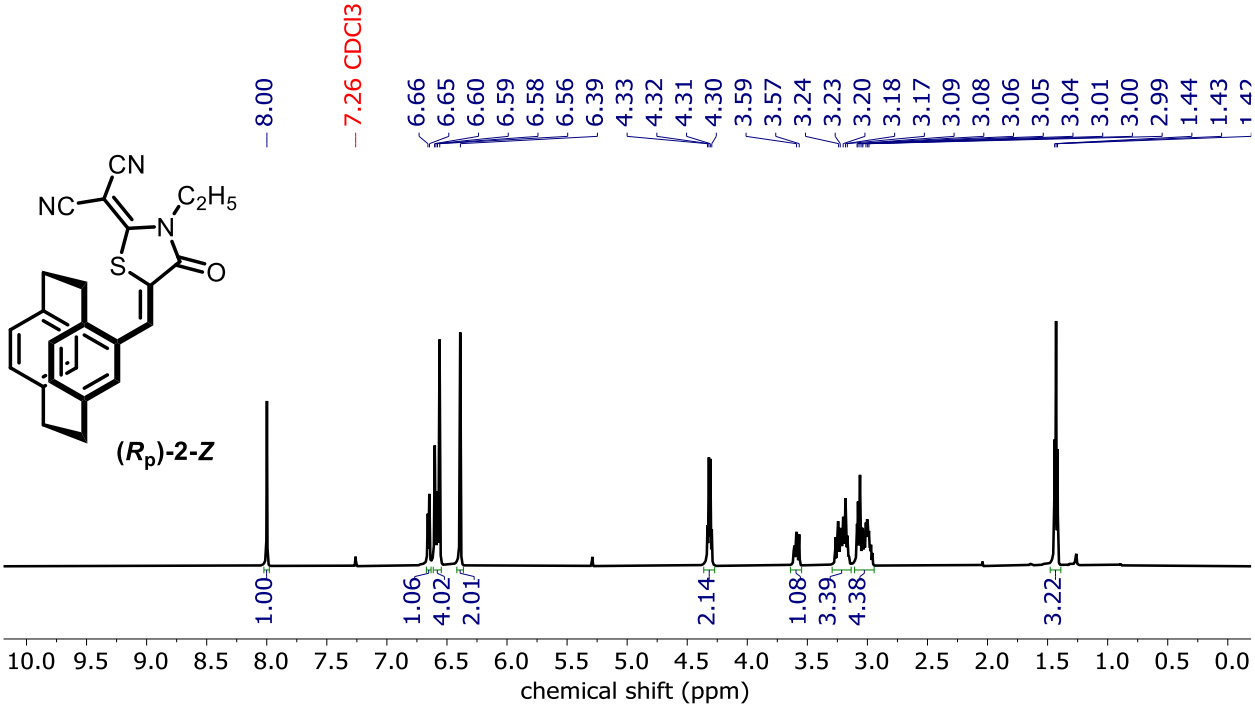

Figure S14. ^{1}H NMR (600 MHz) of **(R_p)-2-*Z*** in chloroform-*d*.

^{13}C {^{1}H} NMR SPECTRA

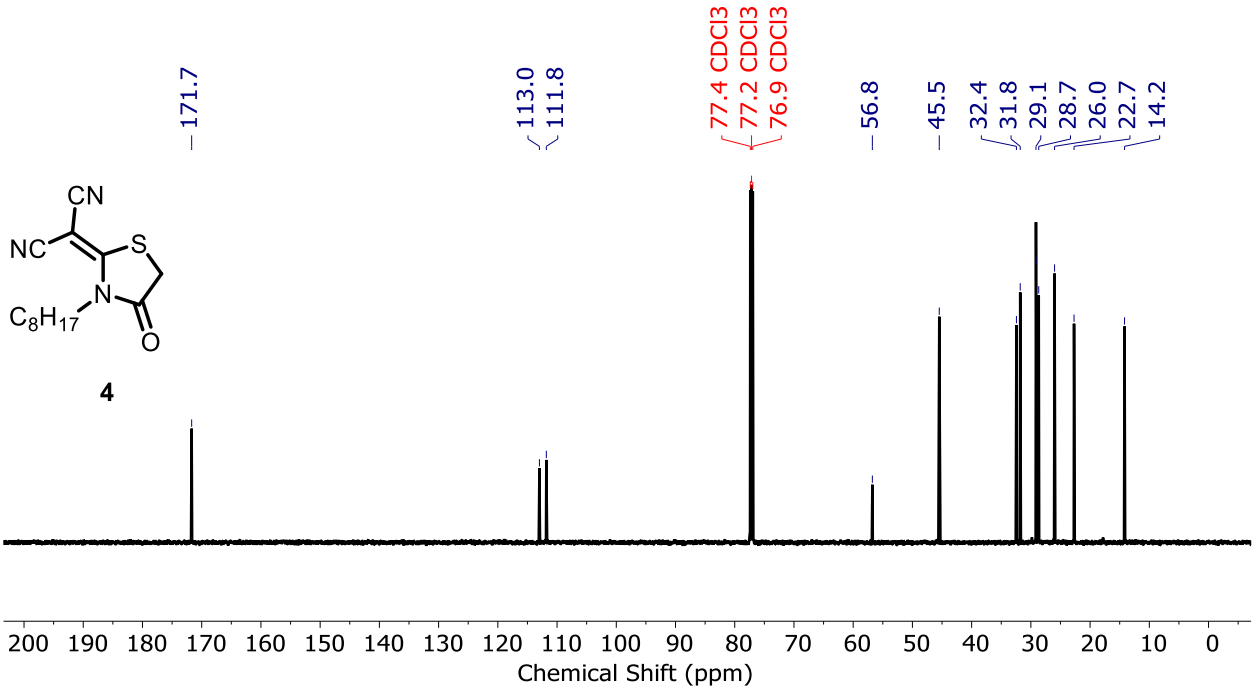

Figure S15. ^{13}C {^{1}H} NMR (150 MHz) of **4** in chloroform-*d*.

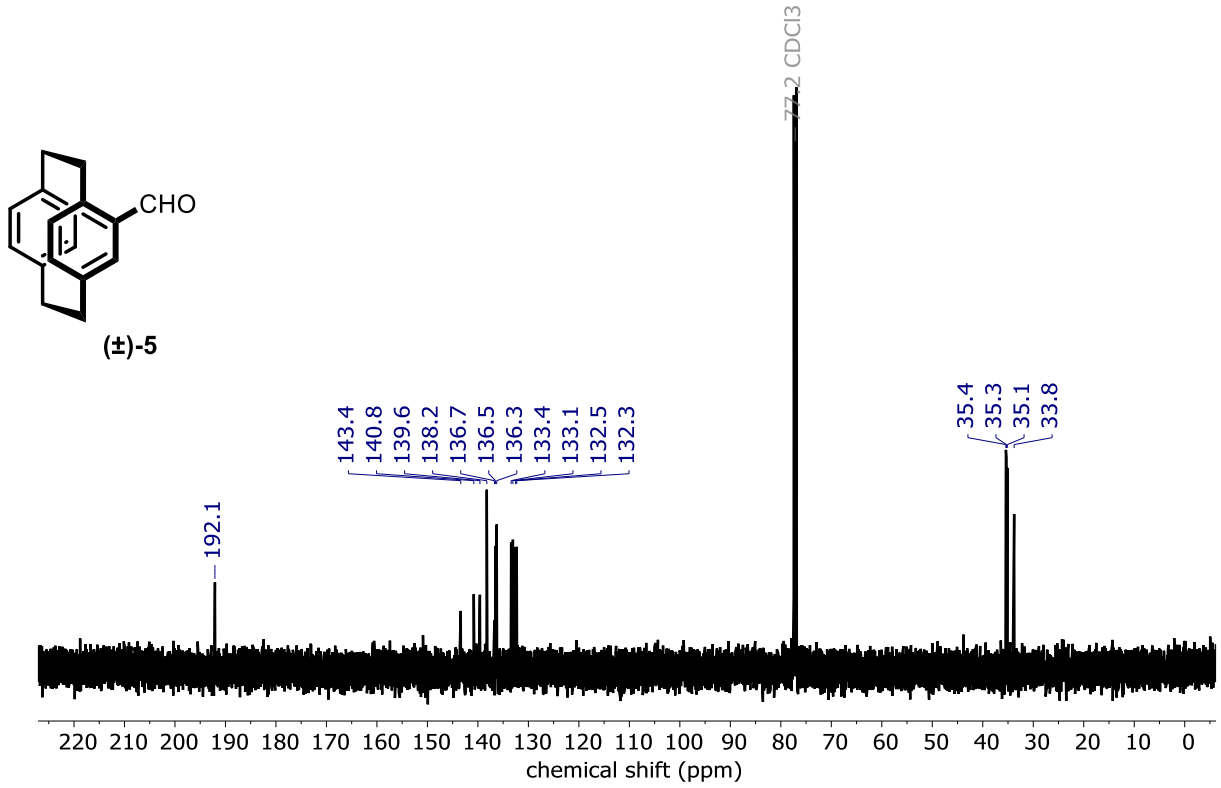

Figure S16. ^{13}C {^{1}H} NMR (126 MHz) of **(±)-5** in chloroform-*d*.

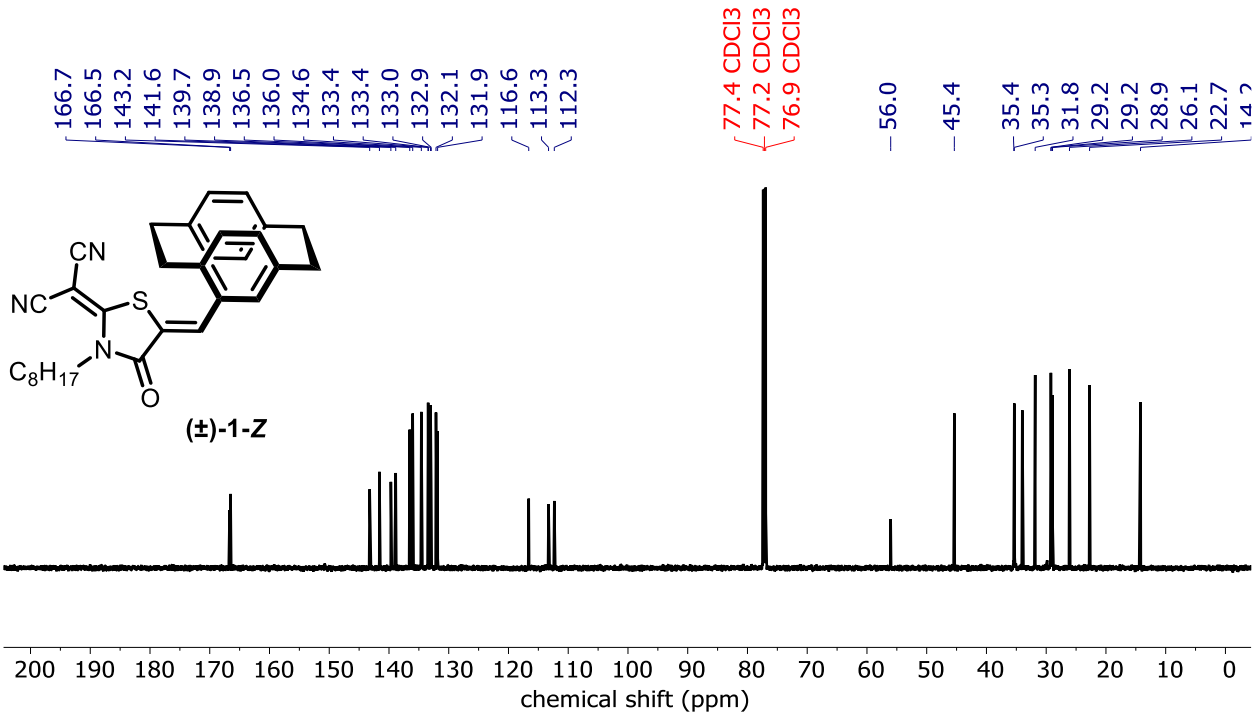

Figure S17. ^{13}C {^{1}H} NMR (150 MHz) of **(±)-1-*Z*** in chloroform-*d*.

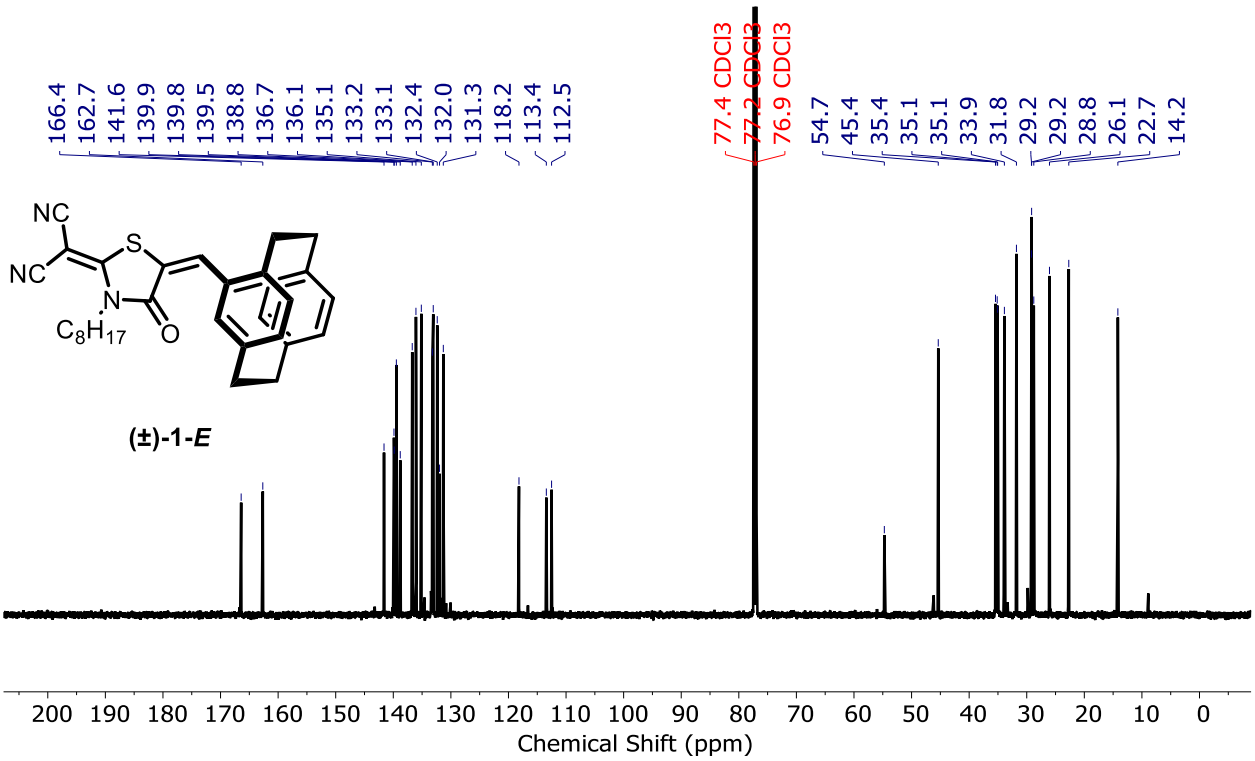

Figure S18. ^{13}C {^{1}H} NMR (150 MHz) of **(±)-1-*E*** (94%) in chloroform-*d*.

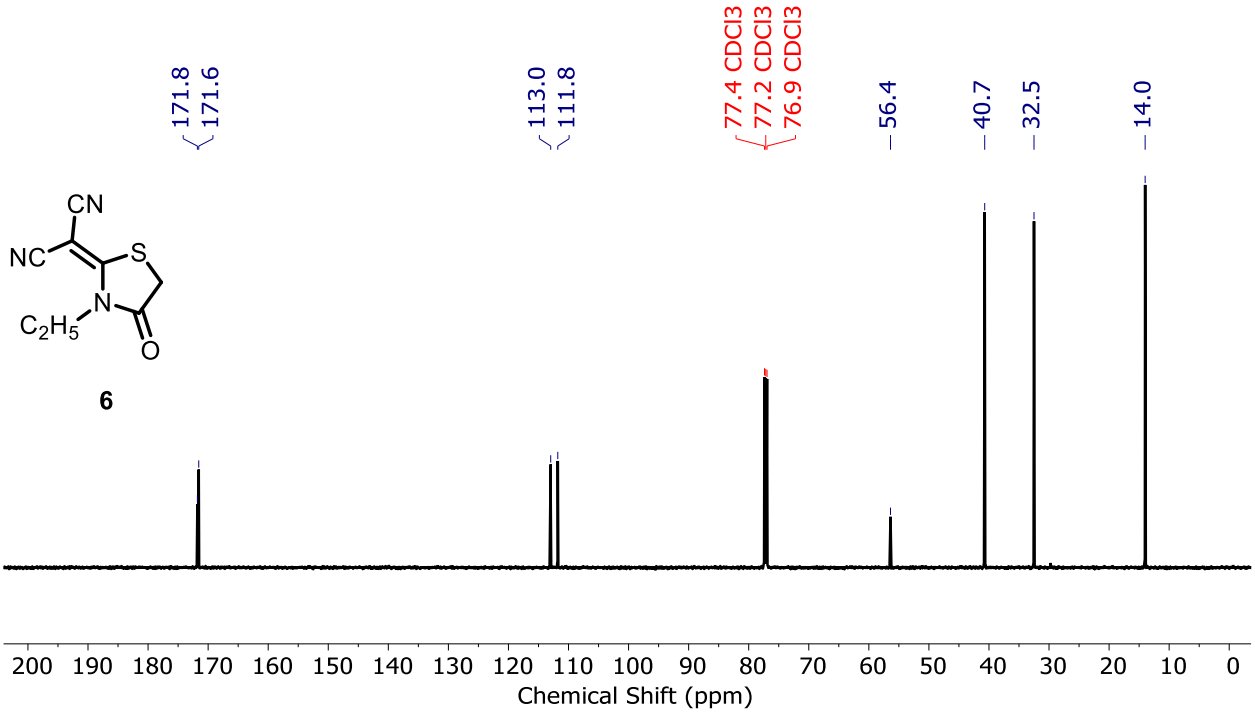

Figure S19. ^{13}C {^{1}H} NMR (150 MHz) of **6** in chloroform-*d*.

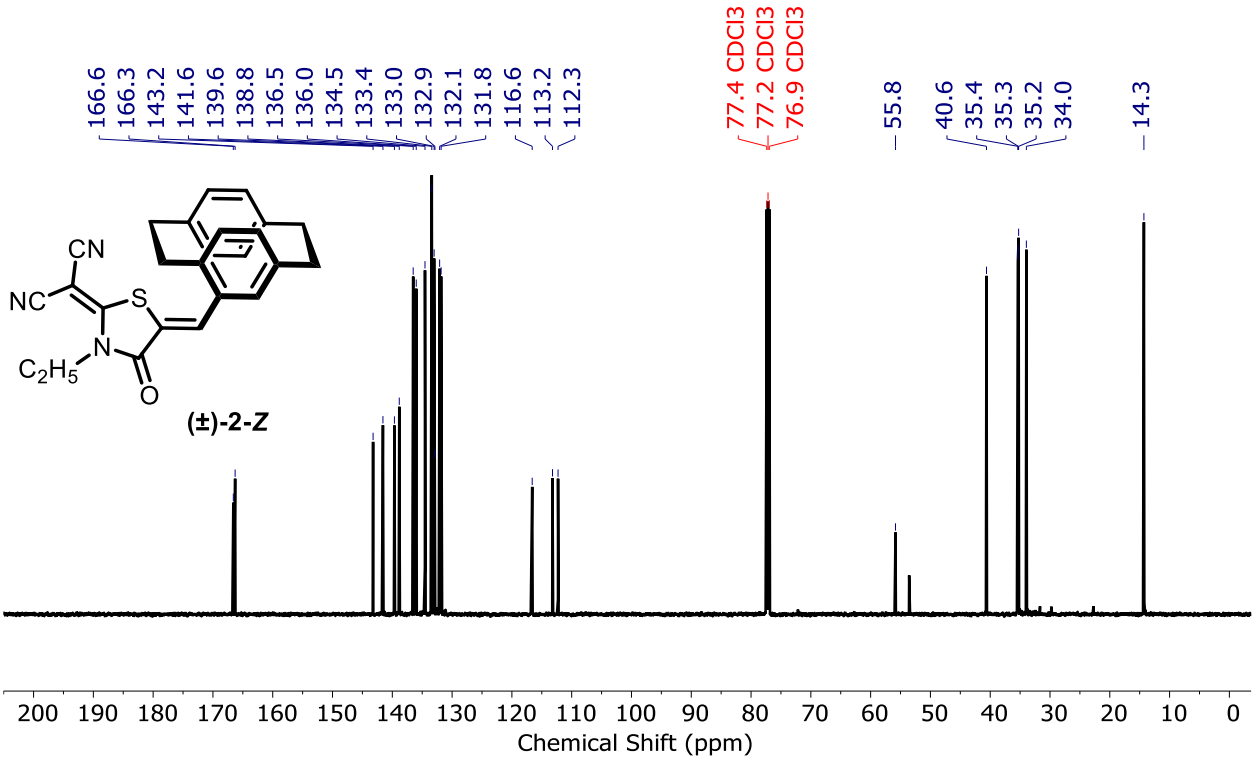

Figure S20. ^{13}C {^{1}H} NMR (150 MHz) of **(±)-2-*Z*** in chloroform-*d*.

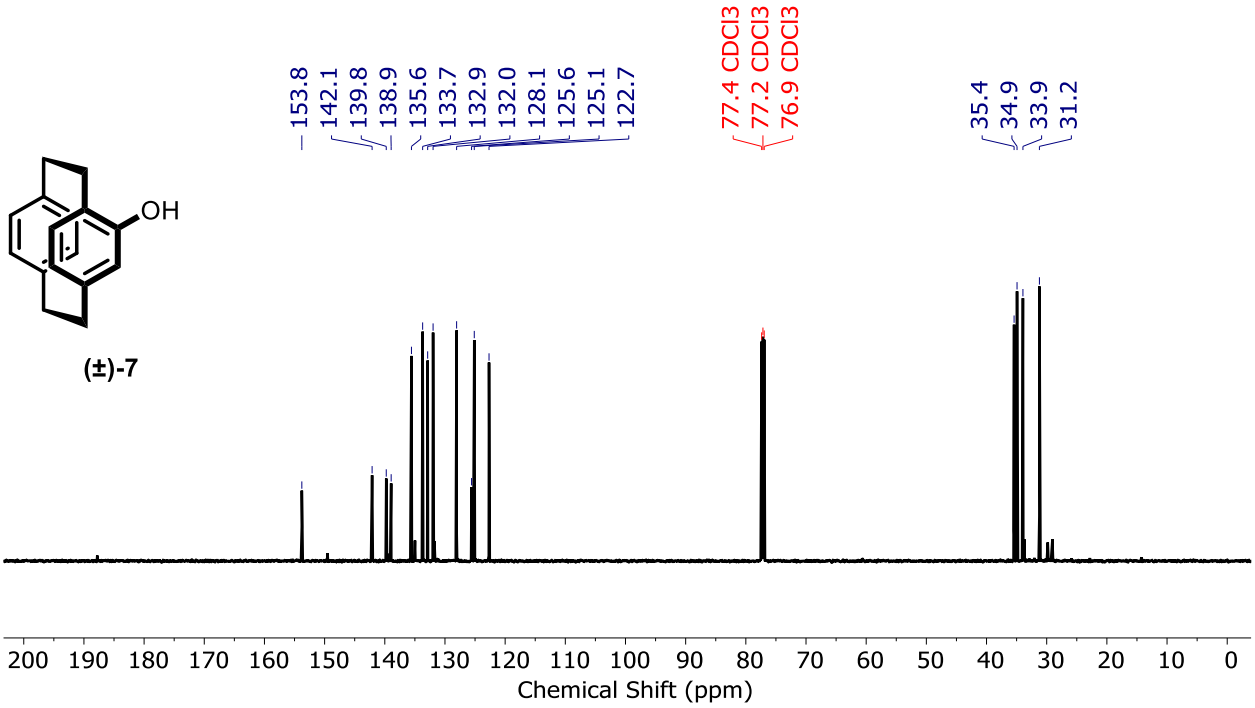

Figure S21. ^{13}C {^{1}H} NMR (150 MHz) of **(±)-7** in chloroform-*d*.

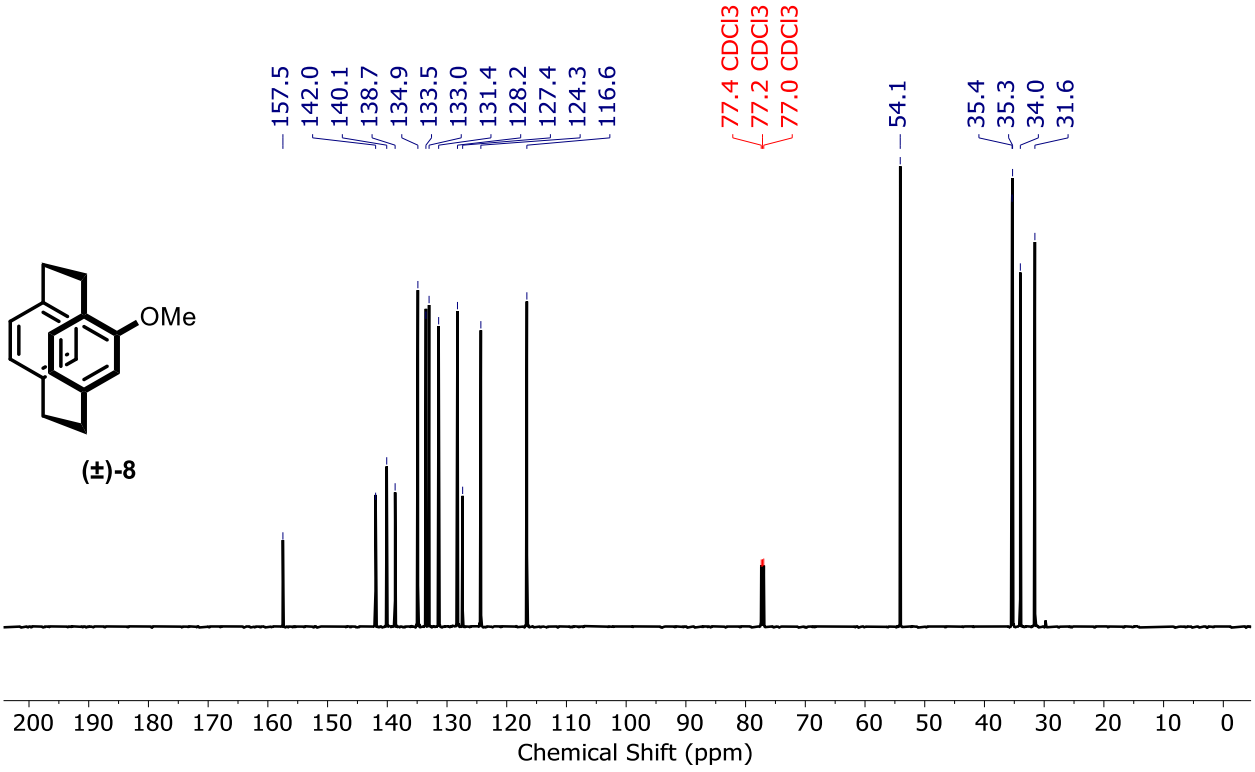

Figure S22. ^{13}C {^{1}H} NMR (150 MHz) of **(±)-8** in chloroform-*d*.

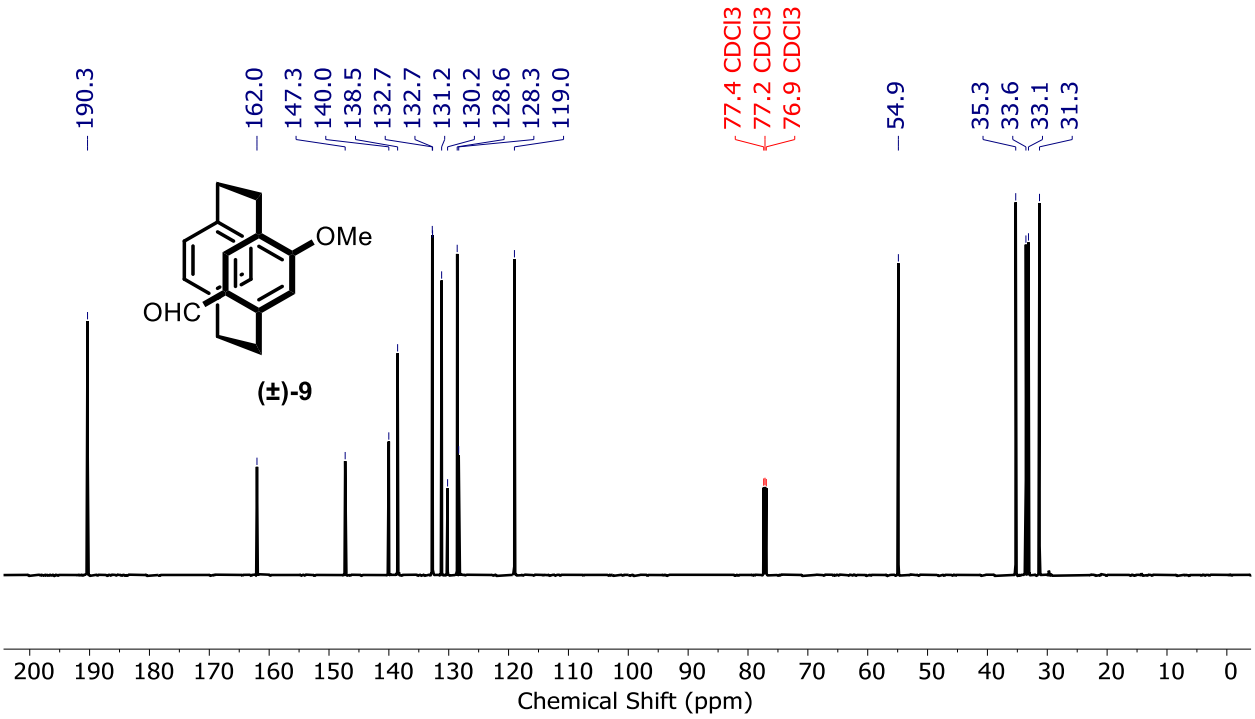

Figure S23. ^{13}C {^{1}H} NMR (150 MHz) of **(±)-9** in chloroform-*d*.

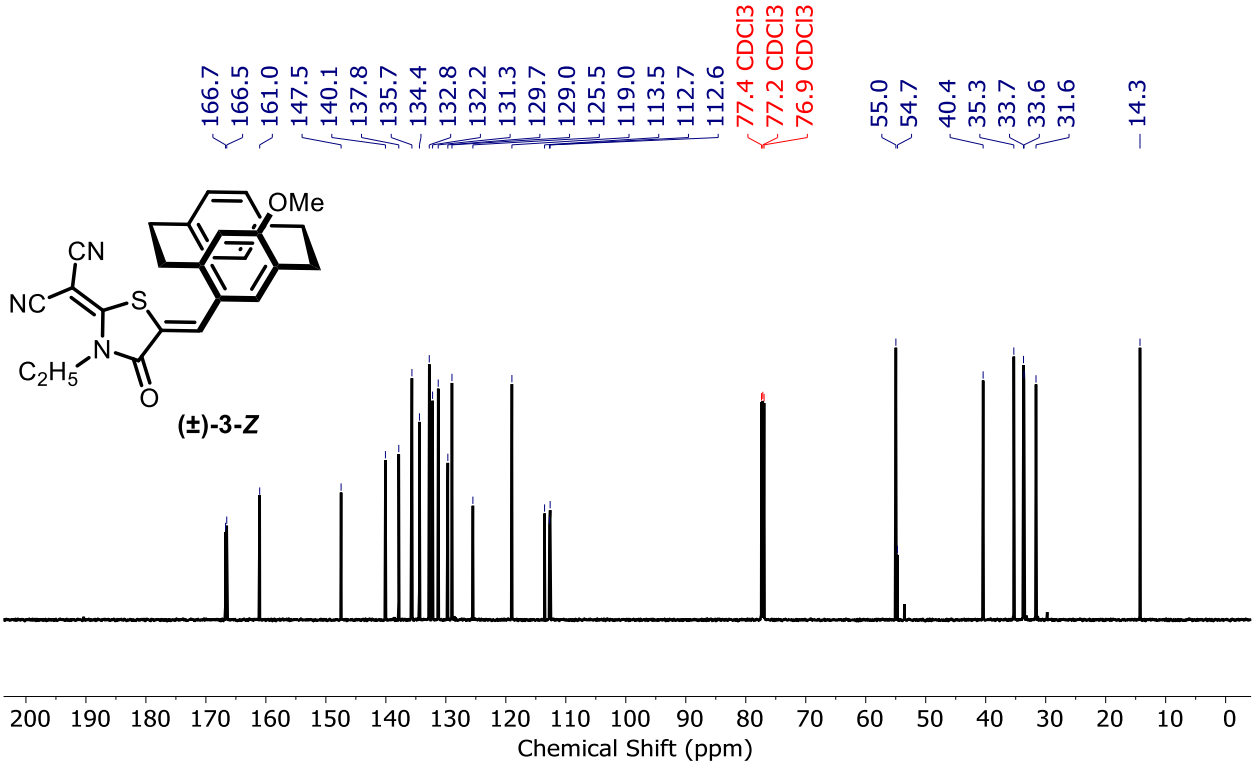

Figure S24. ^{13}C {^{1}H} NMR (150 MHz) of **(±)-3-*Z*** in chloroform-*d*.

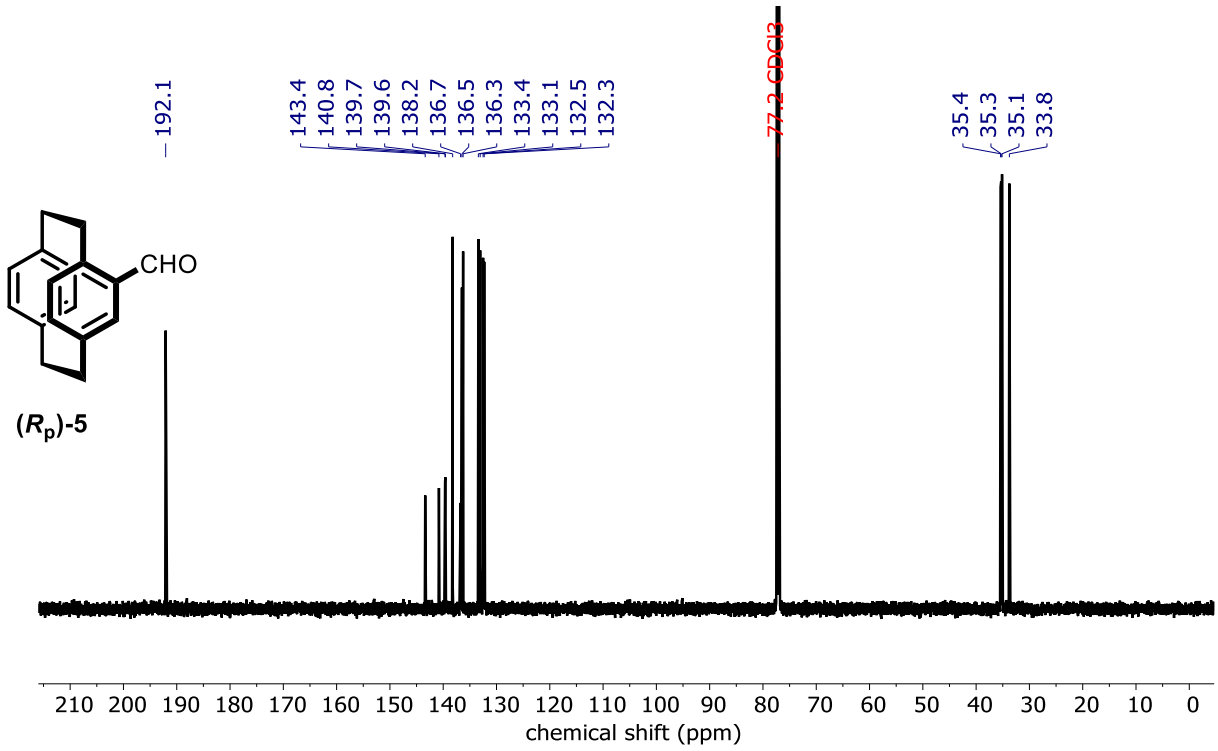

Figure S25. ^{13}C {^{1}H} NMR (150 MHz) of **(R_p)-5** in chloroform-*d*.

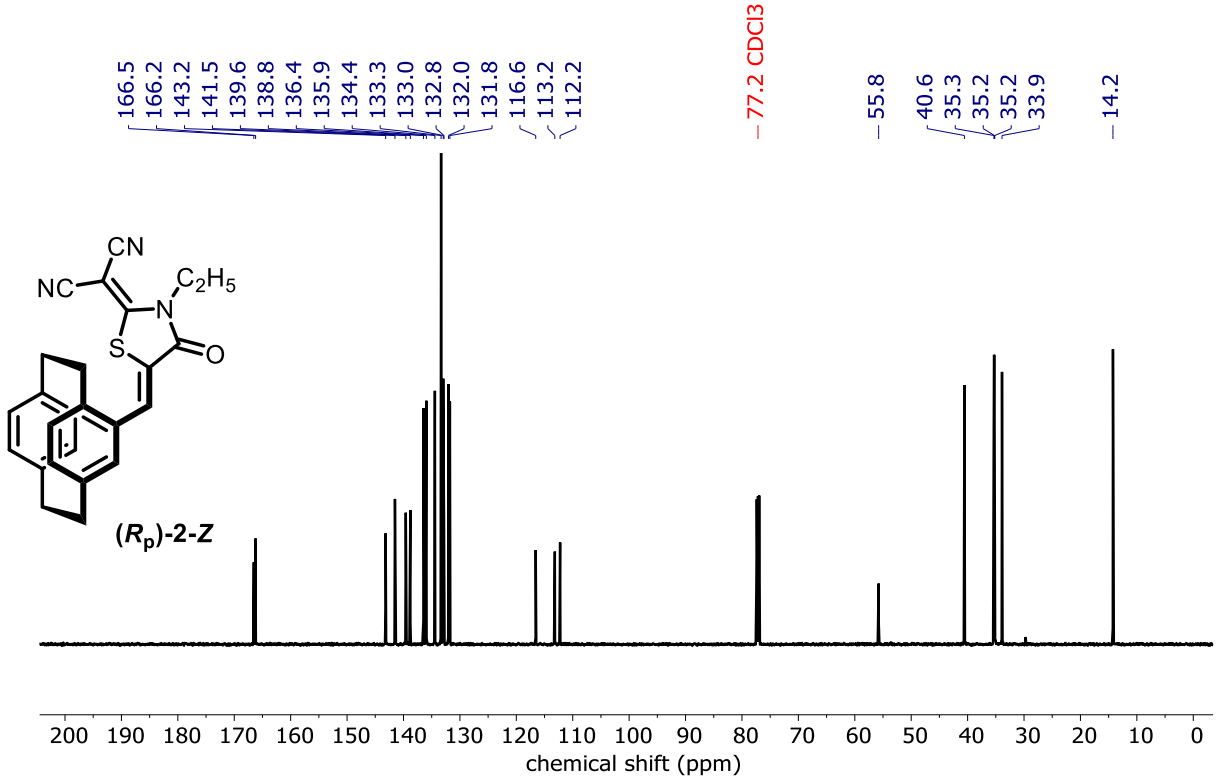

Figure S26. ^{13}C {^{1}H} NMR (150 MHz) of **(R_p)-5-*Z*** in chloroform-*d*.

2D-NMR SPECTRA

Two-dimensional (2D) NMR spectroscopic characterization was performed on a Bruker 600 MHz spectrometer (^{1}H at 600 MHz; ^{13}C at 150 MHz) using acetone-d_6 as the solvent.

(a)

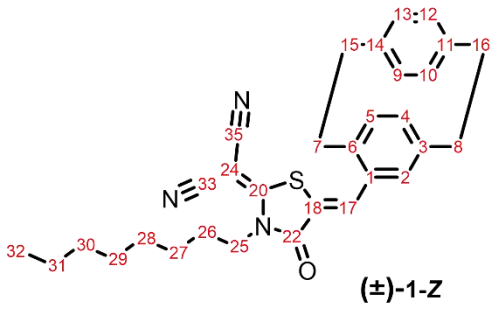

(±)-1-*Z*

(b)

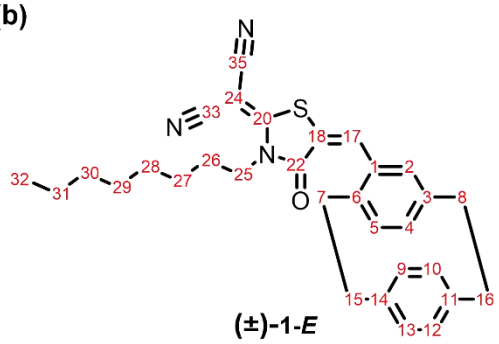

(±)-1-*E*

(c) **Compound (±)-1-*Z***

Assignments		Assignments	
Atom	δ (ppm)	Atom	δ (ppm)
1 C	141.55	17 C	133.53
2 C	133.20	H	8.04
H	6.76	18 C	117.51
3 C	133.17	19 S	
4 C	136.14	20 C	167.11
H	6.77	21 N	
5 C	135.99	22 C	166.25
H	6.72	23 O	
6 C	142.85	24 C	
7 C	33.53	25 C	44.99
H'	3.62	H2	4.24
H''	3.09	26 C	28.38
8 C	34.68	H2	1.79
H'	3.21	27 C	25.86
H''	3.12	H2	1.46
9 C	131.60	28 C	28.95
H	6.48	H2	1.37
10 C	132.03	29 C	28.93
H	6.51	H2	1.40
11 C	139.58	30 C	31.57
12 C	133.37	H2	1.32
H	6.63	31 C	22.47
13 C	133.02	H2	1.34
H	6.65	32 C	13.50
14 C	138.93	H3	0.90
15 C	34.89	33 C	112.56, 113.45
H'	3.27	34 N	
H''	3.03	35 C	112.56, 113.45
16 C	34.93	36 N	
H'	3.21		
H''	3.12		

(d) **Compound (±)-1-*E***

Assignments		Assignments	
Atom	δ (ppm)	Atom	δ (ppm)
1 C	132.59	17 C	140.03
2 C	136.30	H	7.90
H	7.24	18 C	118.45
3 C	139.38	19 S	
4 C	135.96	20 C	167.73
H	6.69	21 N	
5 C	134.89	22 C	162.92
H	6.61	23 O	
6 C	141.75	24 C	
7 C	33.30	25 C	44.75
H'	3.58	H2	4.11
H''	2.96	26 C	28.20
8 C	34.61	H2	1.74
H'	3.16	27 C	25.82
H''	3.01	H2	1.40
9 C	131.27	28 C	28.97
H	6.66	H2	1.36
10 C	132.20	29 C	28.88
H	6.46	H2	1.35
11 C	139.55	30 C	31.59
12 C	133.00	H2	1.29
H	6.63	31 C	22.42
13 C	133.00	H2	1.31
H	6.63	32 C	13.43
14 C	139.18	H3	0.89
15 C	34.31	33 C	112.88, 113.79
H2	3.17	34 N	
16 C	34.93	35 C	112.88, 113.79
H'	3.15	36 N	
H''	3.08		

Figure S27. Atomic numbering schemes used for the 2D NMR chemical shift assignments showing (a) **(±)-1-*Z*** and (b) **(±)-1-*E***. Selected chemical shift values are listed showing ^{1}H signals and ^{13}C signals for compounds (c) **(±)-1-*Z*** and (d) **(±)-1-*E***.

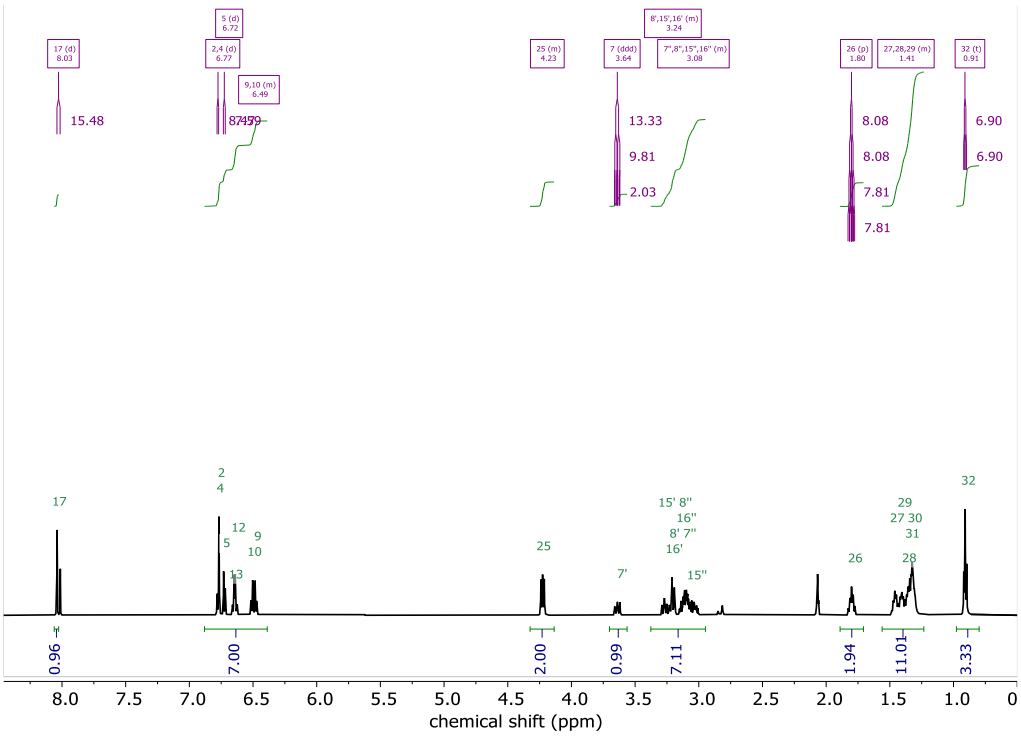

Figure S28. ^{1}H NMR spectrum of **(±)-1-*Z*** in acetone-d_6.

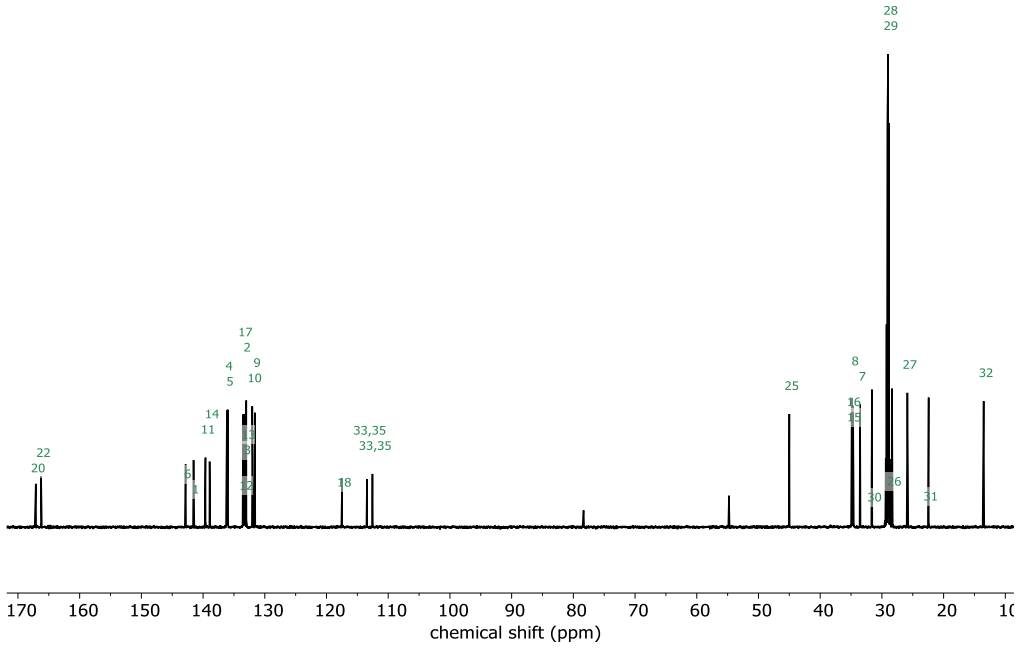

Figure S29. ^{13}C NMR spectrum of **(±)-1-*Z*** in acetone-d_6.

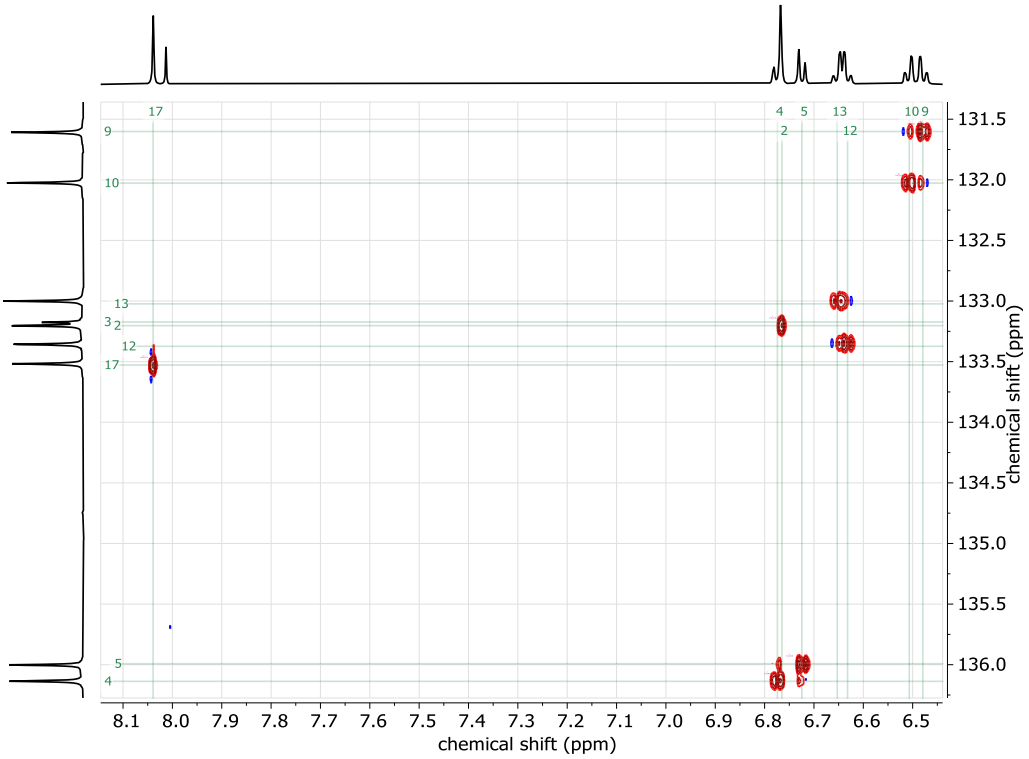

Figure S30. HSQC spectrum of **(±)-1-*Z*** in acetone-d_6 (aromatic region).

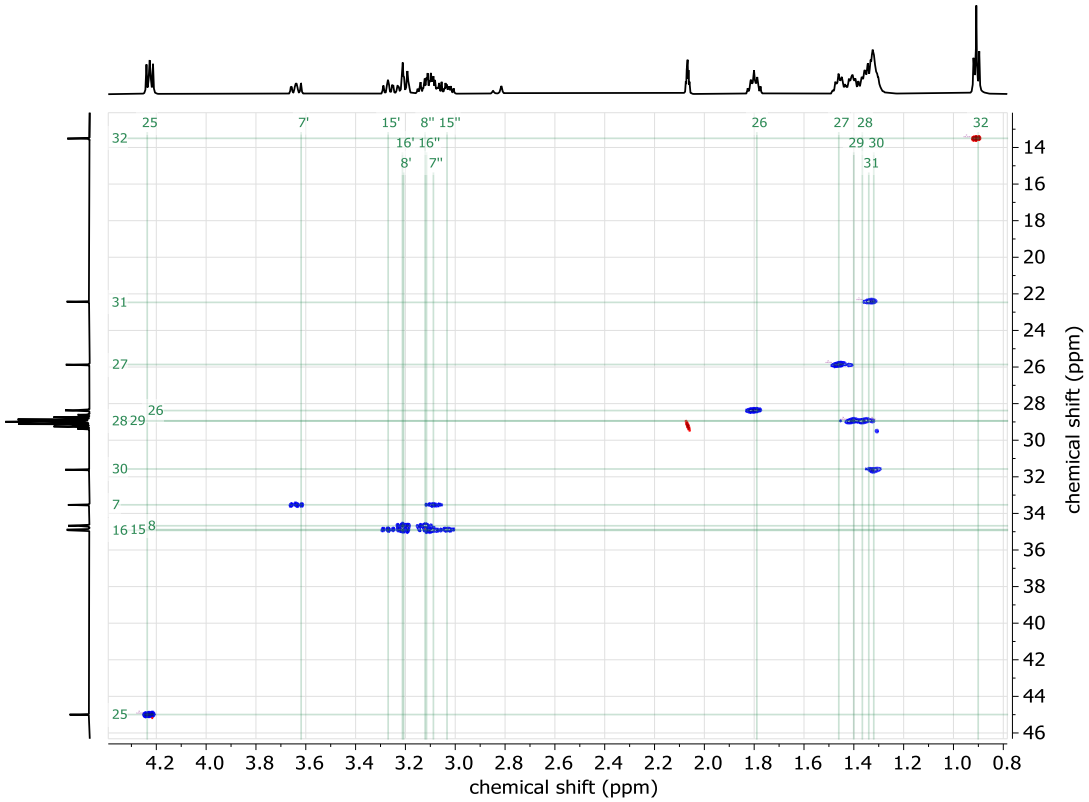

Figure S31. HSQC spectrum of **(±)-1-*Z*** in acetone-d_6 (aliphatic region).

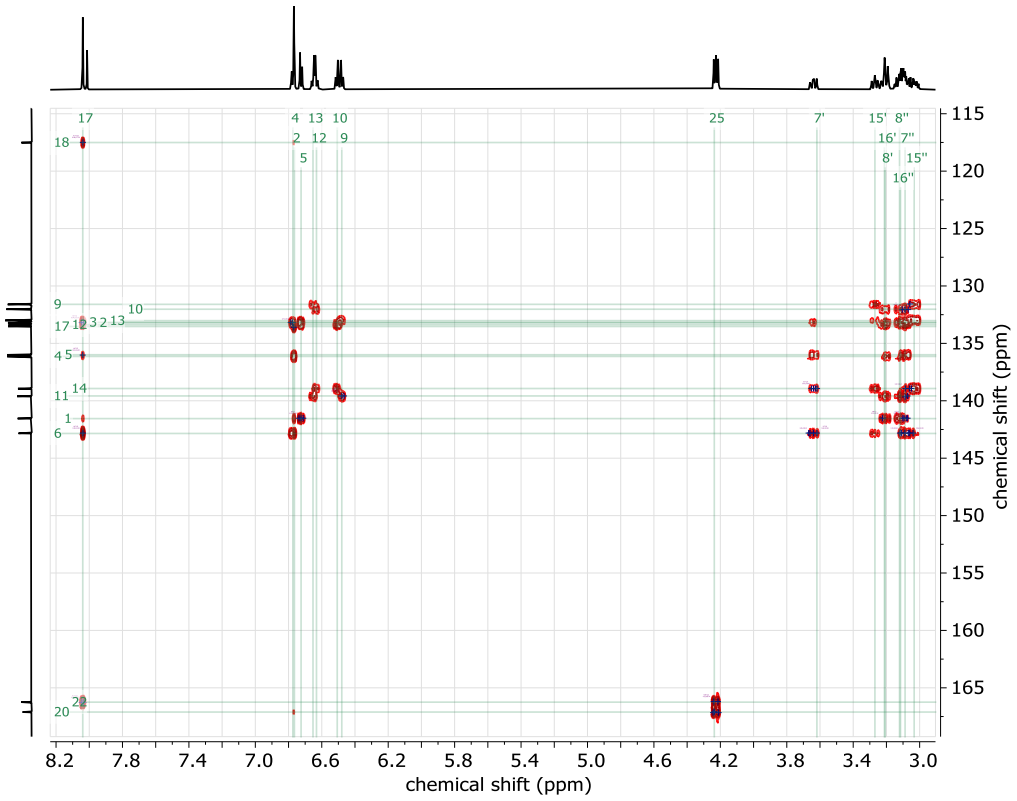

Figure S32. HMBC spectrum of **(±)-1-*Z*** in acetone-d_6 (expanded region).

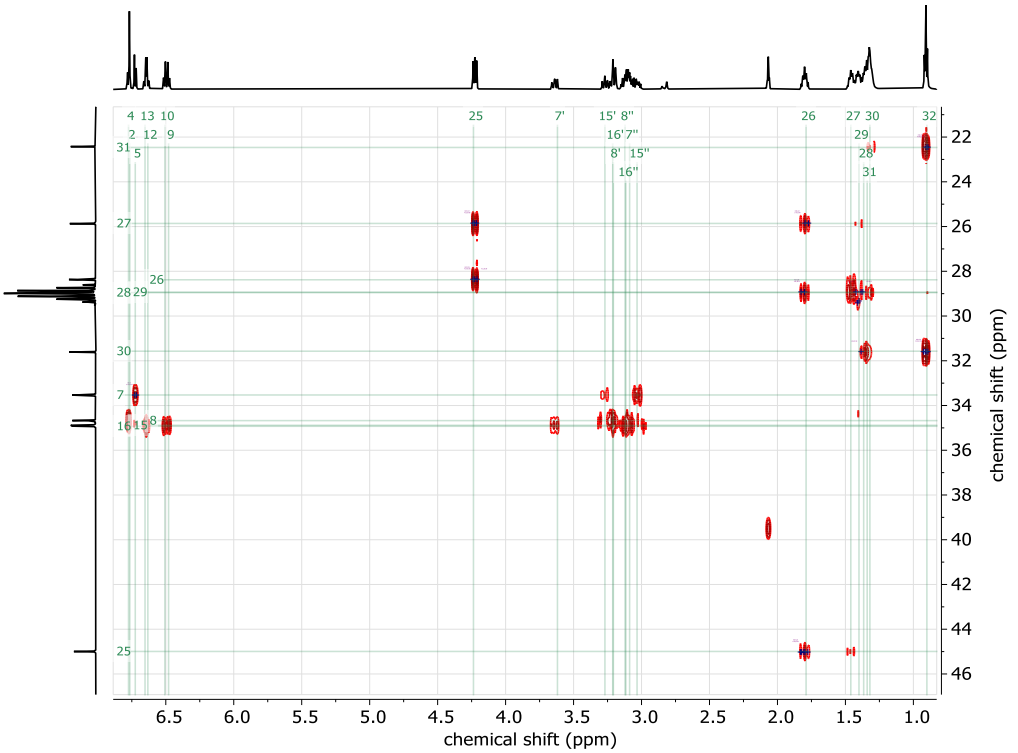

Figure S33. HMBC spectrum of **(±)-1-*Z*** in acetone-d_6 (expanded region).

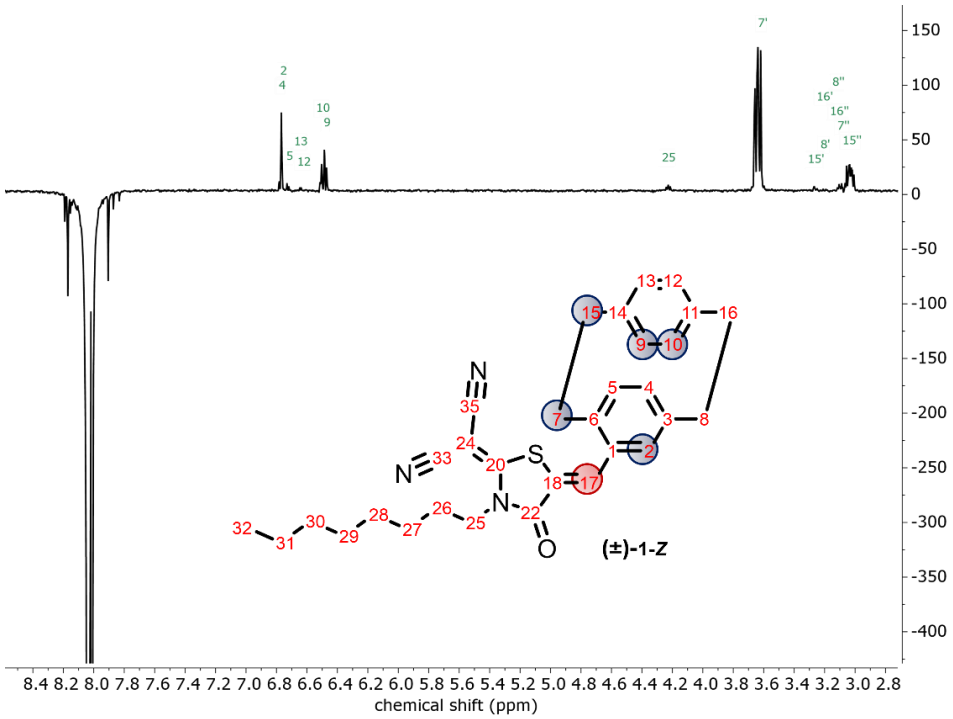

Figure S34. 1D NOESY spectrum with selective inversion of H17 of **(±)-1-*Z*** in acetone-d_6 (expanded region).

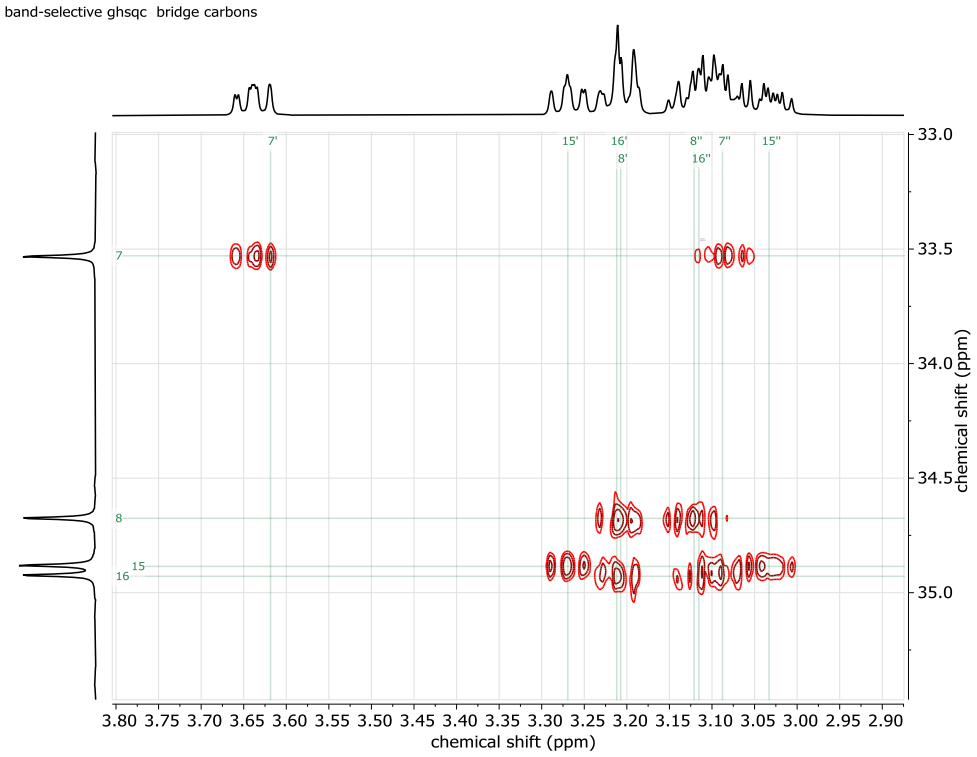

Figure S35. Band-selective HSQC spectrum of **(±)-1-*Z*** in acetone-d_6 (for bridge protons with bridge carbons).

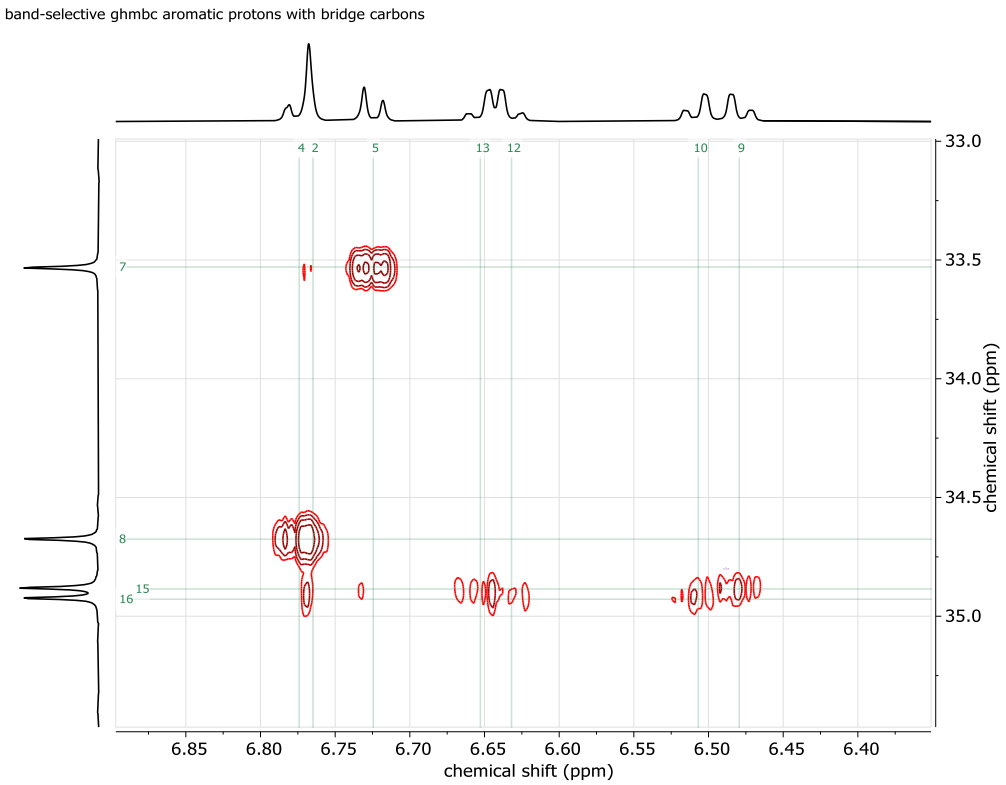

Figure S36. Band-selective HMBC spectrum of **(±)-1-*Z*** in acetone-d_6 (for aromatic protons with bridge carbons).

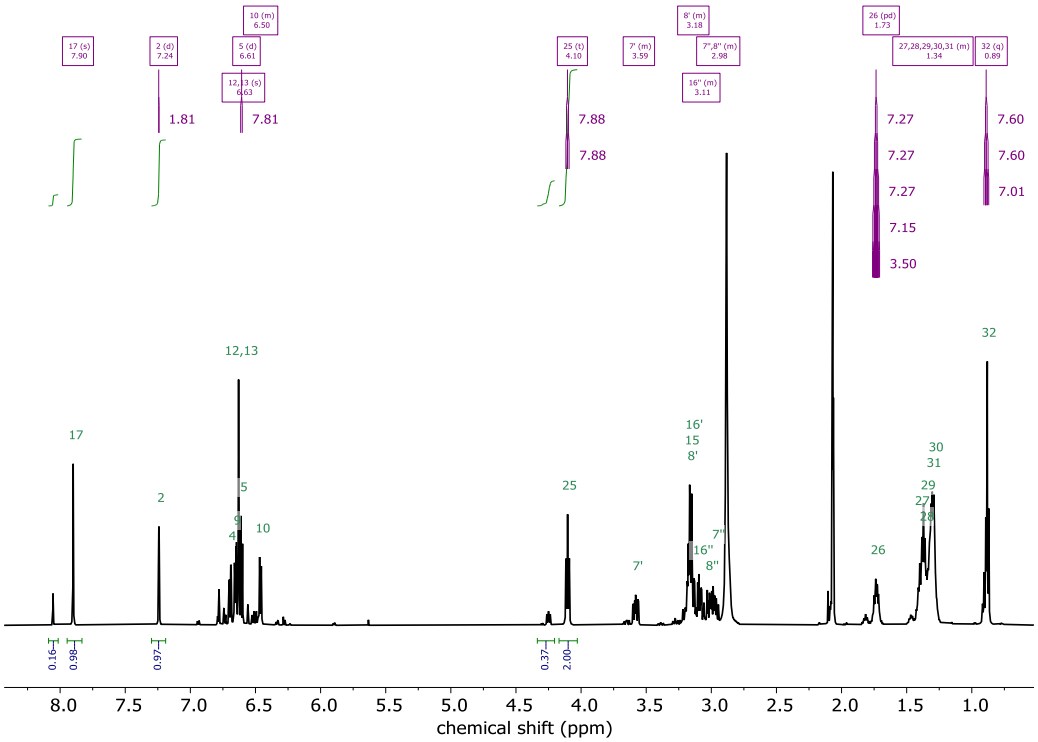

Figure S37. ^{1}H NMR spectrum of **(±)-1-*E*** in acetone-d_6.

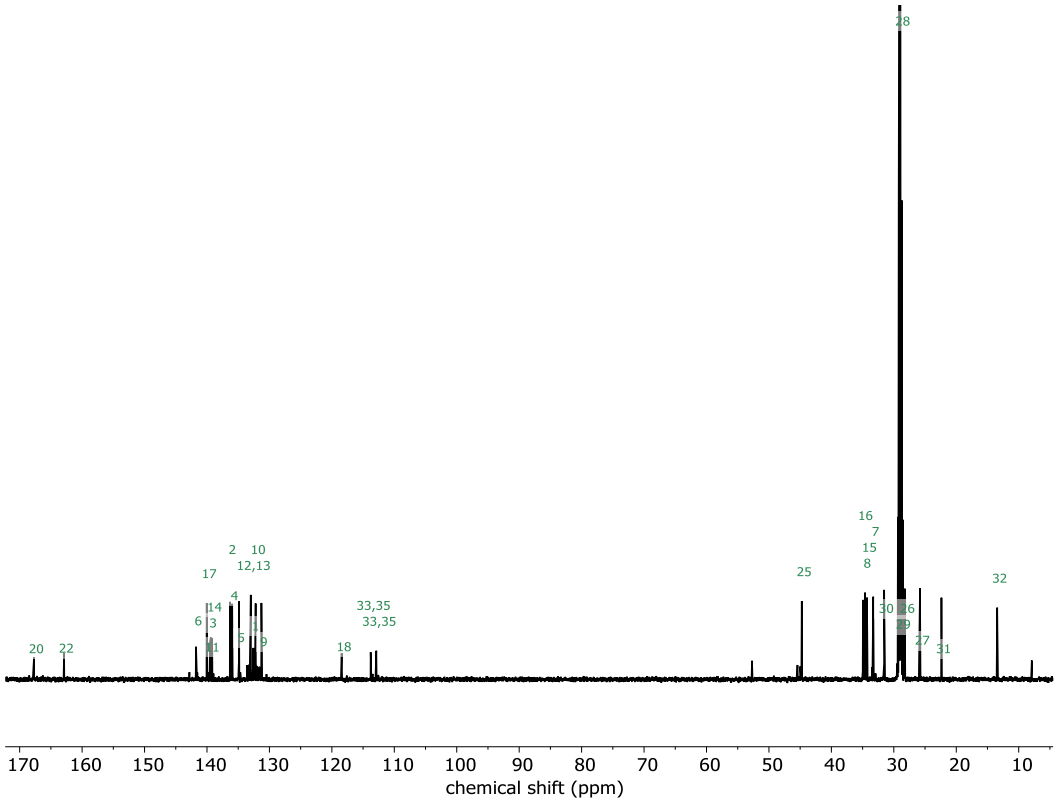

Figure S38. ^{13}C NMR spectrum of **(±)-1-*E*** in acetone-d_6.

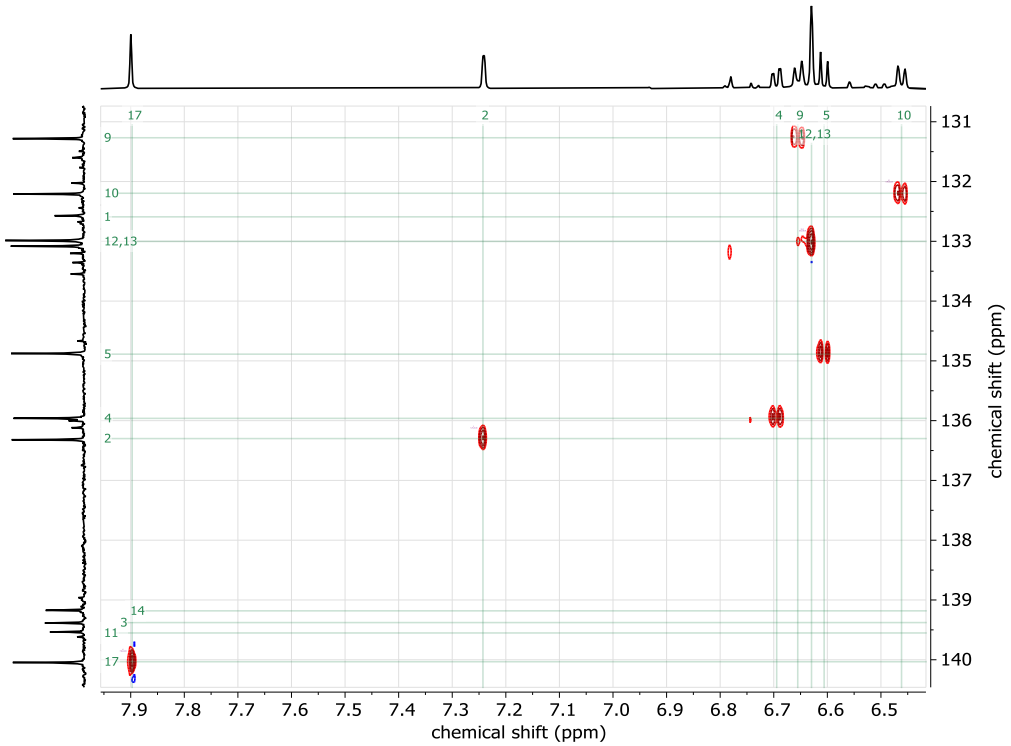

Figure S39. HSQC spectrum of **(±)-1-*E*** in acetone-d_6 (aromatic region).

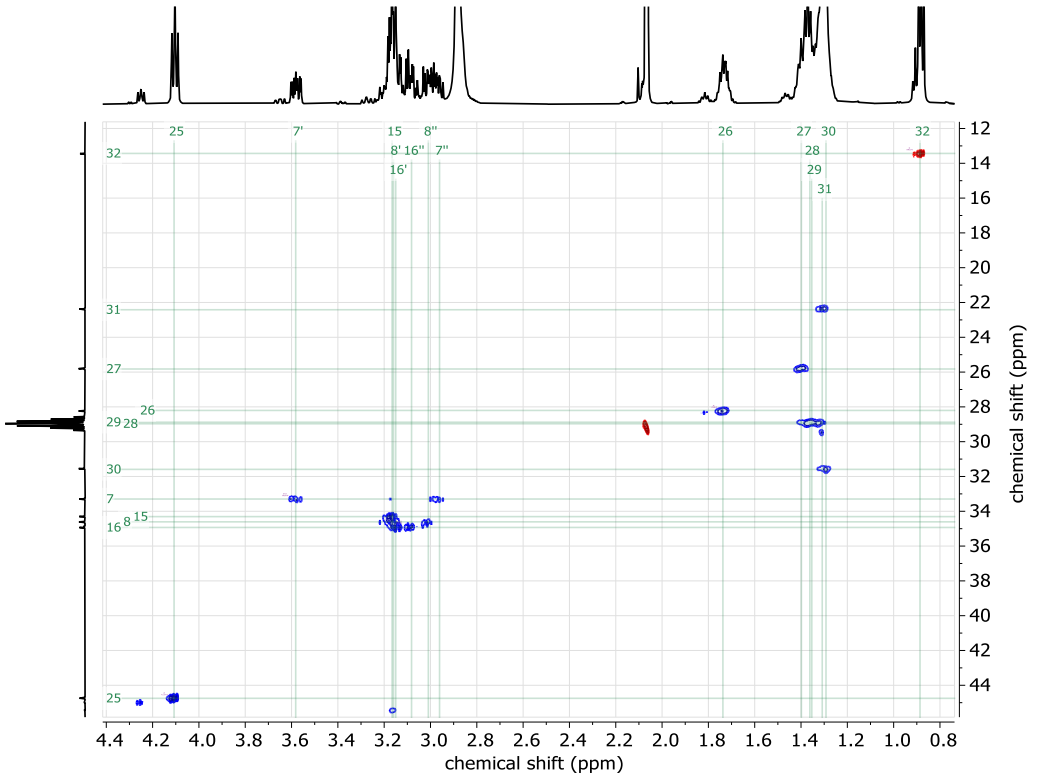

Figure S40. HSQC spectrum of **(±)-1-*E*** in acetone-d_6 (aliphatic region).

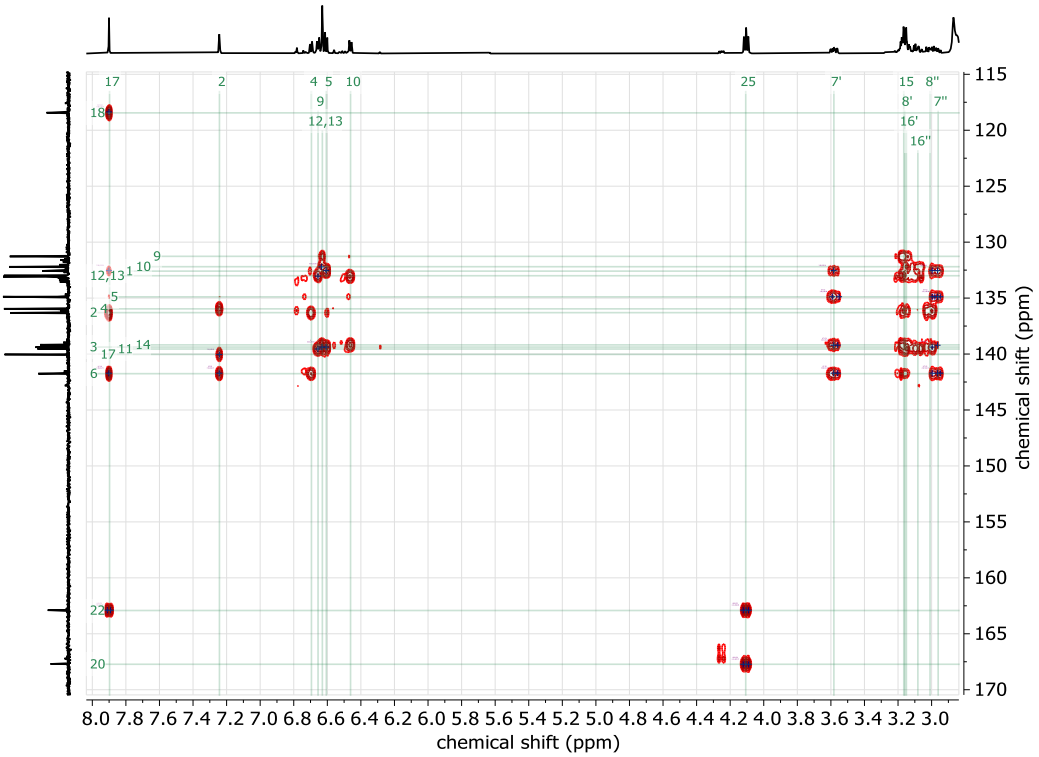

Figure S41. HMBC spectrum of **(±)-1-*E*** in acetone-d_6 (expanded region).

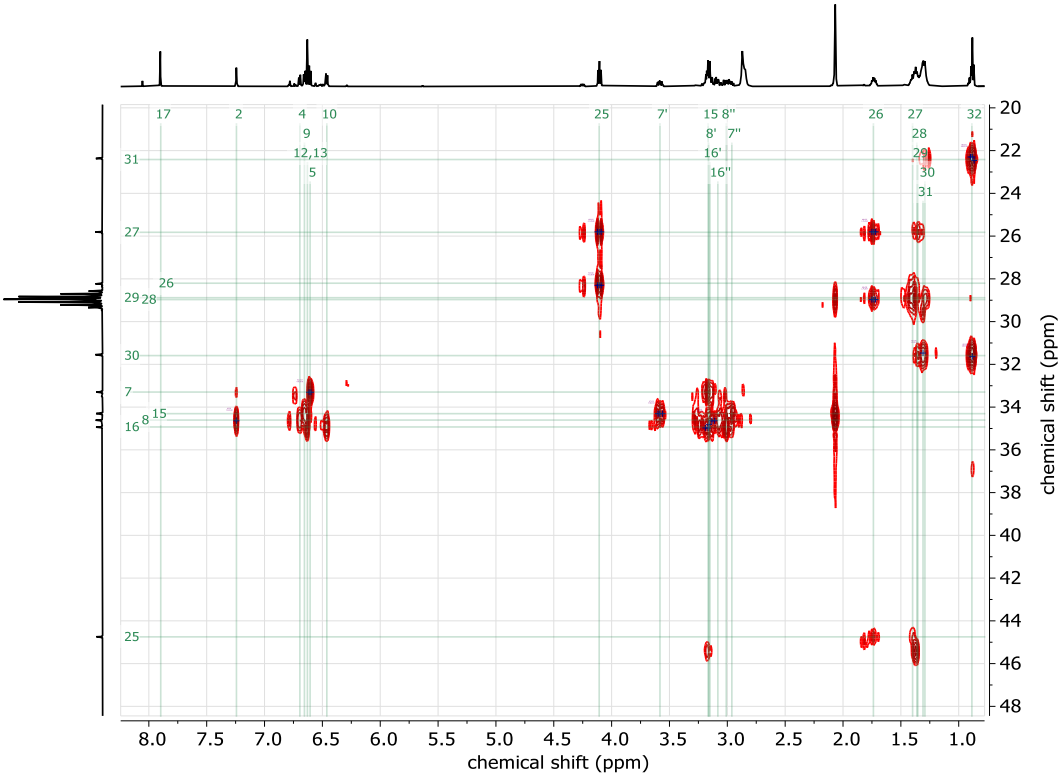

Figure S42. HMBC spectrum of **(±)-1-*E*** in acetone-d_6 (expanded region).

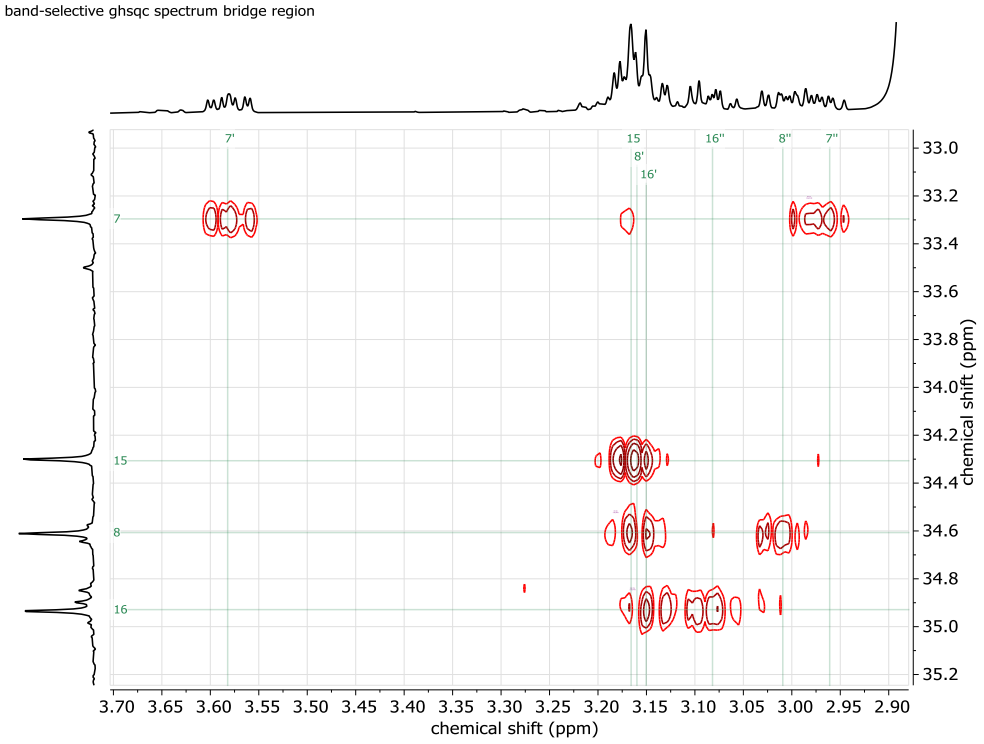

Figure S43. Band-selective HSQC spectrum of **(±)-1-*E*** in acetone-d_6 (for bridge protons with bridge carbons).

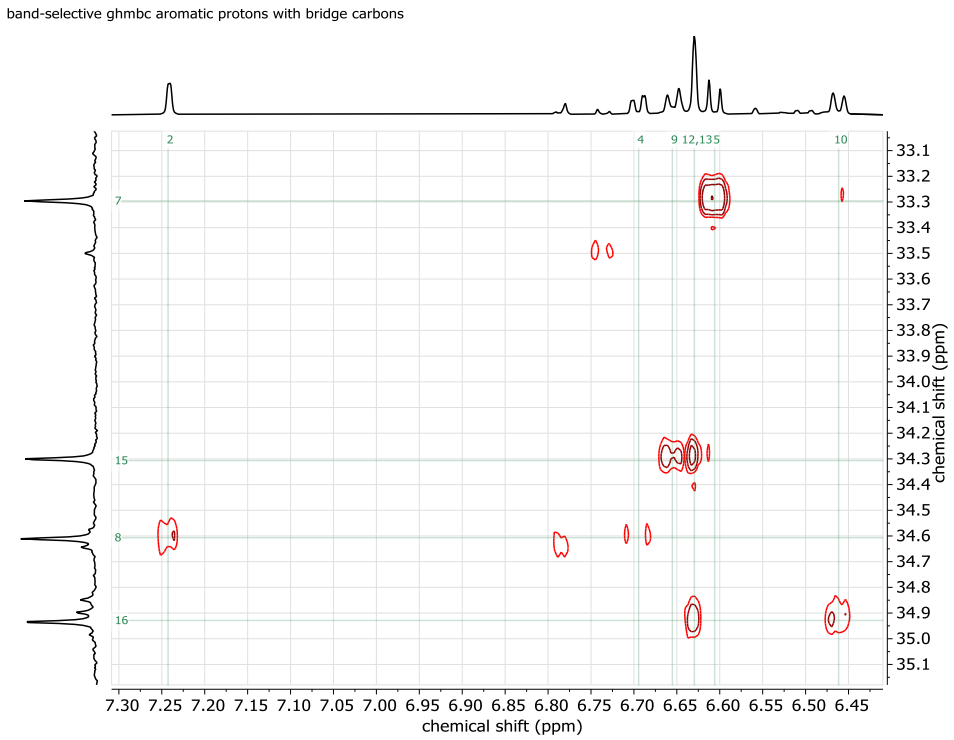

Figure S44. Band-selective HMBC spectrum of **(±)-1-*E*** in acetone-d_6 (for aromatic protons with bridge carbons).

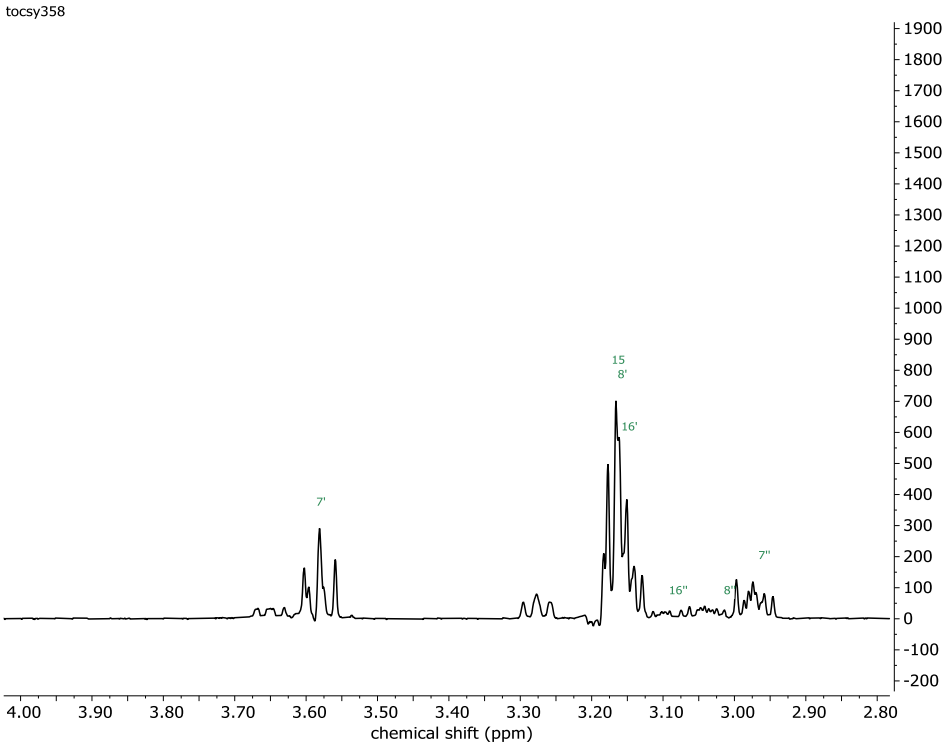

Figure S45. 1D TOCSY spectrum with selective excitation of H7 of **(±)-1-*E*** in acetone-d_6 (expanded region).

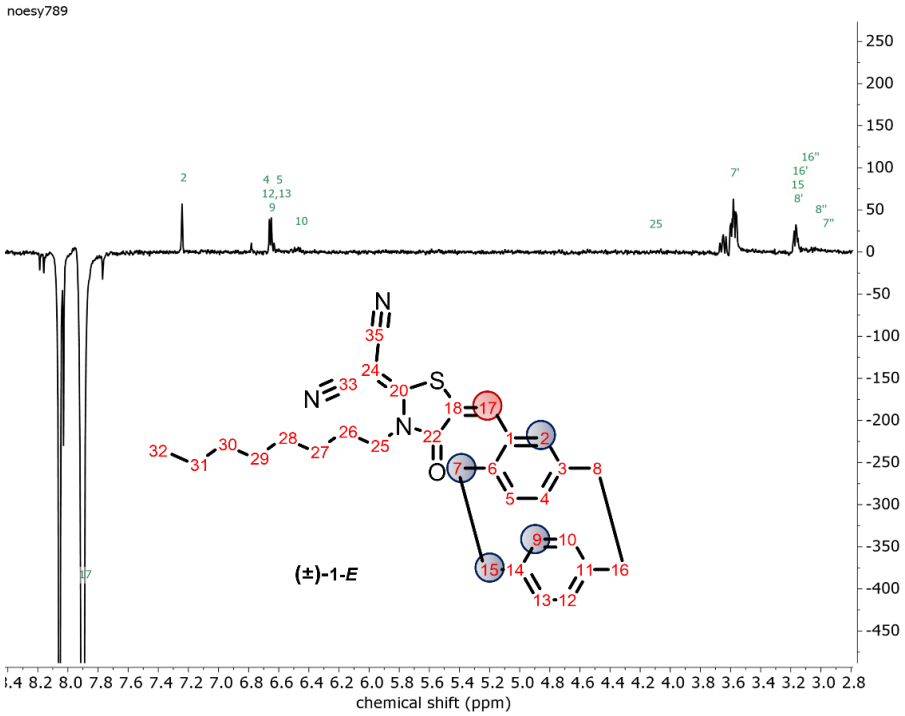

Figure S46. 1D NOESY spectrum with selective inversion of H17 of **(±)-1-*E*** in acetone-d_6 (expanded region).

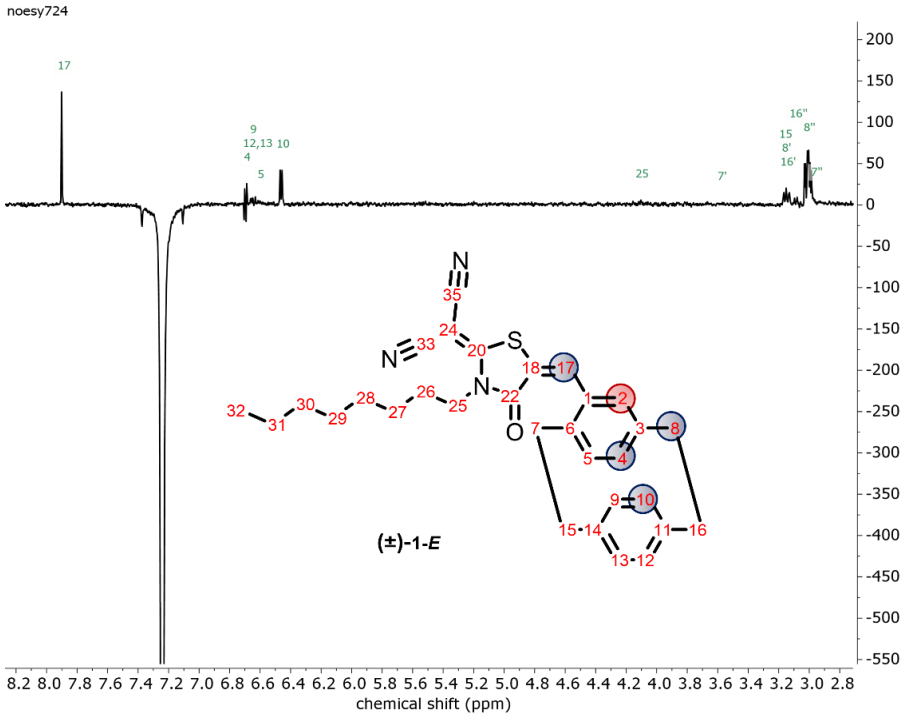

Figure S47. 1D NOESY spectrum with selective inversion of H2 of **(±)-1-*E*** in acetone-d_6 (expanded region).

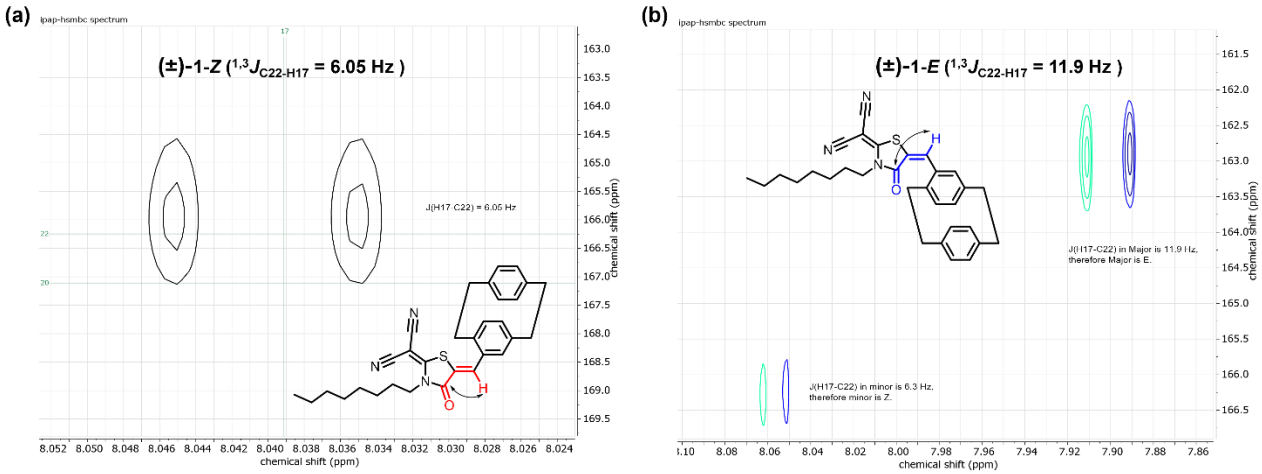

Figure S48. IPAP-gHSMBC spectrum (expanded aromatic region) of (a) **(±)-1-*Z*** and (b) **(±)-1-*E*** in acetone-d_6.

HPLC CHROMATOGRAMS

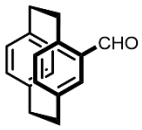

(±)-5

HPLC conditions: Column = Chiralcel OD-H (250 X 4.6 mm); **eluent** = *n*-hexane/*i*-PrOH (98/2); **T** = 298 K; **flow** = 1 ml/min.

Retention time (@λ_{254}): tR $_{Rp}$ = 18.630 min; tR $_{Sp}$ = 26.851 min.

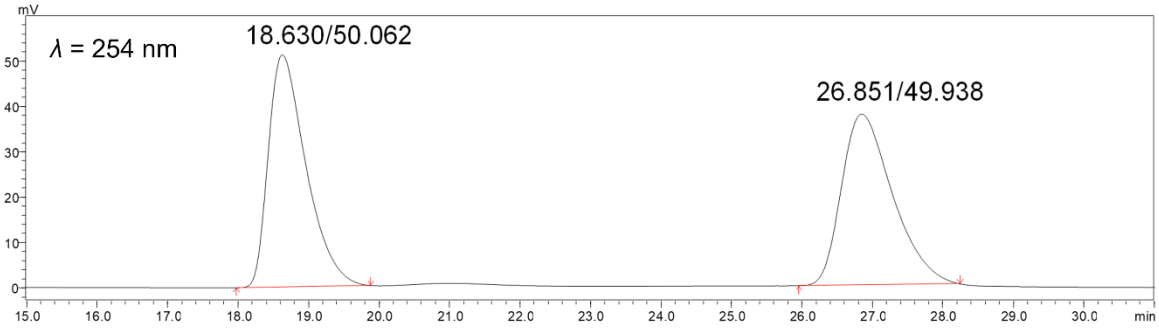

Figure S49. HPLC chromatogram of compound **(±)-5** monitored at λ= 254 nm.

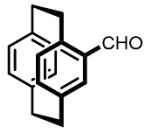

(R_p)-5

HPLC conditions: Column = Chiralcel OD-H (250 X 4.6 mm); **eluent** = *n*-hexane/*i*-PrOH (98/2); **T** = 298 K; **flow** = 1 ml/min.

Retention time (@λ_{254}): tR $_{Rp}$ = 18.890 min; tR $_{Sp}$ = 26.893 min; ~82% ee.

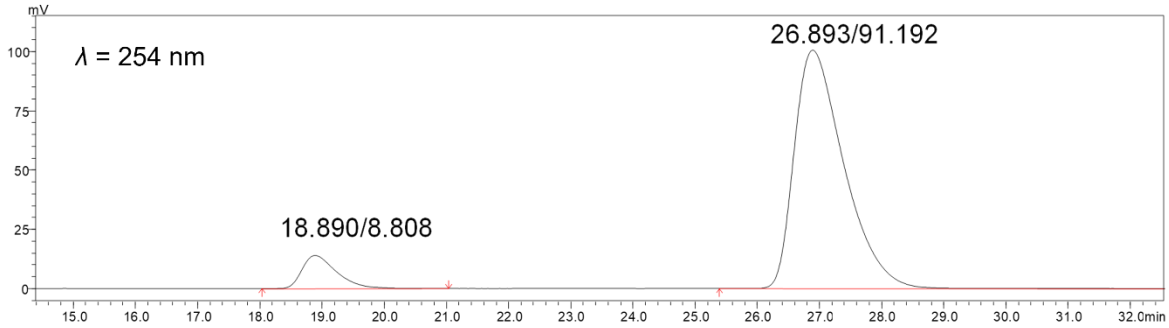

Figure S50. HPLC chromatogram of compound **(R_p)-5** monitored at λ= 254 nm.

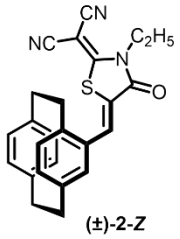

(±)-2-*Z*

HPLC conditions: Column = Chiralcel AD-H (250 X 4.6 mm); **eluent** = *n*-hexane/*i*-PrOH (98/2); **T** = 298 K; **flow** = 1 ml/min.

Retention time (@λ_{254}): tR $_{Rp}$ = 28.633 min; tR $_{Sp}$ = 31.640 min.

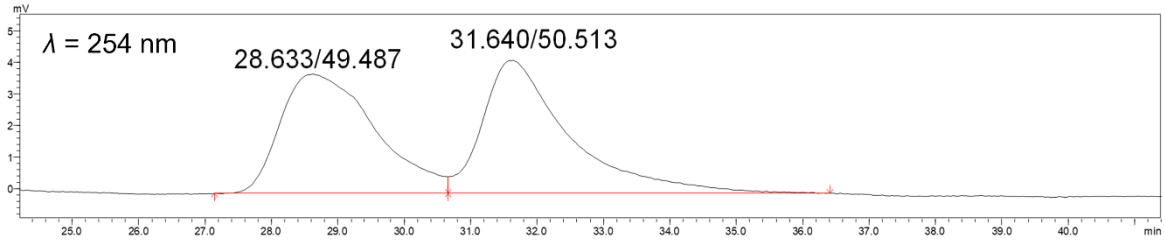

Figure S51. HPLC chromatogram of compound **(±)-2-*Z*** monitored at λ= 254 nm.

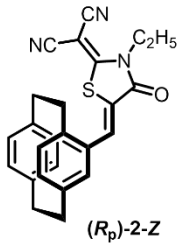

(R_p)-2-*Z*

HPLC conditions: Column = Chiralcel AD-H (250 X 4.6 mm); **eluent** = *n*-hexane/*i*-PrOH (98/2); **T** = 298 K; **flow** = 1 ml/min.

Retention time (@λ_{254}): tR $_{Rp}$ = 28.676 min; tR $_{Sp}$ = 32.052 min; ~90% ee.

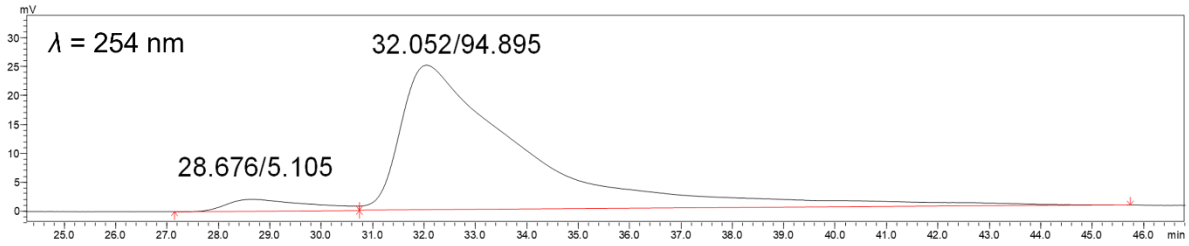

Figure S52. HPLC chromatogram of compound **(R_p)-2-*Z*** monitored at λ= 254 nm.

IRRADIATION SOURCES

General Information

Ultraviolet irradiation (λ_{irr} = 371 nm) was achieved using a MelodySusie (Model No. DR-301C, 110-120 Volt, 36 Watt) UV Gel Nail Polish Dryer emitting a peak ultraviolet irradiation wavelength of 371 nm in addition to residual visible emission (Figure S53).

Violet irradiation was achieved using a violet 10W LED array mounted to a heat sink that was built in-house. The peak irradiation wavelength was measured to be 404 nm.

Blue LED irradiation was achieved using a Westinghouse Lighting (Model No. 3315100) 100-Watt Equivalent PAR38 Flood Blue Outdoor Weatherproof LED Light Bulb (15-Watt, 120 Volt) emitting a peak irradiation wavelength of 454 nm.

Green LED irradiation was achieved using a Westinghouse Lighting (Model No. 3314900) 100-Watt Equivalent PAR38 Flood Green Outdoor Weatherproof LED Light Bulb (15-Watt, 120 Volt) emitting a peak irradiation wavelength of 523 nm.

The absolute irradiance of the LEDs was obtained using a fiber optic cable and Ocean Optics Jaz spectrometer for each LED at their corresponding working distance. The resulting spectra were integrated to obtain the reported light intensities.

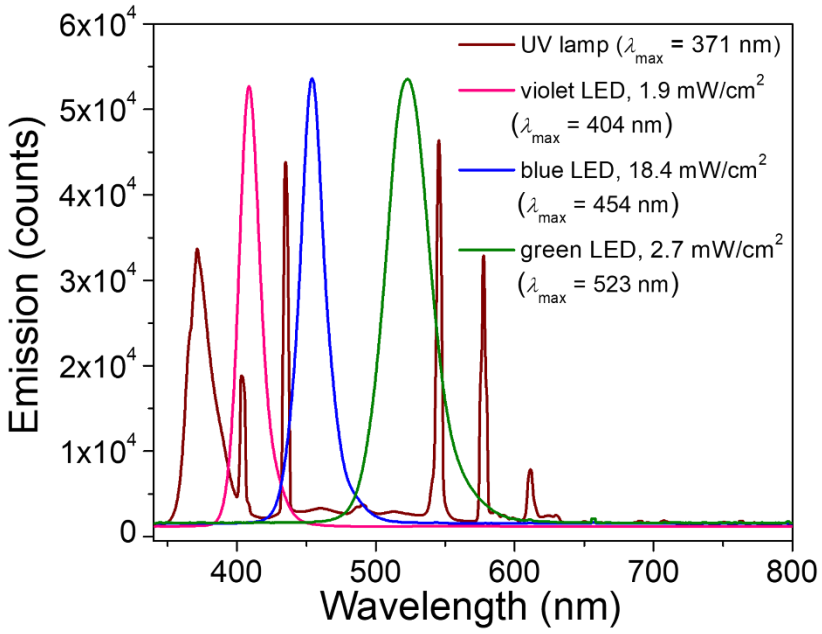

Figure S53. Emission plots of MelodySusie (Model No. DR-301C) UV Gel Nail Polish Dryer (maroon trace), violet LED (pink trace), Westinghouse (Model No. 3315100) blue LED outdoor weatherproof light bulb (blue trace), and Westinghouse (Model No. 3314900) green LED outdoor weatherproof light bulb (green trace).

THIN LAYER CHROMATOGRAPHY

General Information

Thin layer chromatography (TLC) experiments were performed on SiO_2-60 F254 aluminum plates with visualization by visible light. Pure samples (*Z* isomer) were spotted as solutions in dichloromethane. Samples of *Z*/*E* mixture were obtained by irradiating pure *Z* isomer in dichloromethane using a 404 nm LED prior to sample spotting and TLC plate development. The spots were eluted using a 2:1 dichloromethane:hexanes eluent mixture.

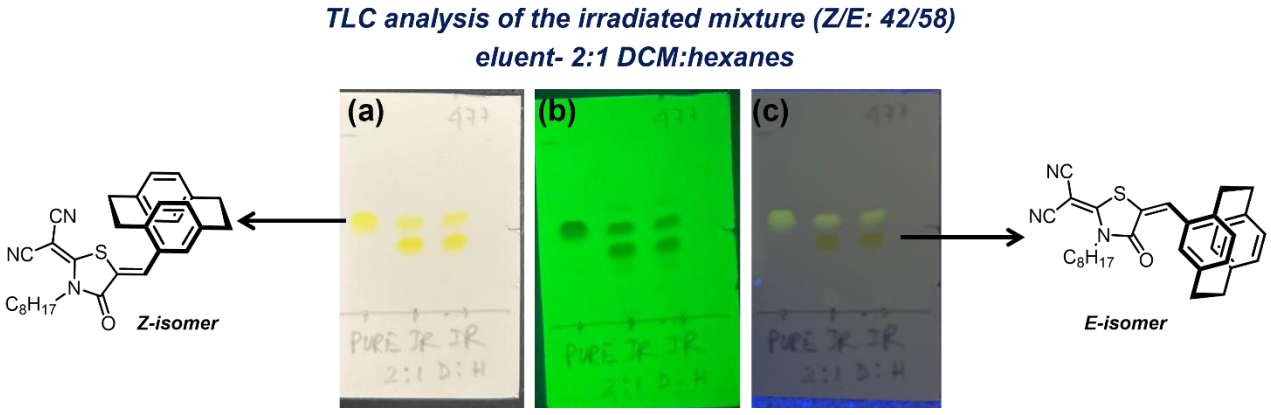

Figure S54. Thin layer chromatography (TLC) data showing pure **(±)-1-*Z*** (left TLC lane) compared with a **(±)-1-*Z*/(±)-1-*E*** mixture (middle and right TLC lanes) obtained post-irradiation (λ_{irr} = 404 nm), under (a) ambient light, (b) short-wave UV light, and (c) long-wave UV light.

SOLUTION NMR PHOTOISOMERIZATION STUDIES

General Procedure (Wavelength-Dependent Studies)

^{1}H NMR were recorded on an INOVA-500 (^{1}H at 500 MHz) and a Bruker 600 MHz spectrometer (^{1}H at 600 MHz). To determine the photostationary state isomeric composition of each RCN-functionalized target molecule (**(±)-1-*Z***, **(±)-2-*Z***, **(±)-3-*Z***, and **(R_p)-2-*Z***), a 15 mM stock solution in chloroform-*d* was prepared. Approximately 0.5 mL of each stock solution was transferred to a conventional glass NMR tube. The samples were exposed to an appropriate irradiation wavelength (λ_{irr} = 371, 404, 454, and 523 nm) and ^{1}H NMR spectra were recorded to monitor the reaction progress. The integration ratios of signals corresponding to *Z* isomers and *E* isomers were compared to calculate a relative percentage of each species in solution. The samples were irradiated for 3 h – 5 h and ^{1}H NMR spectra were recorded until no changes in *Z*/*E* integration ratios were observed.

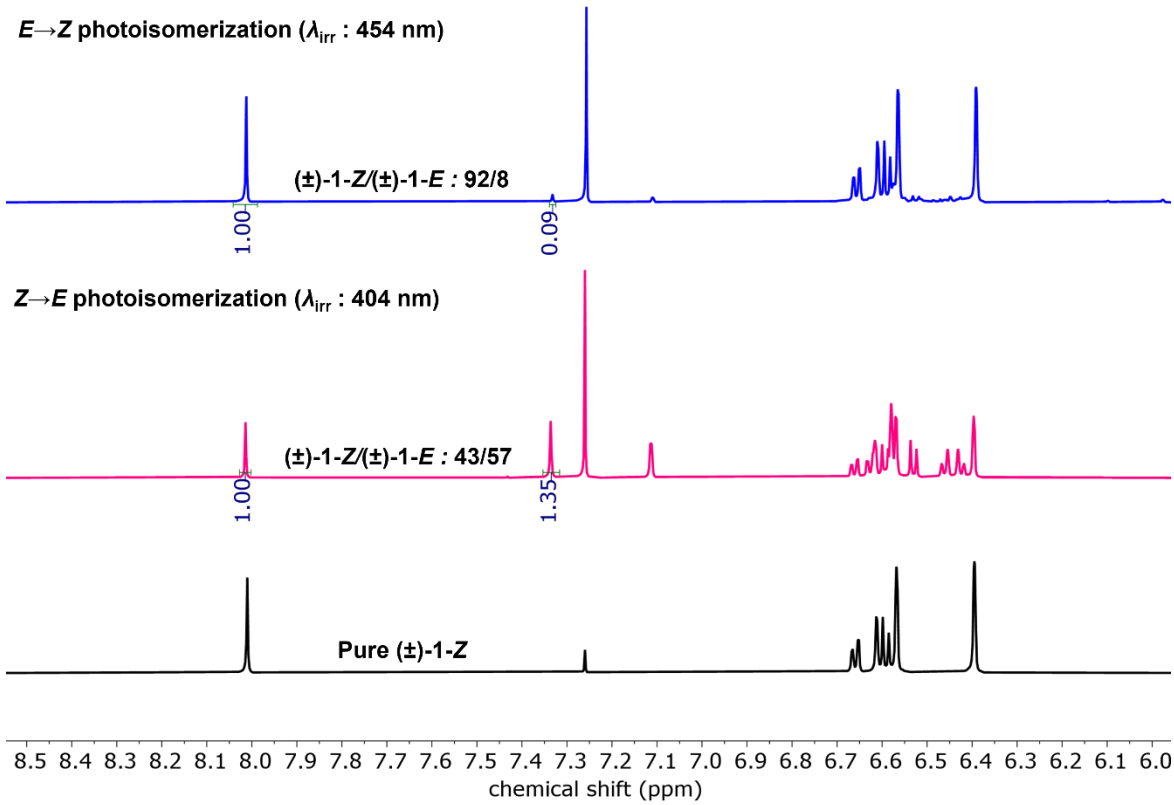

Figure S55. ^{1}H NMR spectra (chloroform-*d*) showing pure **(±)-1-*Z*** (black, bottom spectrum) and **(±)-1-*Z*/(±)-1-*E*** isomeric mixture achieved post-irradiation using 404 nm (pink spectrum, *Z*→*E* isomerization) LED, which was subsequently subjected to 454 nm (blue spectrum, *E*→*Z* isomerization) LED irradiation.

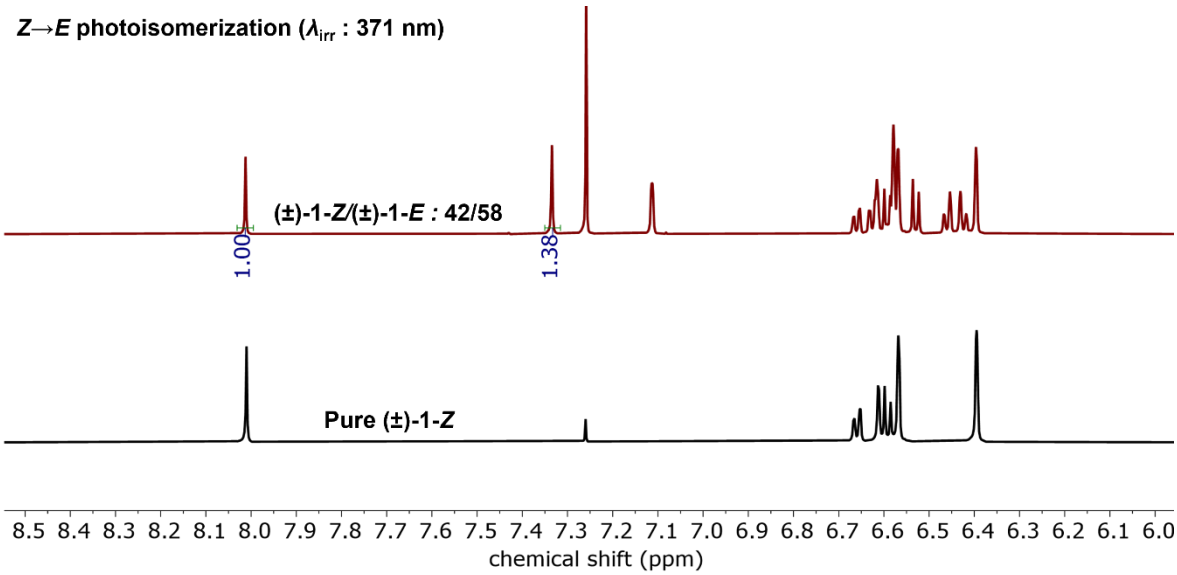

Figure S56. ^{1}H NMR spectra (chloroform-*d*) showing pure **(±)-1-*Z*** (black, bottom spectrum) and **(±)-1-*Z*/(±)-1-*E*** isomeric mixture achieved post-irradiation using 371 nm (maroon spectrum, *Z*→*E* isomerization) UV lamp.

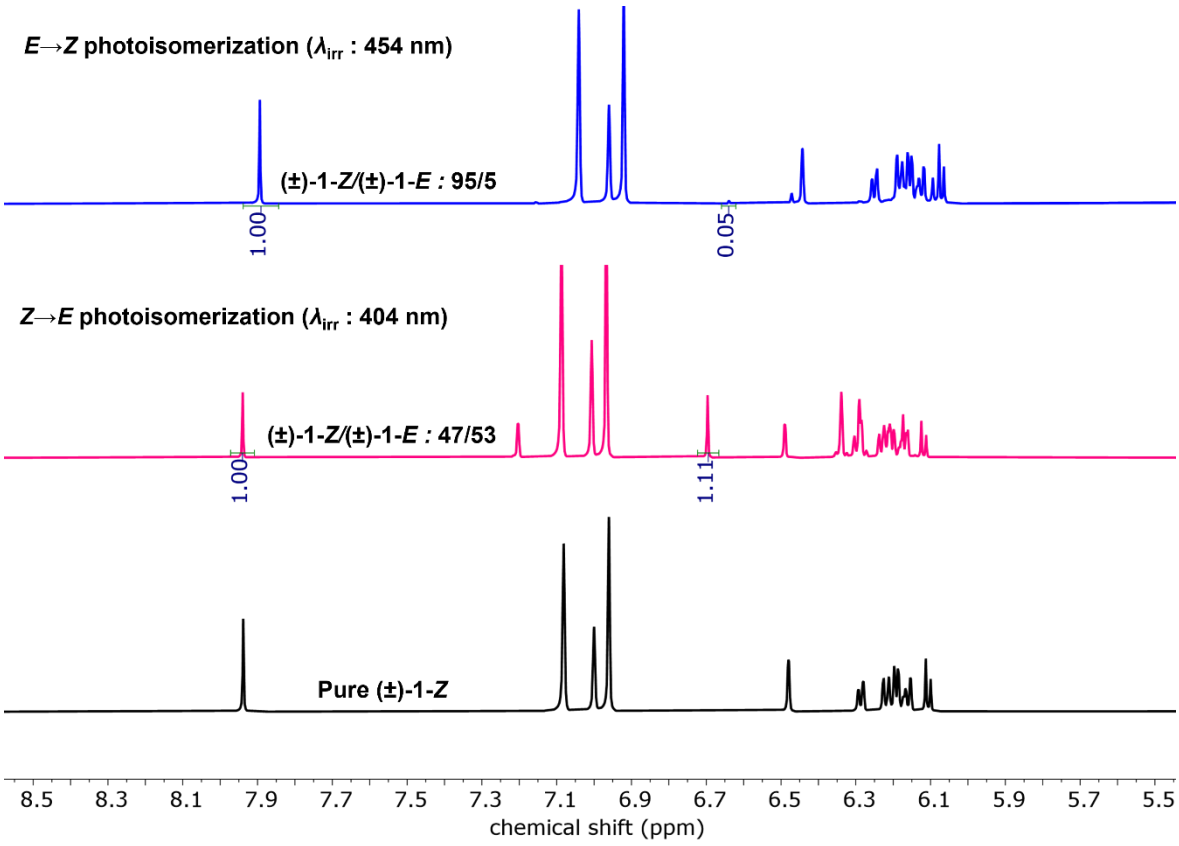

Figure S57. ^{1}H NMR spectra (toluene-d_8) showing pure **(±)-1-*Z*** (black, bottom spectrum) and **(±)-1-*Z*/(±)-1-*E*** isomeric mixture achieved post-irradiation using 404 nm (pink spectrum, *Z*→*E* isomerization) LED, which was subsequently subjected to 454 nm (blue spectrum, *E*→*Z* isomerization) LED irradiation.

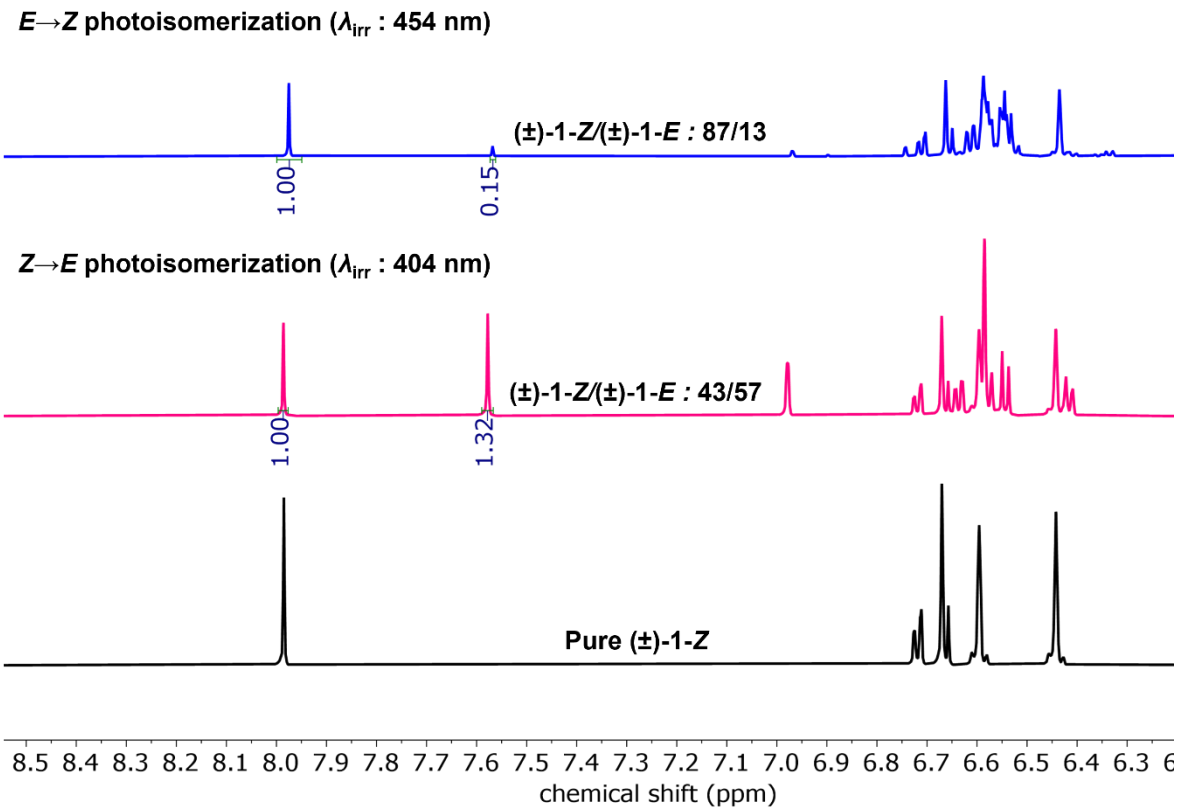

Figure S58. ^{1}H NMR spectra (acetonitrile-d_3) showing pure **(±)-1-*Z*** (black, bottom spectrum) and **(±)-1-*Z*/(±)-1-*E*** isomeric mixture achieved post-irradiation using 404 nm (pink spectrum, *Z*→*E* isomerization) LED, which was subsequently subjected to 454 nm (blue spectrum, *E*→*Z* isomerization) LED irradiation.

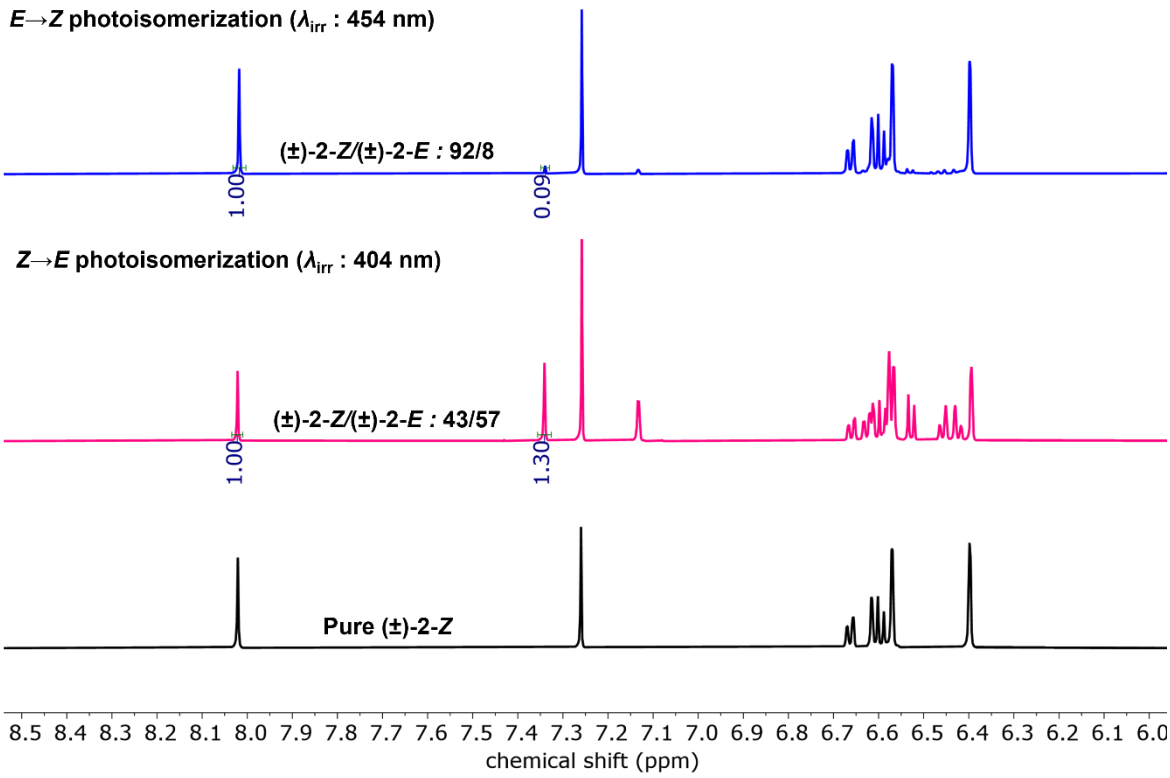

Figure S59. ^{1}H NMR spectra (chloroform-*d*) showing pure **(±)-2-*Z*** (black, bottom spectrum) and **(±)-2-*Z*/(±)-2-*E*** isomeric mixture achieved post-irradiation using 404 nm (pink spectrum, *Z*→*E* isomerization) LED, which was subsequently subjected to 454 nm (blue spectrum, *E*→*Z* isomerization) LED irradiation.

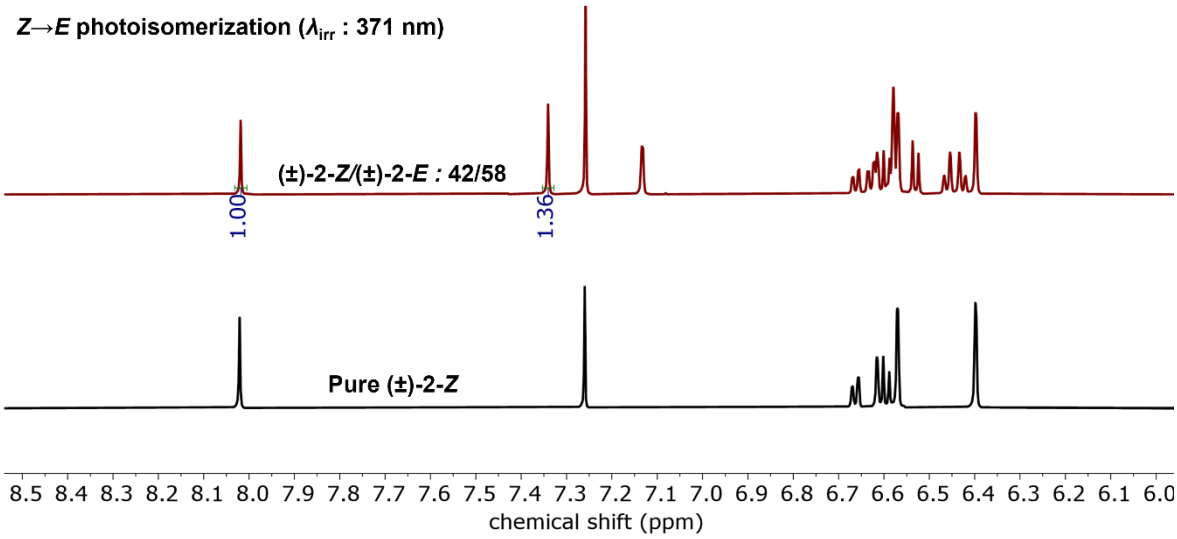

Figure S60. ^{1}H NMR spectra (chloroform-*d*) showing pure **(±)-2-*Z*** (black, bottom spectrum) and **(±)-2-*Z*/(±)-2-*E*** isomeric mixture achieved post-irradiation using 371 nm (maroon spectrum, *Z*→*E* isomerization) UV lamp.

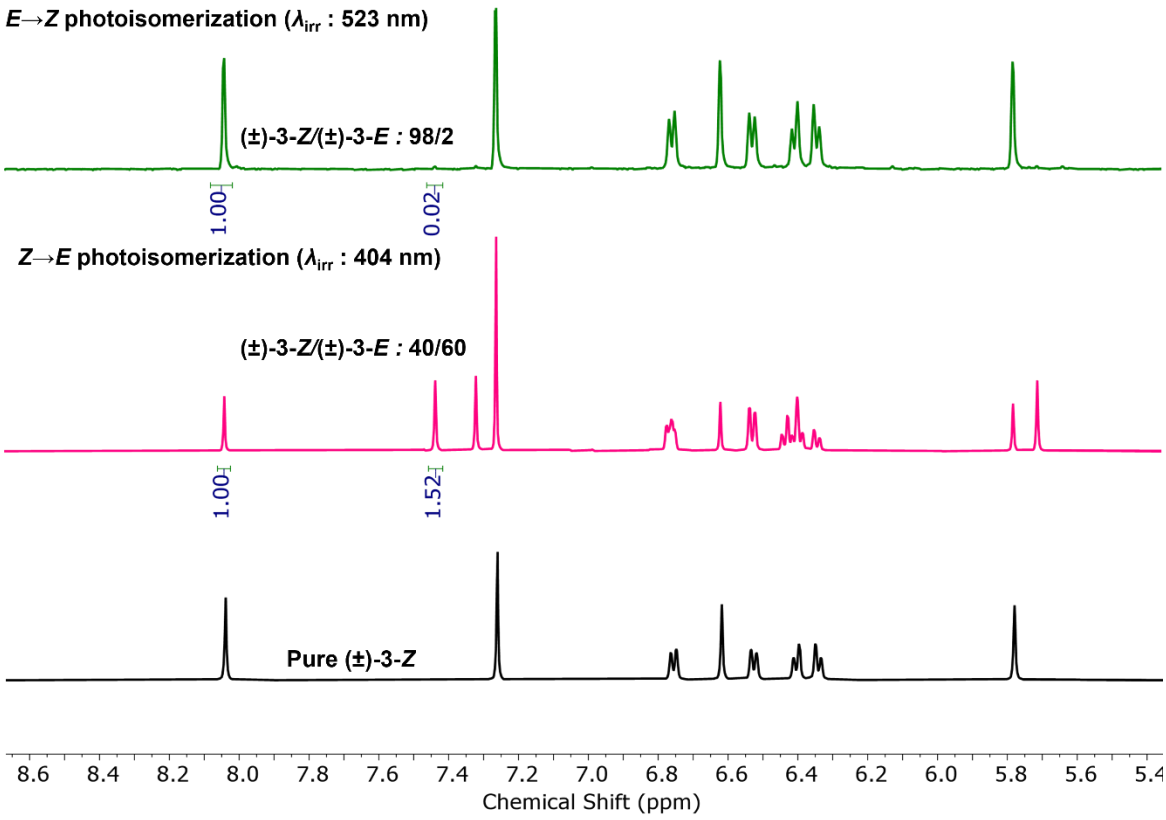

Figure S61. ^{1}H NMR spectra (chloroform-*d*) showing pure **(±)-3-*Z*** (black, bottom spectrum) and **(±)-3-*Z*/(±)-3-*E*** isomeric mixture achieved post-irradiation using 404 nm (pink spectrum, *Z*→*E* isomerization) LED, which was subsequently subjected to 523 nm (green spectrum, *E*→*Z* isomerization) LED irradiation.

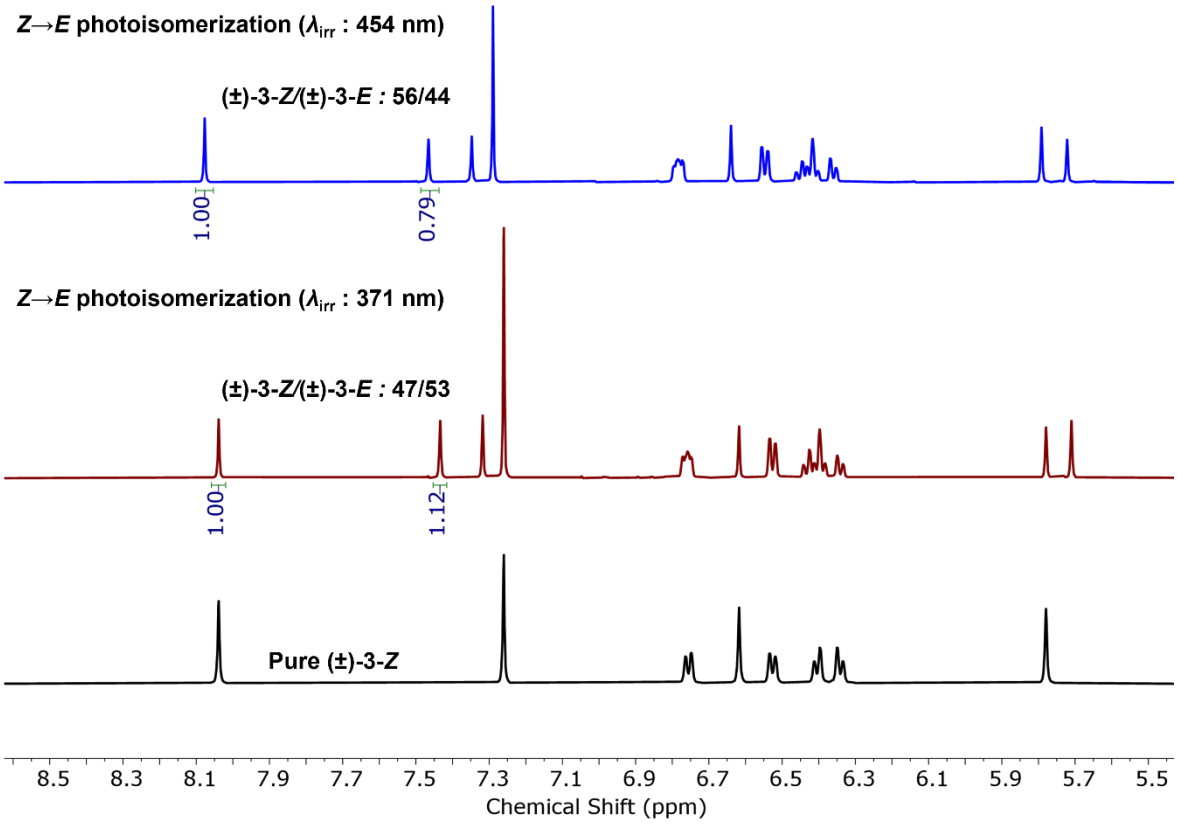

Figure S62. ^{1}H NMR spectra (chloroform-*d*) showing pure **(±)-3-*Z*** (black, bottom spectrum) and **(±)-3-*Z*/(±)-3-*E*** isomeric mixtures achieved post-irradiation using 371 nm (maroon spectrum, *Z*→*E* isomerization) UV lamp, and 454 nm (blue spectrum, *Z*→*E* isomerization).

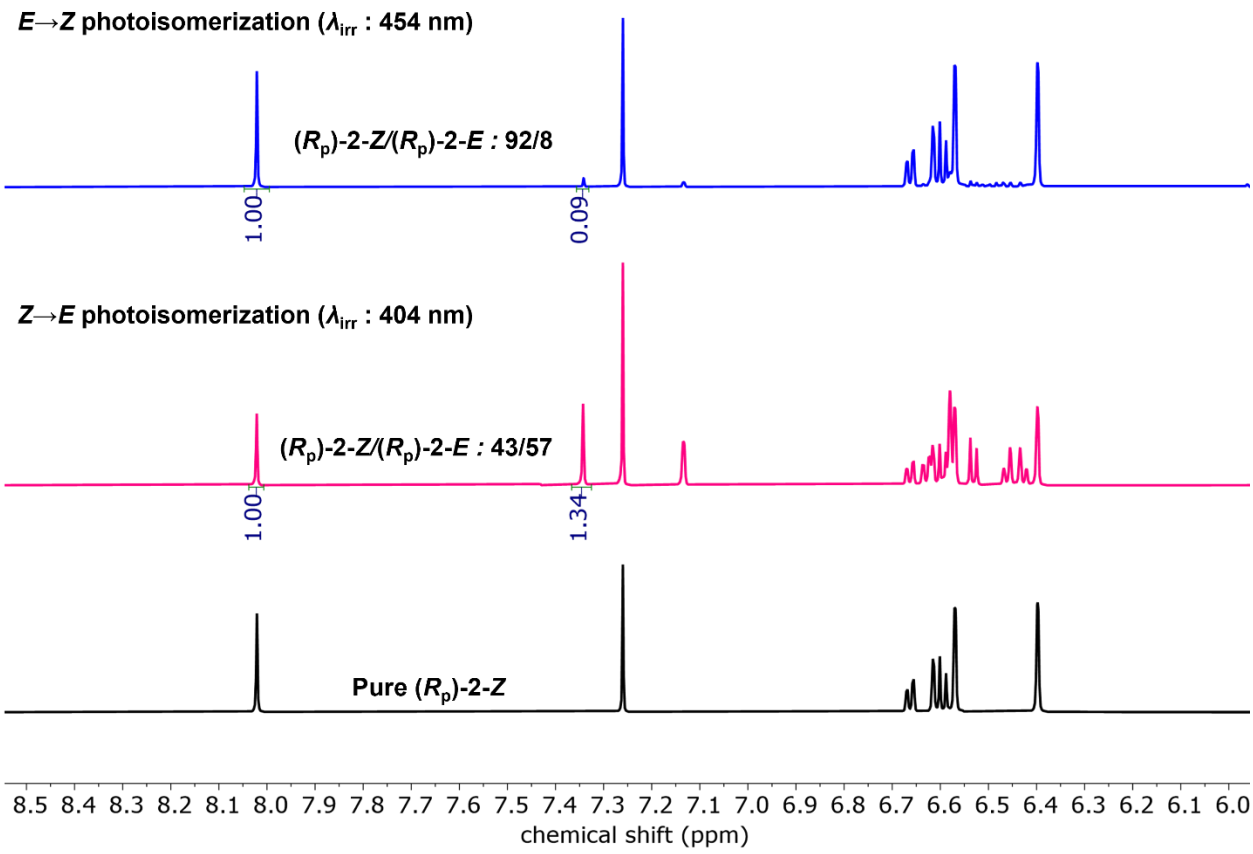

Figure S63. ^{1}H NMR spectra (chloroform-*d*) showing pure **(*R*$_p$)-2-*Z*** (black, bottom spectrum) and **(*R*$_p$)-2-*Z*/(*R*$_p$)-2-*E*** isomeric mixture achieved post-irradiation using 404 nm (pink spectrum, *Z*→*E* isomerization) LED, which was subsequently subjected to 454 nm (green spectrum, *E*→*Z* isomerization) LED irradiation.

KINETICS OF *Z*→*E* PHOTOISOMERIZATION

General Procedure

^{1}H NMR were recorded on a Bruker 600 MHz spectrometer (^{1}H at 600 MHz). To evaluate the kinetics of *Z*→*E* photoisomerization, a 15 mM stock solution in chloroform-*d* was prepared for compounds **(±)-2-*Z*** and **(±)-3-*Z*** each. Approximately 0.5 mL of each stock solution was transferred to a conventional glass NMR tube. The samples were exposed to an irradiation wavelength (λ_{irr} = 404 nm) and ^{1}H NMR spectra were recorded to monitor the reaction progress until no changes in *Z*/*E* integration ratios were observed. Each sample was irradiated for 36 min and ^{1}H NMR spectra were recorded every 3 minutes.

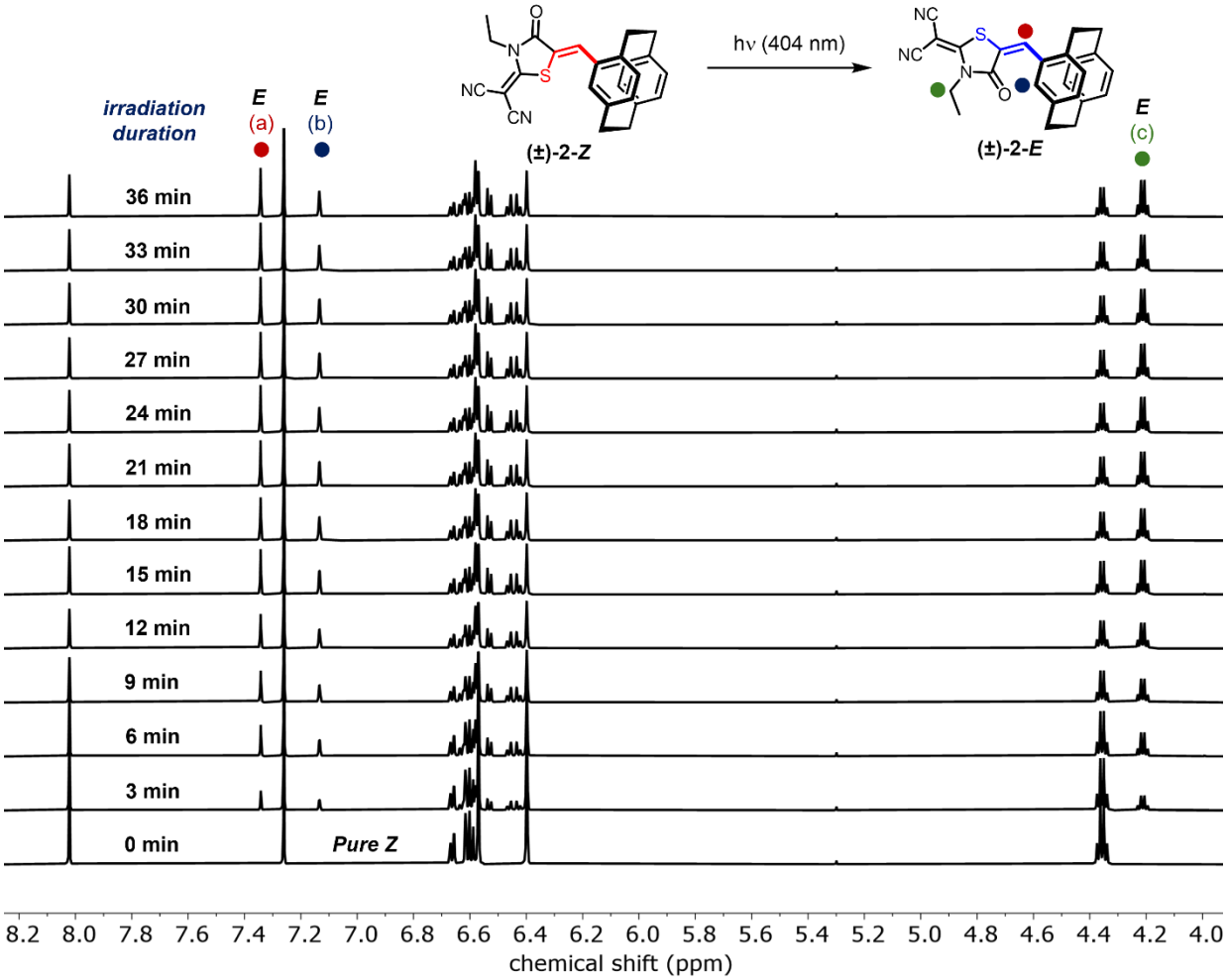

Figure S64. Stacked ^{1}H NMR spectra (15 mM, $CDCl_3$, 600 MHz) of compound **(±)-2** with pure **(±)-2-*Z*** spectrum (bottom) and **(±)-2-*Z*/(±)-2-*E*** irradiated mixtures obtained upon 404 nm excitation. The change in *Z* and *E* isomer peak integrals were monitored until a PSS was reached.

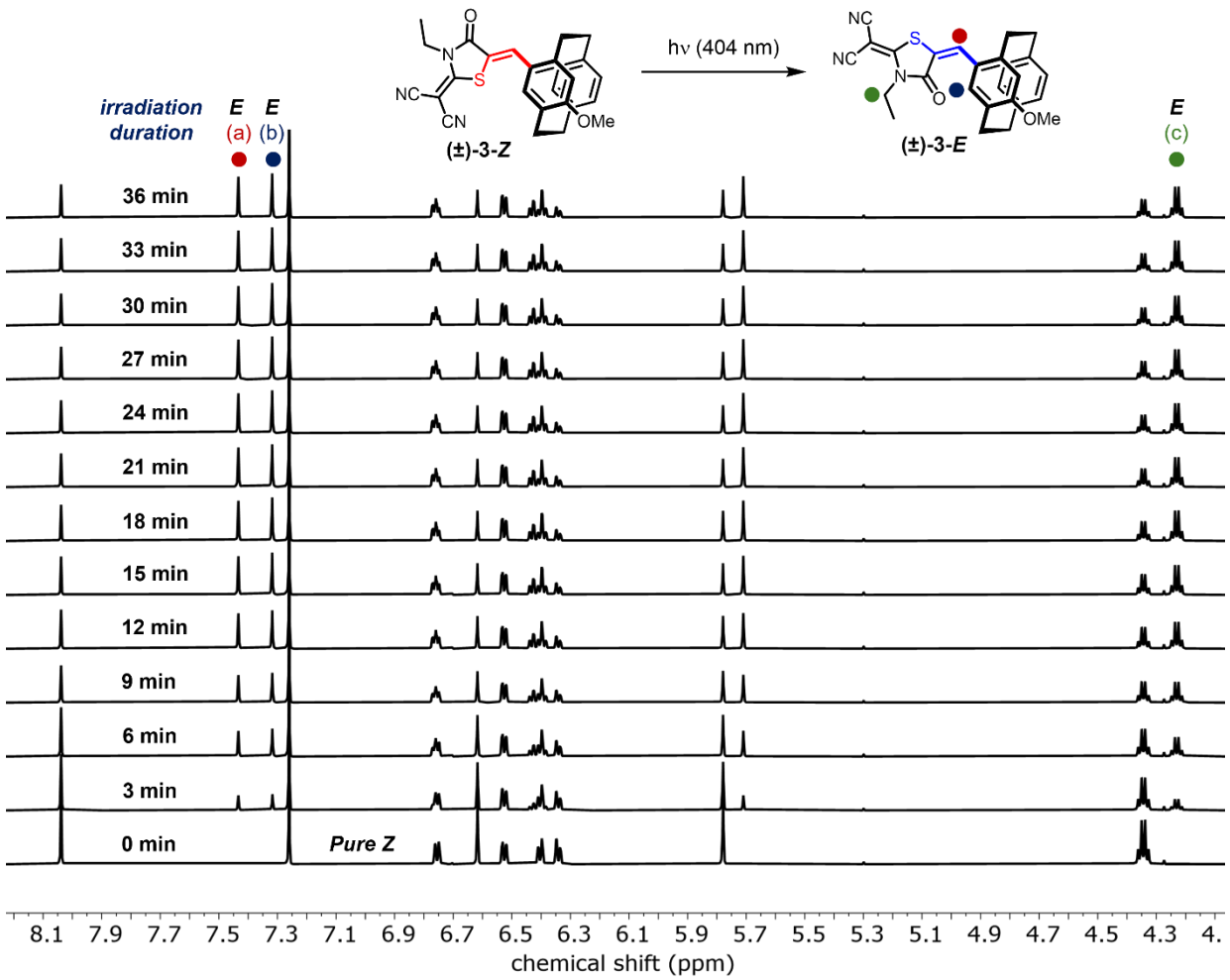

Figure S65. Stacked ^{1}H NMR spectra (15 mM, $CDCl_3$, 600 MHz) of compound **(±)-3** with pure **(±)-3-*Z*** spectrum (bottom) and **(±)-3-*Z*/(±)-3-*E*** irradiated mixtures obtained upon 404 nm excitation. The change in *Z* and *E* isomer peak integrals were monitored until a PSS was reached.

Considering the *Z*→*E* photoisomerization process will follow first-order kinetics, we have used a "three-parameter exponential fit equation" (eq. 1) to calculate the rate constants using the MestReNova software.

$$\mathbf{y = B + F * exp\,(-x * G)} \quad \text{.....eq. 1}$$

We have chosen three peaks (the exocyclic olefin proton, *E*(a); one aromatic proton of the top phenyl deck, *E*(b); and one aliphatic proton signal of the RCN unit, *E*(c)) to monitor the photoisomerization of both the compounds to measure the rate constants as accurately as possible.

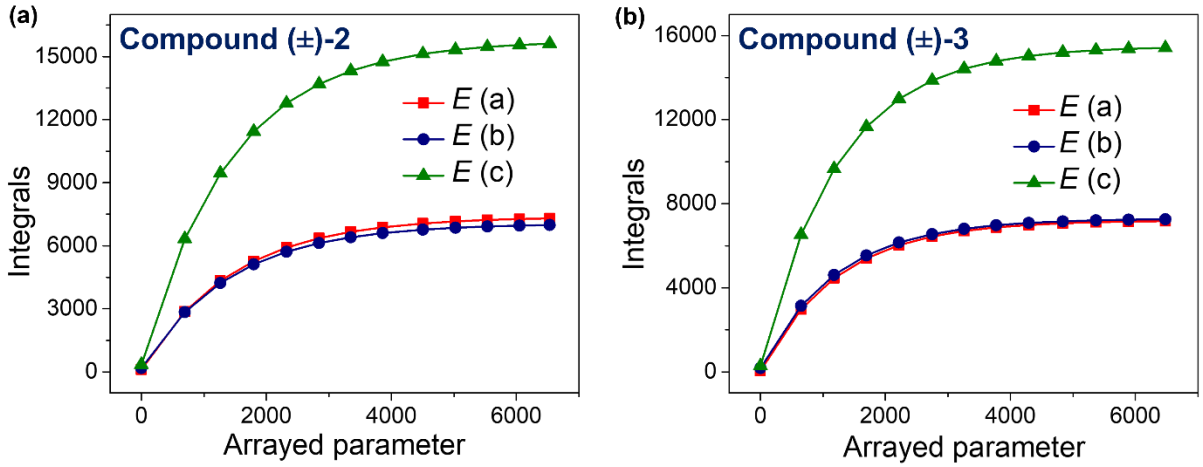

Figure S66. The change in the integrals of the proton peaks of *E*(a), *E*(b), and *E*(c) as the *Z*→*E* photoisomerization reaction progresses with time; for compounds (a) **(±)-2**, and (b) **(±)-3**.

Table S1. The rate constants calculated for the *Z*→*E* photoisomerization based on the proton peaks of *E*(a), *E*(b), and *E*(c); for compounds (a) **(±)-2**, and (b) **(±)-3**.

NMR peaks	Rate constants (in 10^{-4} S^{-1})	Error (in 10^{-5} S^{-1})	B values	F values
Compound (±)-2				
E (a)	6.879	2.462	7388	-7276
E (b)	7.052	2.502	7054	-6875
E (c)	7.063	2.460	15768	-15423
Average (**(±)-2**)	6.998	2.475		
Compound (±)-3				
E (a)	8.104	2.553	7212	-7157
E (b)	8.252	2.667	7295	-7107
E (c)	8.123	2.476	15496	-15215
Average (**(±)-3**)	8.160	2.565		

Using eq.1, the rate constants calculated for the *Z*→*E* photoisomerization based on the proton peaks of *E*(a), *E*(b), and *E*(c) are found to be (7.00±0.25)×10^{-4} sec^{-1} for compound **(±)-2**, and (8.16±0.26)×10^{-4} sec^{-1} for compound **(±)-3**.

SOLUTION NMR THERMAL ISOMERIZATION STUDIES

General Procedure

^{1}H NMR were recorded on a BRUKER-600 (^{1}H at 600 MHz) spectrometer. Solutions (15 mM) of compounds **(±)-1-*Z***, **(±)-2-*Z***, and **(±)-3-*Z*** were prepared in chloroform-*d*, toluene-d_8, or acetonitrile-d_3, as specified. Approximately 0.5 mL of each stock solution was transferred to a conventional glass NMR tube, which was subjected to selective wavelength irradiation (λ_{irr} = 404 nm) to promote the *Z*→*E* isomerization. The NMR tube with the *Z*/*E* mixture was placed in a pre-heated water bath with a set temperature of 60 °C (for samples prepared in acetonitrile-d_3). The entire experimental setup was covered with aluminum foil to minimize the possibility of unintentional photoisomerization in the laboratory. The NMR spectra at specific time intervals were recorded at 25 °C as quickly as possible to minimize the possibility of reverse isomerization upon change of the temperature.

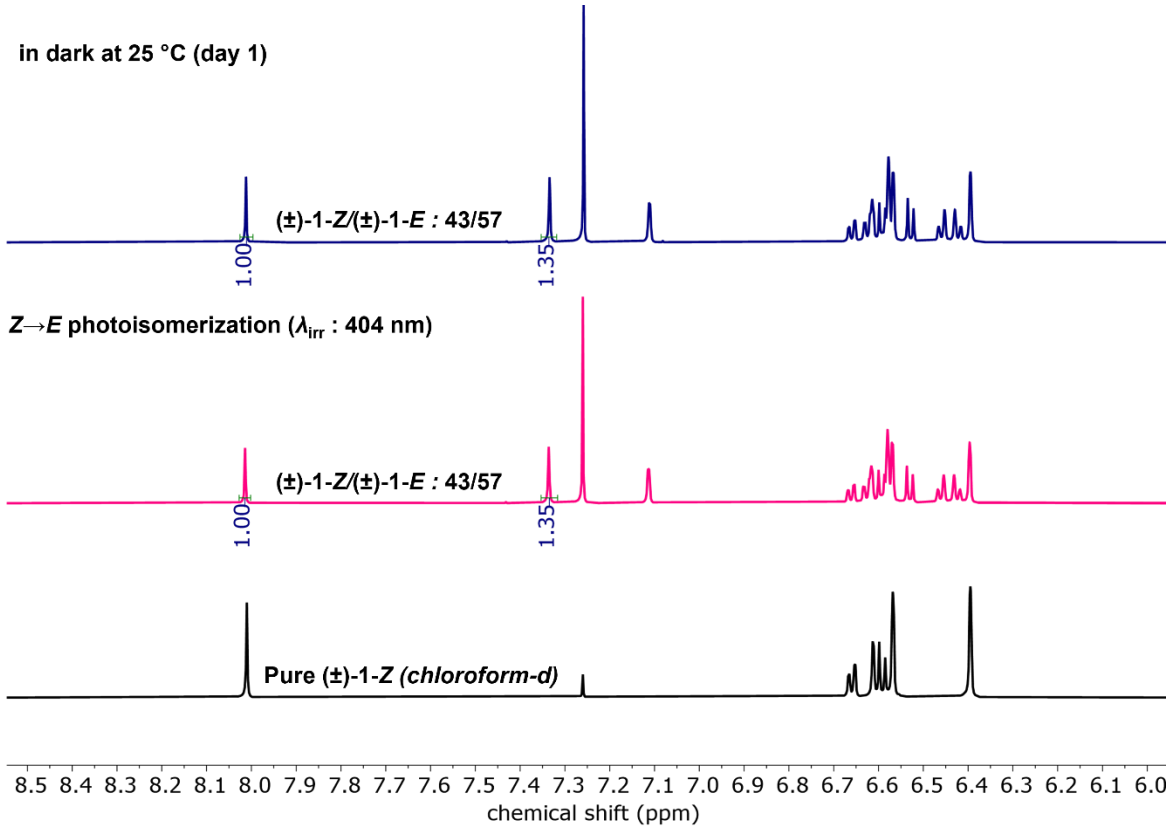

Figure S67. ^{1}H NMR spectra (chloroform-*d*) showing pure **(±)-1-*Z*** (black, bottom spectrum) and **(±)-1-*Z*/(±)-1-*E*** isomeric mixture achieved post-irradiation using 404 nm (pink spectrum, *Z*→*E* isomerization) LED, which was subsequently kept in dark at 25 °C for 1 day (navy blue, top spectrum) showing no thermal *E*→*Z* isomerization at this conditions.

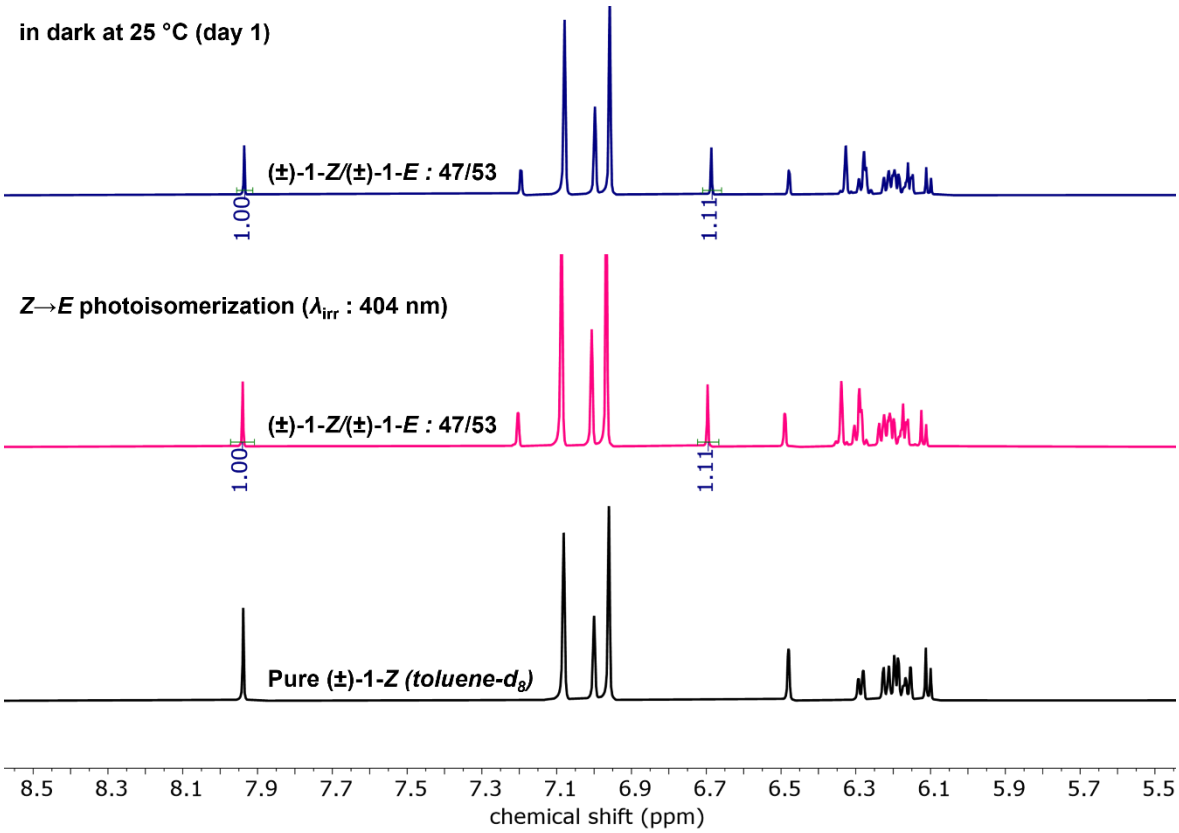

Figure S68. ^{1}H NMR spectra (toluene-d_8) showing pure **(±)-1-*Z*** (black, bottom spectrum) and **(±)-1-*Z*/(±)-1-*E*** isomeric mixture achieved post-irradiation using 404 nm (pink spectrum, *Z*→*E* isomerization) LED, which was subsequently kept in dark at 25 °C for 1 day (navy blue, top spectrum) showing no thermal *E*→*Z* isomerization at this conditions.

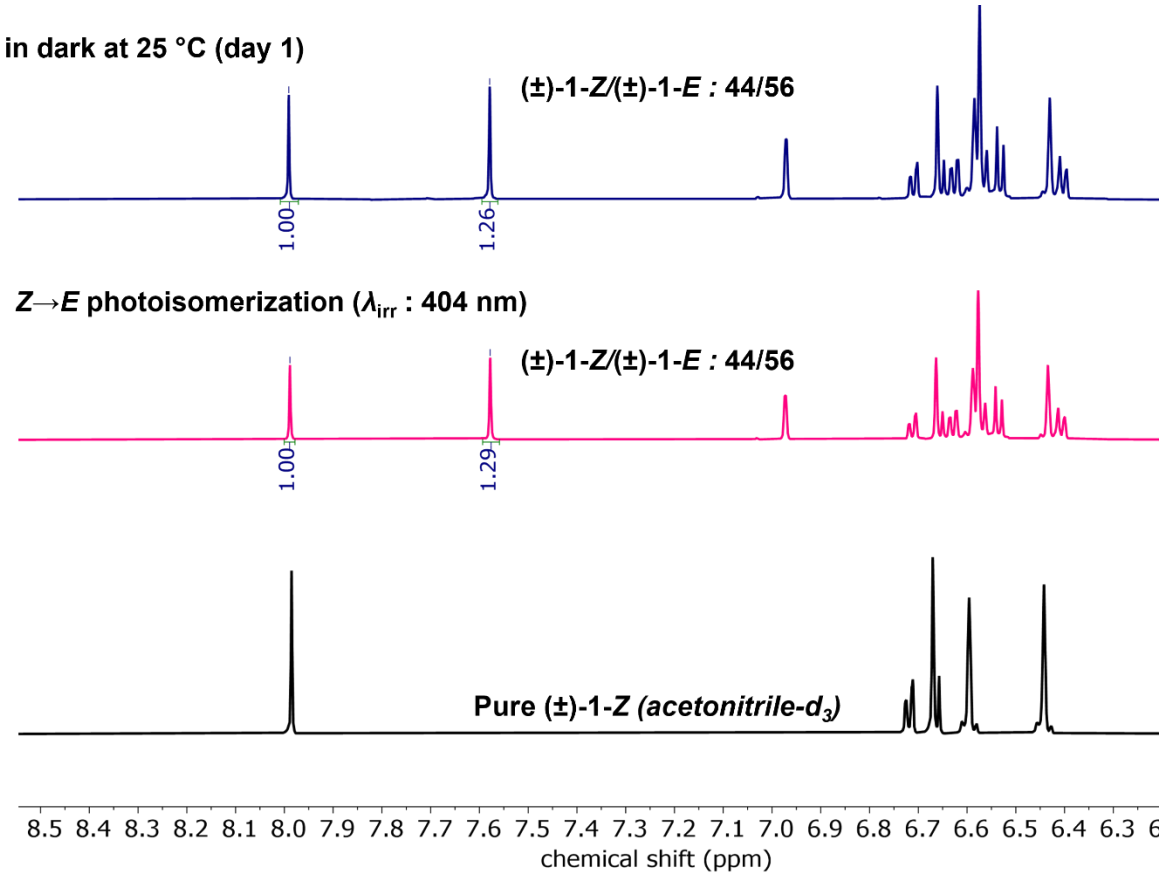

Figure S69. ^{1}H NMR spectra (acetonitrile-d_3) showing pure **(±)-1-*Z*** (black, bottom spectrum) and **(±)-1-*Z*/(±)-1-*E*** isomeric mixture achieved post-irradiation using 404 nm (pink spectrum, *Z*→*E* isomerization) LED, which was subsequently kept in dark at 25 °C for 1 day (navy blue, top spectrum) showing no thermal *E*→*Z* isomerization at this conditions.

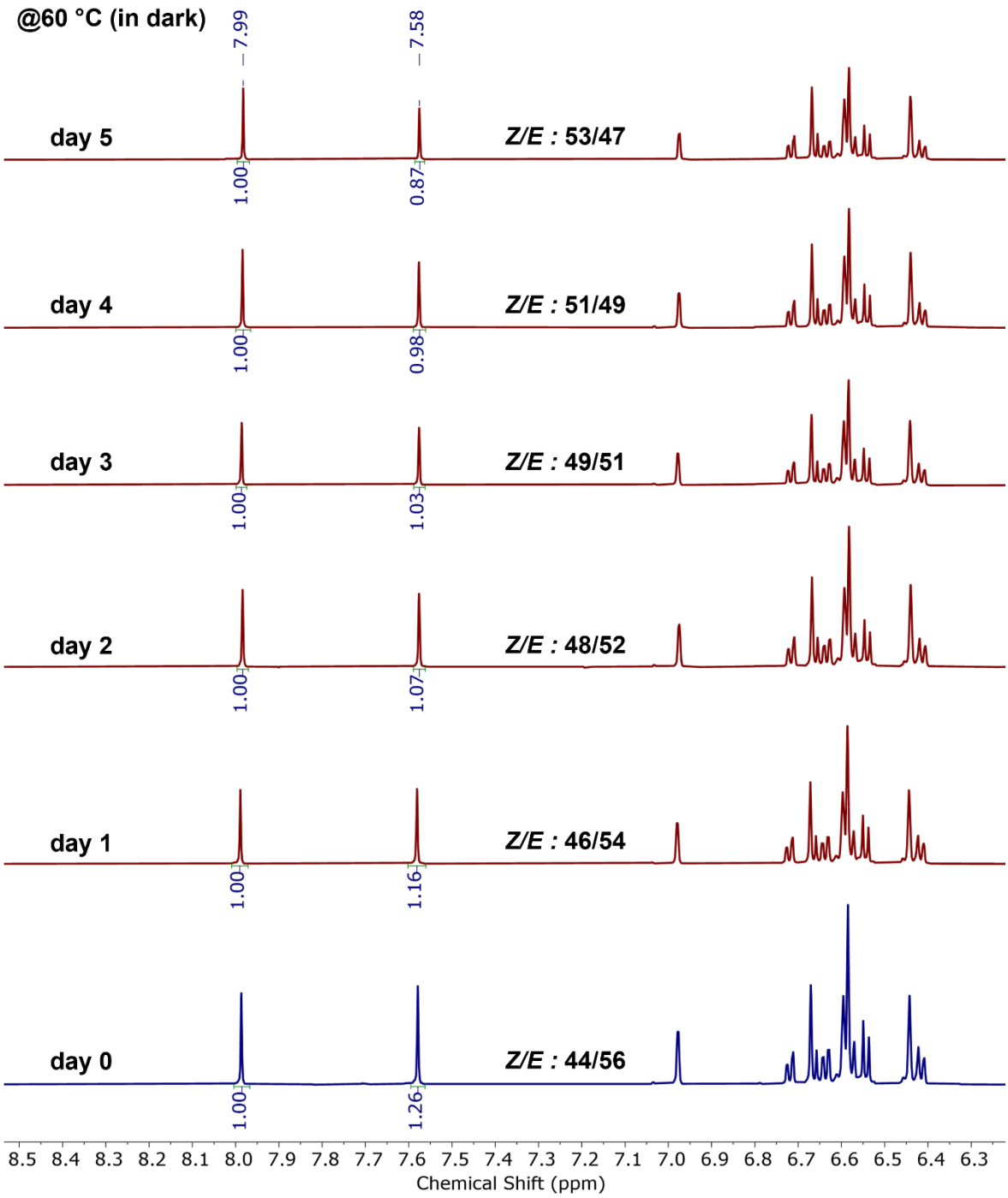

Figure S70. ^{1}H NMR spectra (acetonitrile-d_3) of **(±)-1-*Z*/(±)-1-*E*** isomeric mixture showing thermal *E*→*Z* isomerization at 60 °C over 5 days.

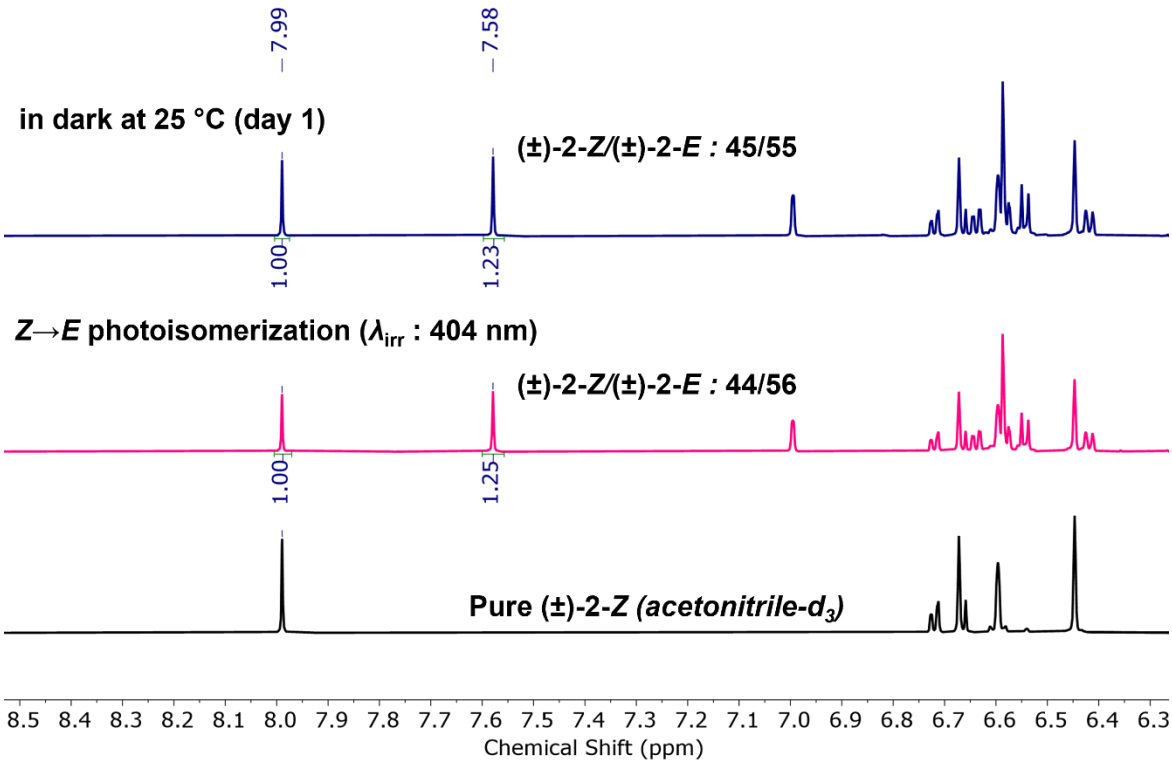

Figure S71. ^{1}H NMR spectra (acetonitrile-d_3) showing pure **(±)-2-*Z*** (black, bottom spectrum) and **(±)-2-*Z*/(±)-2-*E*** isomeric mixture achieved post-irradiation using 404 nm (pink spectrum, *Z*→*E* isomerization) LED, which was subsequently kept in dark at 25 °C for 1 day (navy blue, top spectrum) showing no thermal *E*→*Z* isomerization at this conditions.

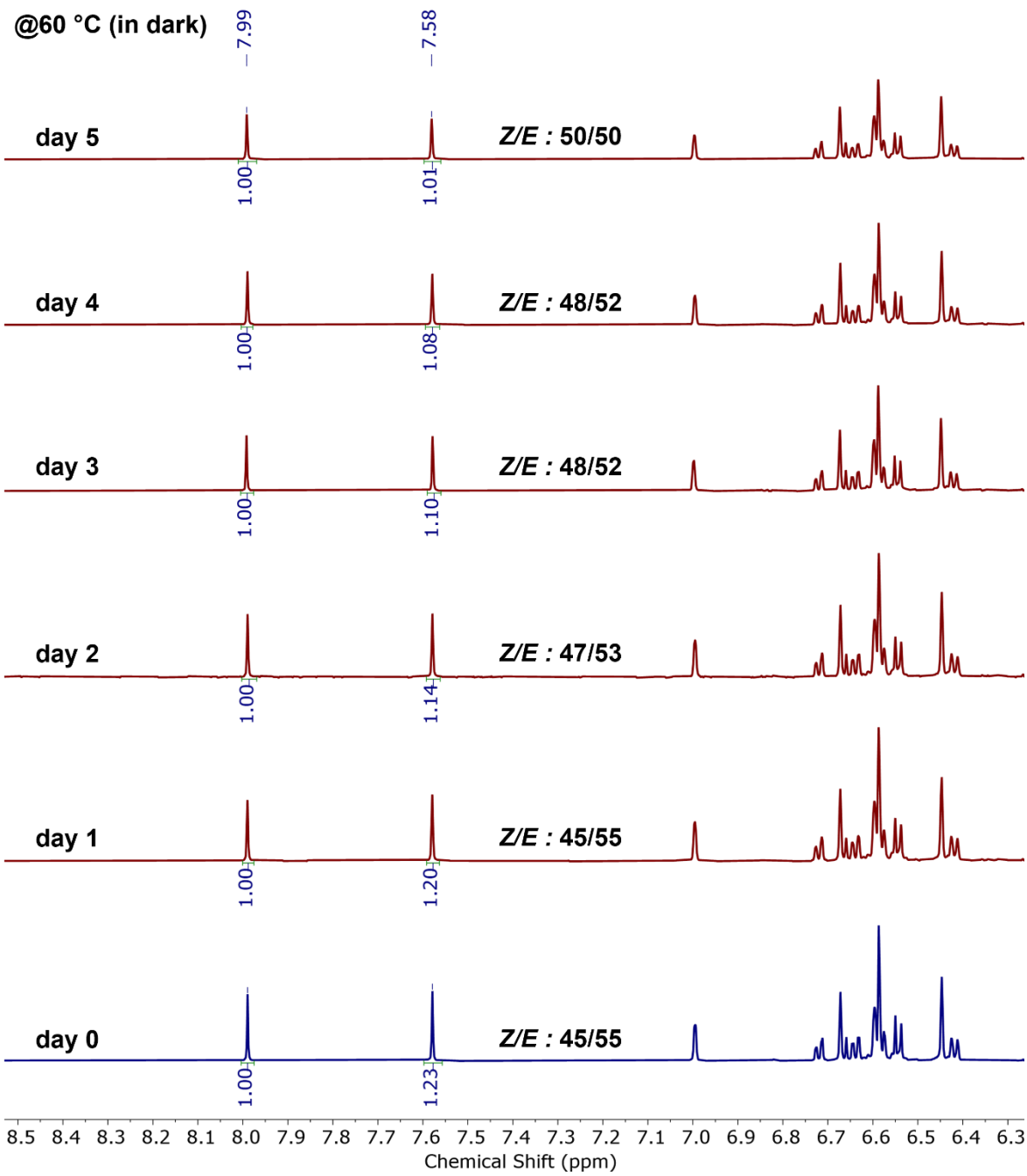

Figure S72. ^{1}H NMR spectra (acetonitrile-d_3) of **(±)-2-*Z*/(±)-2-*E*** isomeric mixture showing thermal *E*→*Z* isomerization at 60 °C over 5 days.

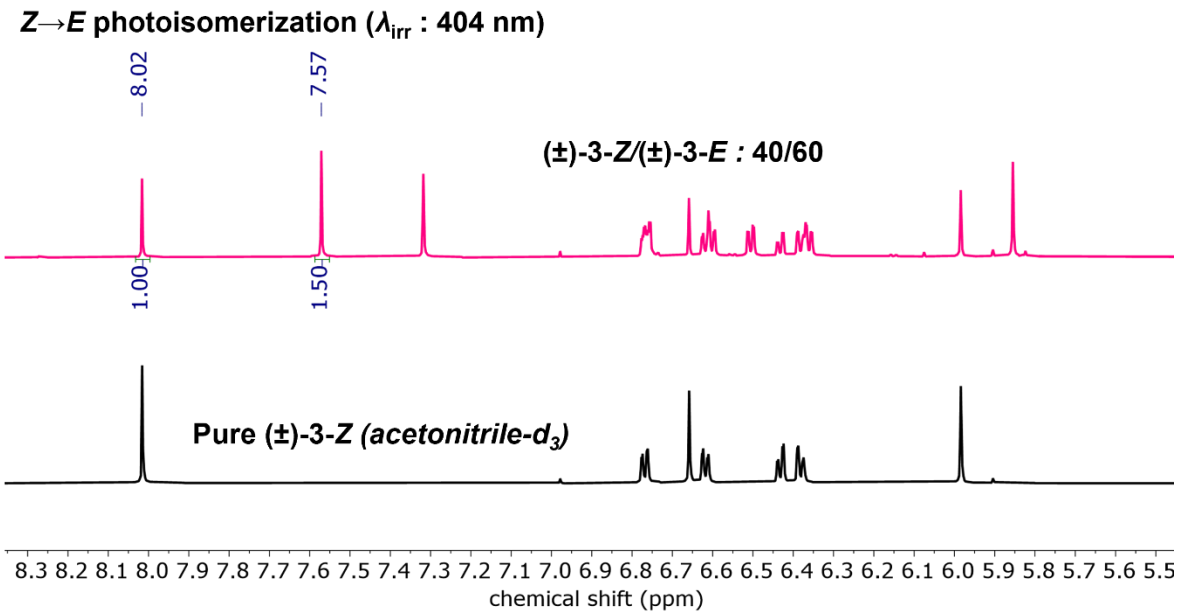

Figure S73. ^{1}H NMR spectra (acetonitrile-d_3) showing pure **(±)-3-*Z*** (black, bottom spectrum) and **(±)-3-*Z*/(±)-3-*E*** isomeric mixture achieved post-irradiation using 404 nm (pink spectrum, *Z*→*E* isomerization) LED.

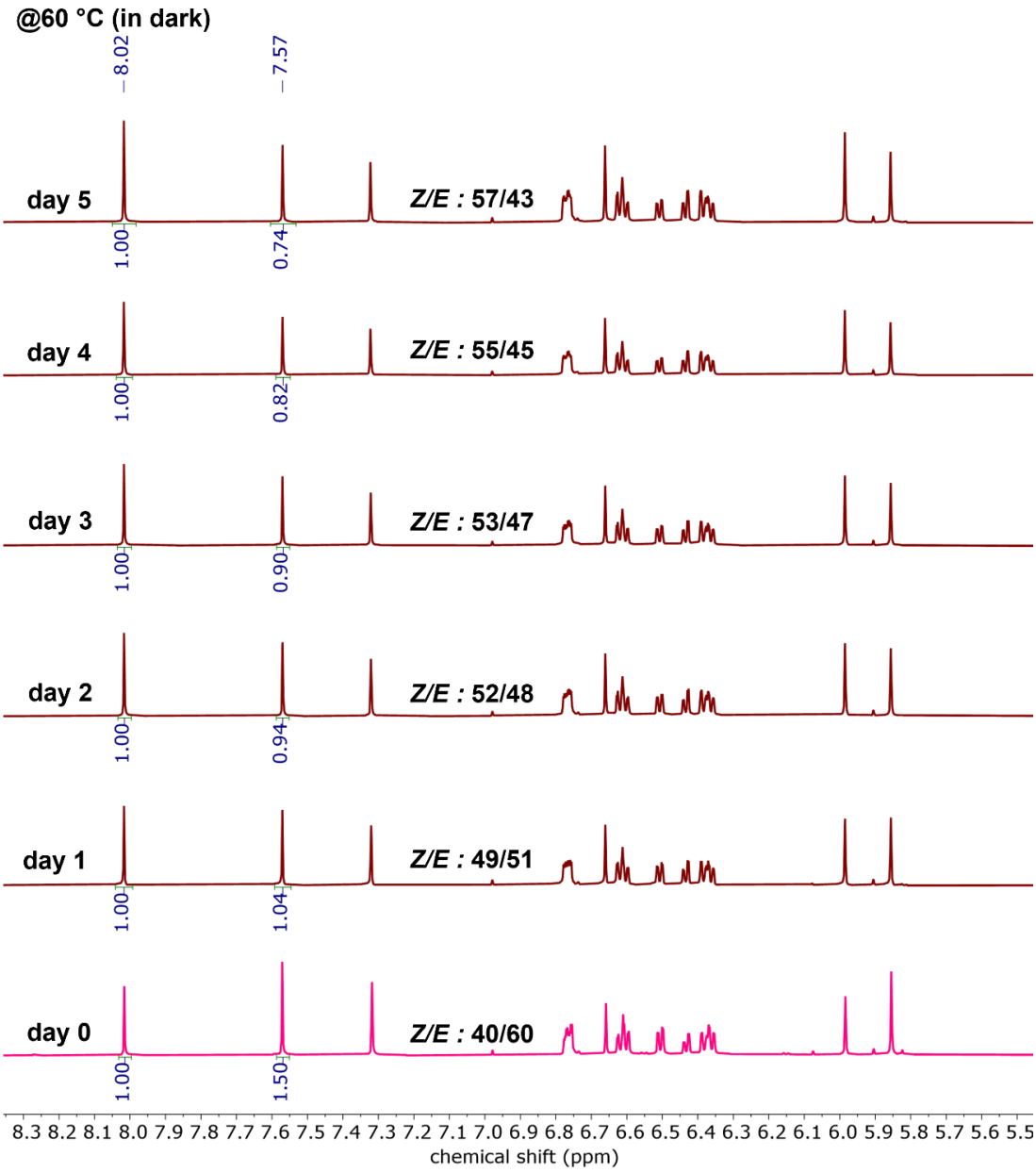

Figure S74. ^{1}H NMR spectra (acetonitrile-d_3) of **(±)-3-*Z*/(±)-3-*E*** isomeric mixture showing thermal *E*→*Z* isomerization at 60 °C over 5 days.

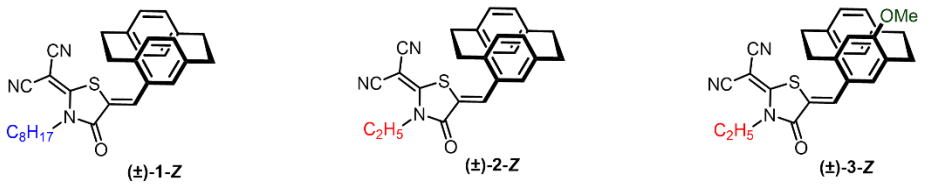

Figure S75. Extent of *E*→*Z* thermal isomerization (in acetonitrile-d_3) for compounds **(±)-1-*Z***, **(±)-2-*Z*** and **(±)-3-*Z*** monitored at 60 °C over 5 days.

VARIABLE TEMPERATURE NMR STUDY

General Procedure

^{1}H NMR were recorded on INOVA-500 (1H at 500 MHz) spectrometer. To evaluate the possible dimeric association for compound **(±)-3-*Z*** in solution, a 15 mM stock solution in tetrachloroethane-d_2 (TCE-d_2) was prepared. Approximately 0.5 mL of stock solution was transferred to a conventional glass NMR tube. ^{1}H NMR spectra were monitored from changing the temperature 25 °C to 90 °C, with each spectrum recorded at every 5 °C rise in temperature.

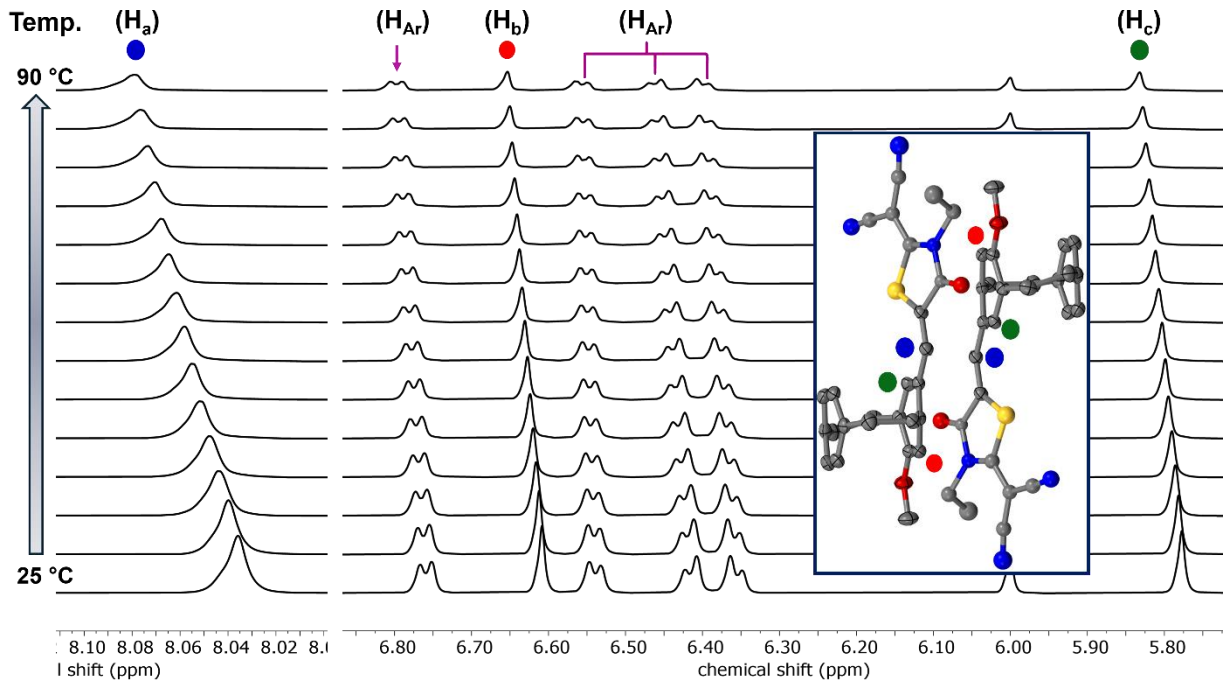

Figure S76. Stacked ^{1}H NMR spectra (15 mM, TCE-d_2, 500 MHz) of compound **(±)-3-*Z*** as monitored through a temperature change from 25 °C (bottom spectrum) to 90 °C (top spectrum) with every 5 °C interval. A deshieding of all the proton peaks in the aromatic regions was observed with increasing temperature, consistent with possible disruption of π–π interactions.

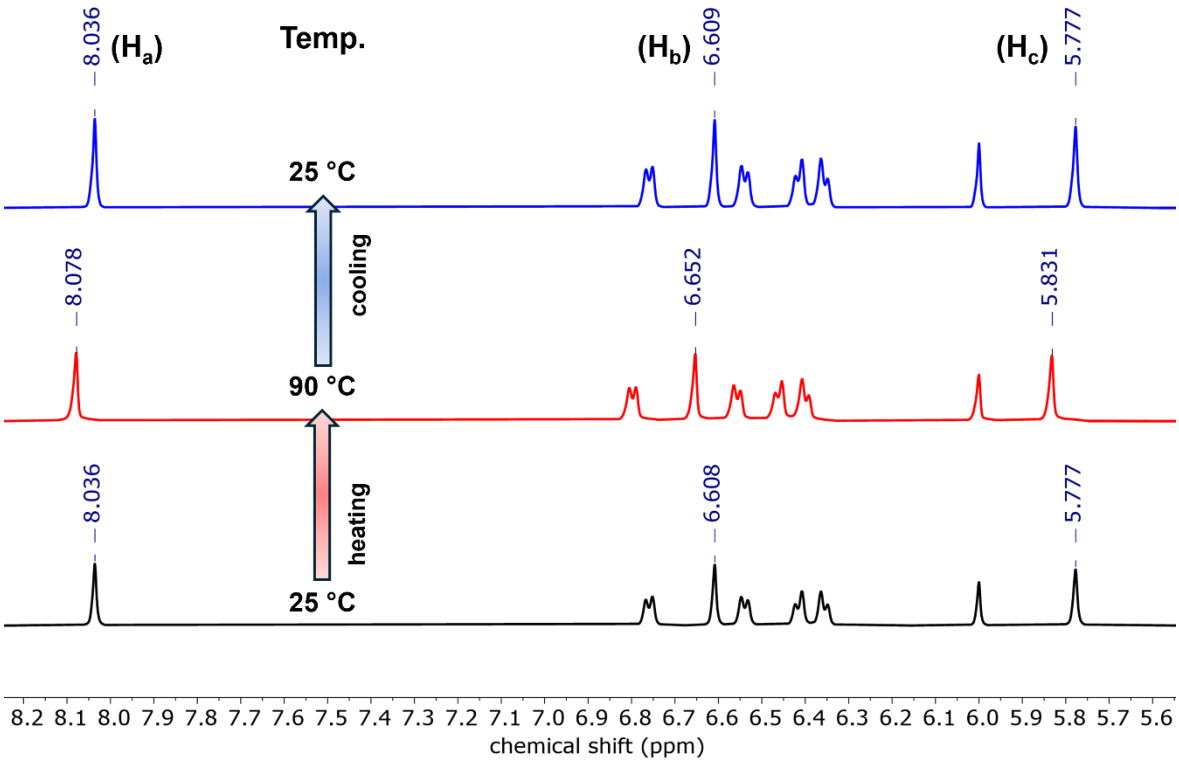

Figure S77. Stacked ^{1}H NMR spectra (15 mM, TCE-d_2, 500 MHz) of compound **(±)-3-*Z*** as monitored through a temperature range from 25 °C (bottom and top spectrum) to 90 °C (middle spectrum), showing reversible change in chemical shift upon heating and cooling.

UV-VIS PROFILES (SOLUTION AND TD-DFT)

General Procedure

Solution absorption spectra were measured on a Perkin-Elmer Lambda 25 dual beam absorption spectrometer and a Cary 100 Bio spectrophotometer in chloroform (and methylcyclohexane, toluene, acetonitrile; as specified) using 20 μM solutions in 1 cm quartz cells for all RCN-functionalized target molecules **(±)-1-*Z***, **(±)-2-*Z***, and **(±)-3-*Z***. Spectrophotometric grade solvents were used for all absorption studies. Solutions were prepared and transferred into a quartz cuvette for immediate UV-vis absorption measurements.

Excited state Time-dependent DFT (TD-DFT) calculations were performed at the CAM-B3LYP/cc-pVDZ level of theory in the gas phase (or using IEFPCM solvent model as specified) starting with the structural coordinates obtained from previously optimized geometries. All octyl chains were truncated to methyl groups to reduce the computational cost. As model compounds **(±)-1** and **(±)-2** only differ in the alkyl group connected to the nitrogen atom of the RCN unit, both have been calculated as a common structure, using the alkyl groups as methyl. Different conformers have been assigned for both the *Z* and *E* isomers, which have been determined based on the olefin proton (H17, marked in red, *vide infra*) pointing towards the nearest bridge (Conformer A, $\mathbf{C_A}$), or opposite to the bridge (Conformer B, $\mathbf{C_B}$).

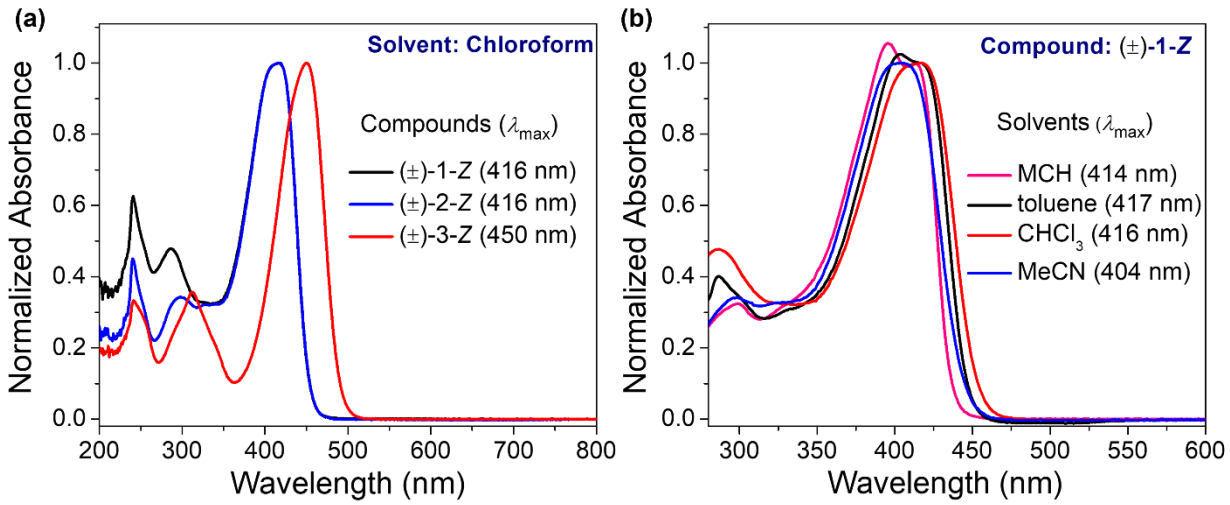

Figure S78. (a) Experimental normalized absorption profiles (chloroform, 20 μM) of pure **(±)-1-*Z*** (black trace), **(±)-2-*Z*** (red trace), and **(±)-3-*Z*** (blue trace). (b) Experimental normalized absorption profiles of pure **(±)-1-*Z*** in four different solvents: methylcyclohexane or MCH (pink trace), toluene (black trace), chloroform (red trace), and acetonitrile or MeCN (blue trace).

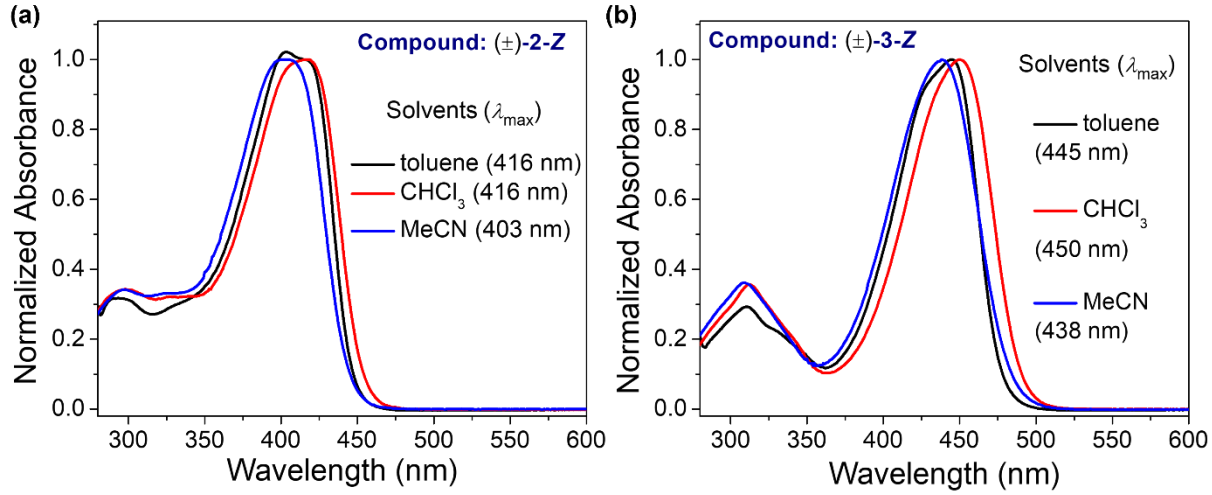

Figure S79. Experimental normalized absorption profiles of pure (a) **(±)-2-*Z*** and (b) **(±)-3-*Z*** in three different solvents: toluene (black trace), chloroform (red trace), and acetonitrile or MeCN (blue trace).

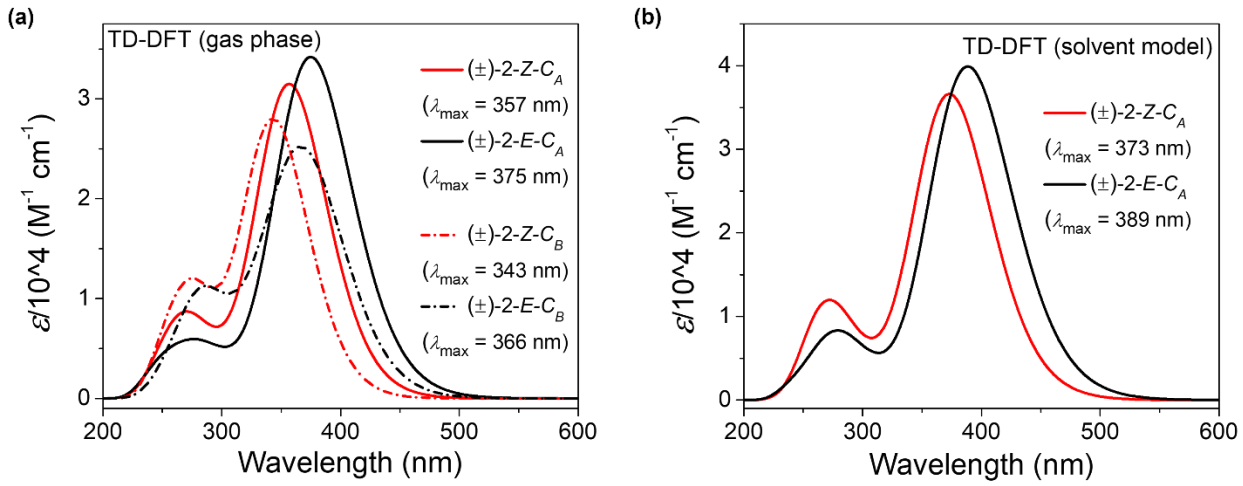

Figure S80. TD-DFT absorbance profiles of **(±)-2-*Z*** (red traces) and **(±)-2-*E*** (black traces) in different conformers $\mathbf{C_A}$ (solid lines) and $\mathbf{C_B}$ (dashed lines) at the CAM-B3LYP/cc-pVDZ level of theory (a) in gas phase, and (b) using IEFPCM solvent model.

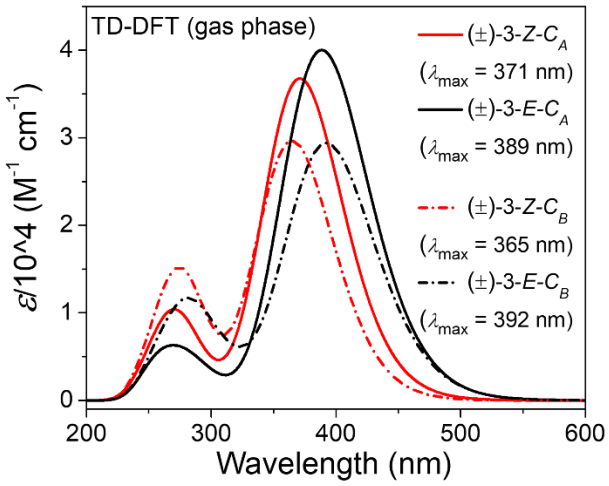

Figure S81. TD-DFT absorbance profiles of **(±)-3-*Z*** (red traces) and **(±)-3-*E*** (black traces) in different conformers $\mathbf{C_A}$ (solid lines) and $\mathbf{C_B}$ (dashed lines) at the CAM-B3LYP/cc-pVDZ level of theory in gas phase.

UV-VIS PHOTOISOMERIZATION STUDIES

General Procedure (Wavelength-Dependent UV-vis Studies)

Solution absorption spectra were measured on a Perkin-Elmer Lambda 25 dual beam absorption spectrometer and a Cary 100 Bio spectrophotometer in chloroform (and methylcyclohexane, toluene, acetonitrile; as specified) using 20 μM solutions in 1 cm quartz cells for all RCN-functionalized target molecules **(±)-1-*Z***, **(±)-2-*Z***, **(±)-3-*Z***, and **(R_p)-2-*Z***. Spectrophotometric grade solvents were used for all

absorption studies. Solutions were prepared and transferred into a quartz cuvette for immediate UV-vis absorption measurements. The cuvettes were removed from the spectrophotometer and covered with a glass container while irradiated at an appropriate wavelength of excitation (λ_{irr} = 371, 404, 454, and 523 nm) and absorption spectra were recorded to monitor the changes in the UV-vis spectrum attributed to the isomerization process. The samples were irradiated for 60–300 s until no changes in the UV-vis spectra were observed, indicating that the respective photostationary states (PSS) were reached.

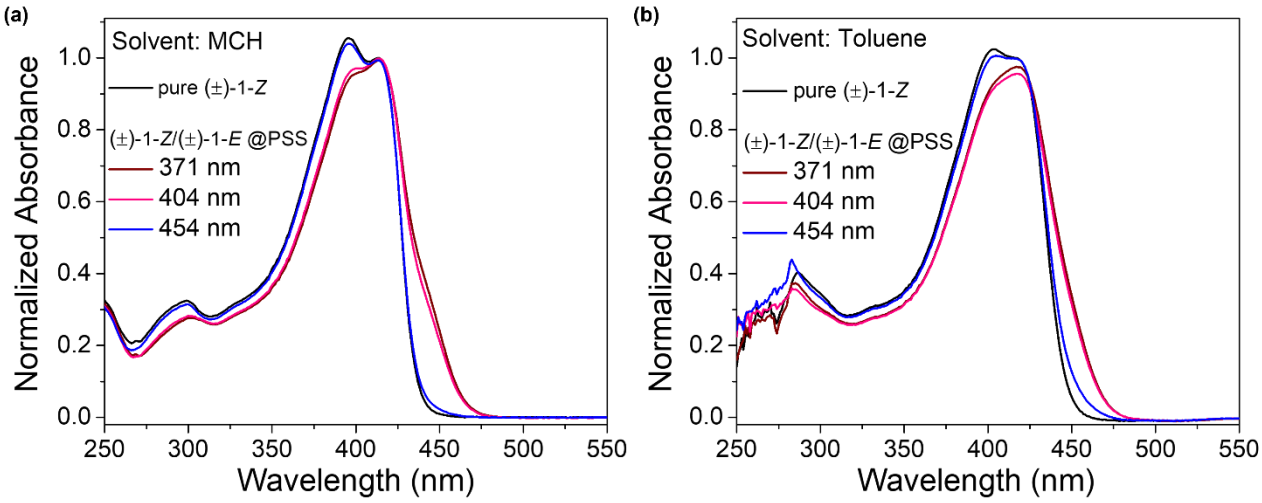

Figure S82. Experimental absorption profiles (20 μM) for compound **(±)-1-*Z*** in (a) Methylcyclohexane (MCH) and (b) Toluene, showing solution UV-vis for pure **(±)-1-*Z*** (black trace), and **(±)-1-*Z*/(±)-1-*E*** mixtures obtained after 371 nm irradiation (maroon trace), 404 nm irradiation (pink trace), and 454 nm irradiation (blue trace).

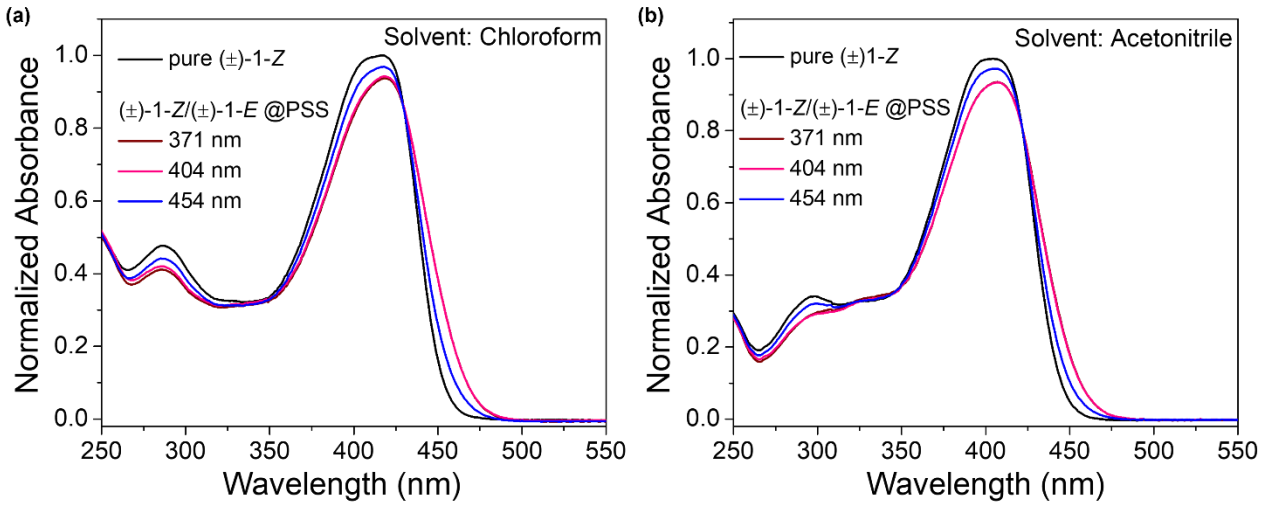

Figure S83. Experimental absorption profiles (20 μM) for compound **(±)-1-*Z*** in (a) Chloroform and (b) Acetonitrile, showing solution UV-vis for pure **(±)-1-*Z*** (black trace), and **(±)-1-*Z*/(±)-1-*E*** mixtures obtained after 371 nm irradiation (maroon trace), 404 nm irradiation (pink trace), and 454 nm irradiation (blue trace).

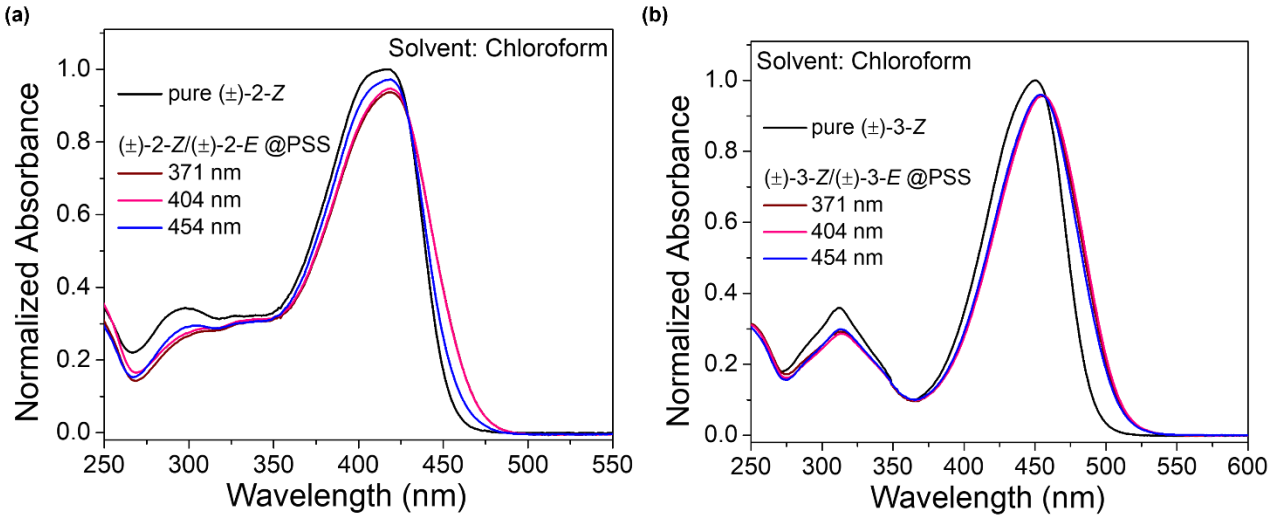

Figure S84. Experimental absorption profiles (chloroform, 20 μM) for compound (a) **(±)-2-*Z*** and (b) **(±)-3-*Z***, showing solution UV-vis for pure *Z* isomer (black trace), and *Z*/*E* mixtures obtained after 371 nm irradiation (maroon trace), 404 nm irradiation (pink trace), and 454 nm irradiation (blue trace).

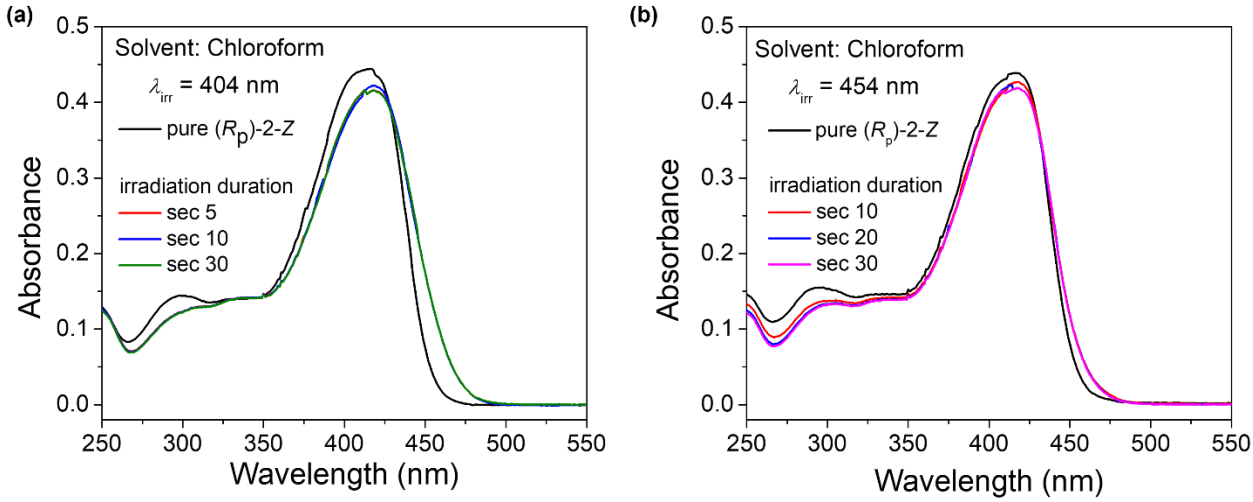

Figure S85. Experimental absorption profiles (chloroform, 20 μM) for compound **(*R*$_p$)-2-*Z*** upon (a) 404 nm and (b) 454 nm irradiation. Spectra showing solution UV-vis for pure *Z* isomer (black trace), and *Z*/*E* mixtures obtained after irradiation.

VARIABLE TEMPERATURE UV–VIS STUDY

General Procedure

UV–vis absorption spectra (20 μM, tetrachloroethane) were recorded using an Applied Photophysics Chirascan-plus spectrophotometer controlled by Chirascan software in quartz cells of 1 cm path length. To evaluate the possible dimeric association for compound **(±)-3-*Z*** in solution, a 20 μM stock solution in tetrachloroethane (TCE) was prepared. Approximately 3.0 mL of stock solution was transferred to a conventional quartz cuvette. The absorption profiles were monitored from changing the temperature 25 °C to 90 °C, with each spectrum recorded at every 5 °C rise in temperature.

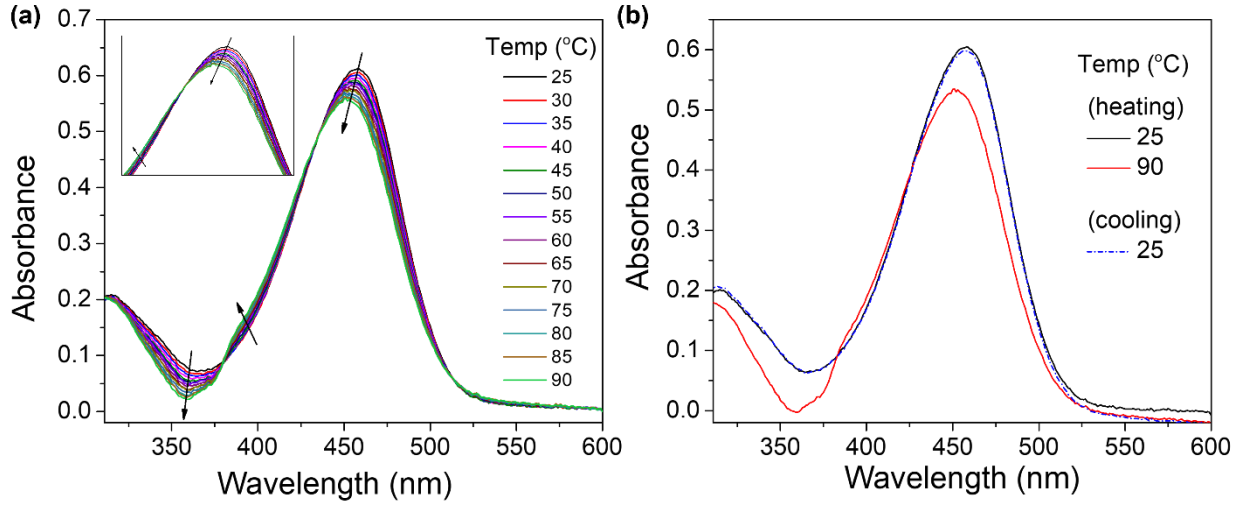

Figure S86. Experimental absorption profiles (tetrachloroethane, 20 μM) of compound **(±)-3-*Z*** (a) as monitored through a temperature change from 25 °C (black trace) to 90 °C (green trace) with every 5 °C interval. A gradual blue-shift along with decrease in absorbance was observed with increasing temperature, consistent with possible disruption of π–π interaction. (b) Reversible change in the UV–vis absorption profiles upon heating and cooling.

UV-VIS PHOTOSWITCHING STUDY

General Procedure

Solution absorption spectra were measured on a Cary 100 Bio spectrophotometer in chloroform using 20 μM solution in 1 cm quartz cells for compound **(±)-3-*Z***. Solution was prepared and transferred into a quartz cuvette for immediate UV-vis absorption measurements. The cuvettes were removed from the spectrophotometer and covered with a glass container while irradiated at an appropriate wavelength of excitation (λ_{irr} = 404, and 523 nm) and absorption spectra were recorded to monitor the changes in the UV-vis spectrum attributed to the isomerization process. The reversible absorbance change at 488 nm was monitored upon 404 nm and subsequent 523 nm irradiation up to ten switching cycles.

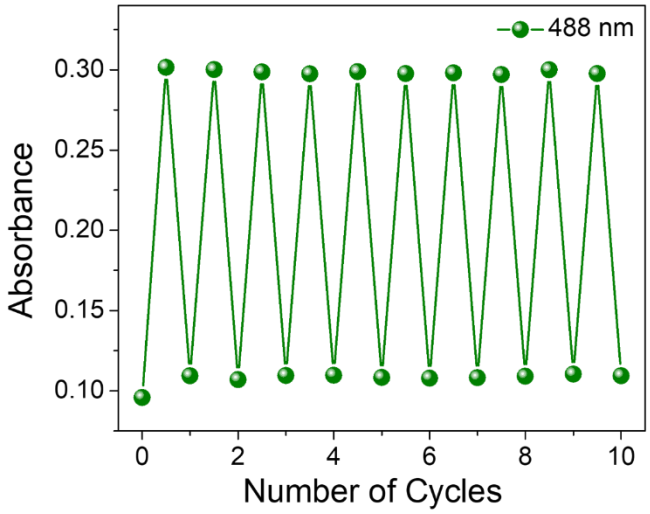

Figure S87. Photoisomerization cycles of compound **(±)-3-*Z*** (chloroform, 20 μM). The absorbance change at 488 nm was monitored while alternating between 404 nm and 523 nm wavelengths of irradiation.

CIRCULAR DICHROISM STUDIES

General Procedure

Circular dichroism (CD) spectroscopic measurements (20 μM in chloroform) were recorded using an Applied Photophysics Chirascan-plus spectrophotometer controlled by Chirascan software in quartz cells of 1 cm path length. Time-dependent DFT (TD-DFT) calculations were performed in the gas phase at the B3LYP/6-31+G(d) level of theory.

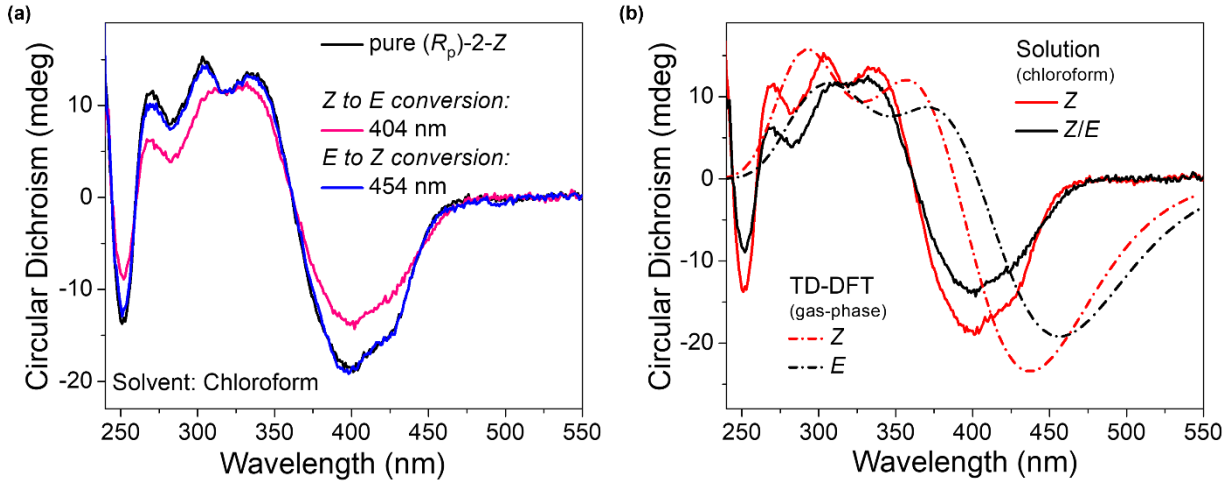

Figure S88. (a) Experimental CD spectra (chloroform, 20 μM) of pure **(R_p)-2-*Z*** (black trace), and upon *Z*→*E* photoisomerization (using 404 nm irradiation, pink trace) using 404 nm irradiation, and reverse *E*→*Z* photoisomerization (using 454 nm irradiation, blue trace). (b) TD-DFT predicted CD profiles (dashed lines) and solution CD spectra (solid lines) of the *Z* (red trace) and *E* (black trace) isomer.

COMPUTATIONAL DETAILS

General Information

Ground state geometries were optimized in the gas phase at the B3LYP/6-31+G(d) level of theory as implemented in Gaussian 09.[9] All final geometries were verified to be a true minima using standard frequency calculations to ensure the absence of imaginary frequencies. All octyl chains were truncated to methyl groups to reduce the computational cost. Excited state calculations were performed at the CAM-B3LYP/cc-pVDZ level of theory in the gas phase starting with the structural coordinates obtained from previously optimized geometries. Solution phase DFT and Time-dependent DFT (TD-DFT) studies were performed using the Integral Equation Formalism Polarizable Continuum Model (IEFPCM, solvent: chloroform). Molecular orbital shapes were visualized from the Gaussian output files using Avogadro molecular editor and CYLview visualization software.

As model compounds **(±)-1** and **(±)-2** only differ in the alkyl group connected to the nitrogen atom of the RCN unit, both have been calculated as a common structure, using the alkyl groups as methyl.

Different conformers have been assigned for both the *Z* and *E* isomers, which have been determined based on the olefin proton (H17, marked in red) pointing towards the nearest bridge (Conformer A, $\mathbf{C_A}$), or opposite to the bridge (Conformer B, $\mathbf{C_B}$).

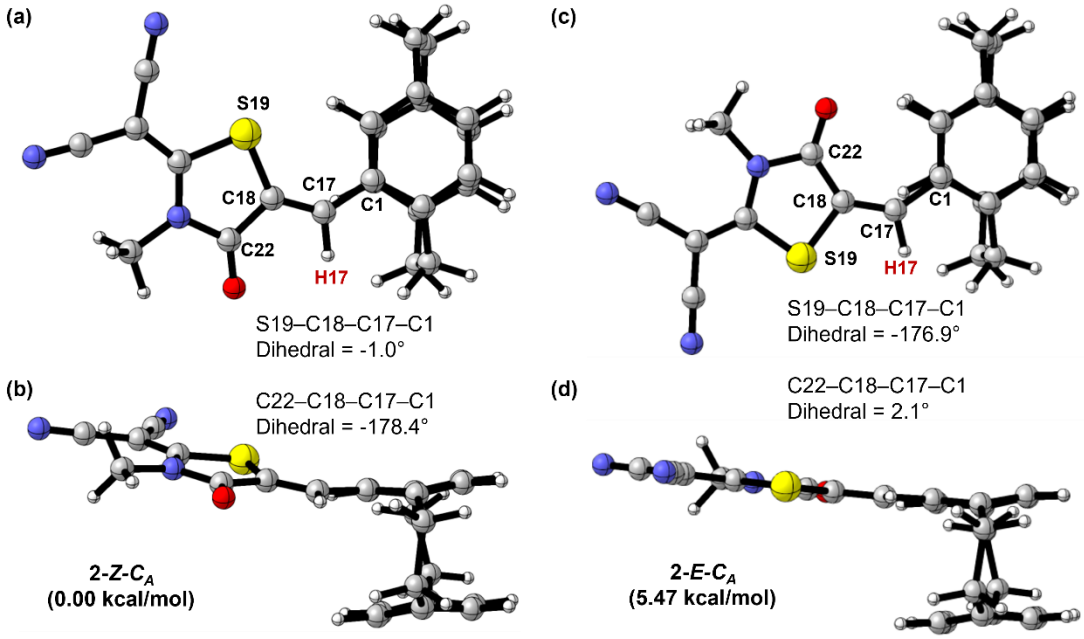

Figure S89. DFT optimized geometries of compounds **(±)-2-*Z*** (a and b) and **(±)-2-*E*** (c and d), adopting Conformation A ($\mathbf{C_A}$), calculated in the gas-phase at the B3LYP/6-31+G(d) level of theory. To be noted, the olefin proton (H17, marked in red) is pointing towards the nearest bridge.

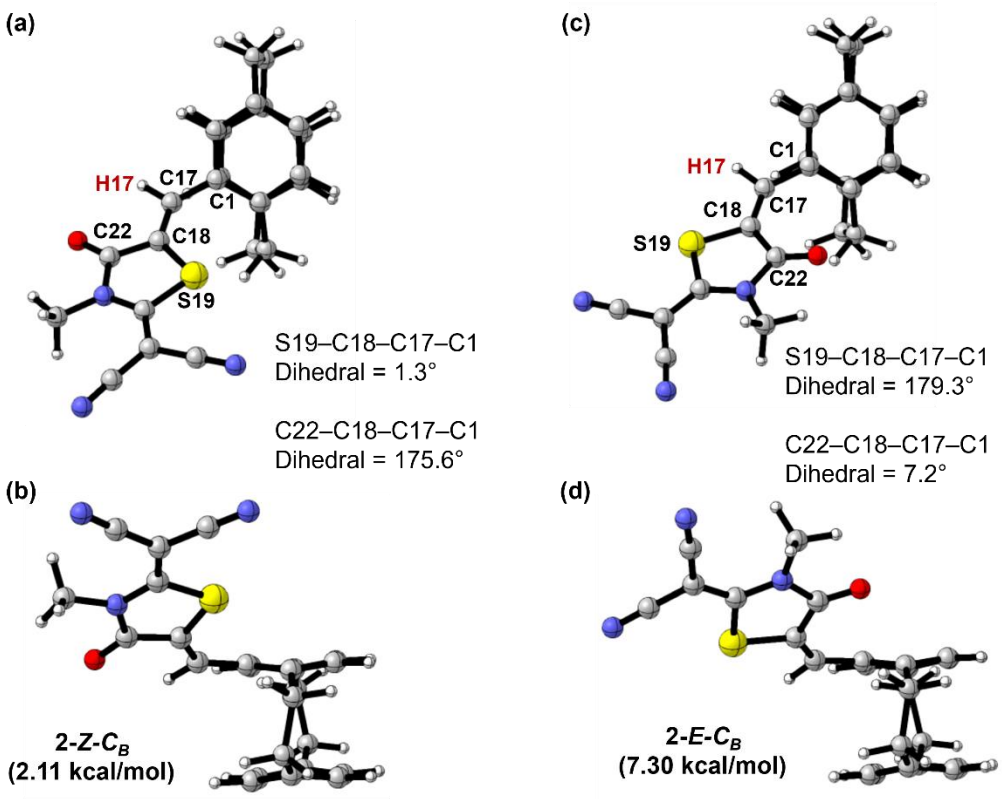

Figure S90. DFT optimized geometries of compounds **(±)-2-*Z*** (a and b) and **(±)-2-*E*** (c and d), adopting Conformation B ($\mathbf{C_B}$), calculated in the gas-phase at the B3LYP/6-31+G(d) level of theory. To be noted, the olefin proton (H17, marked in red) is pointing opposite to the nearest bridge.

Table S2. DFT and TD-DFT data summary for compounds **(±)-2-*Z*** and **(±)-2-*E*** in Conformation A ($\mathbf{C_B}$), and B ($\mathbf{C_B}$), calculated in the gas-phase at the CAM-B3LYP/cc-pVDZ level of theory.

Compound	Energy (in Hartree)	Relative energy (kcal/mol)	HOMO (in eV)	LUMO (in eV)	Δ*E*g (in eV)	Dipole moment (D)	λ_{max} TDDFT (nm)
2-*Z*-C_A	-1563.6267707	0.00	-6.406	-3.140	3.266	8.233	357
2-*E*-C_A	-1563.6180547	5.47	-6.328	-3.198	3.130	9.366	375
2-*Z*-C_B	-1563.6234031	2.11	-6.468	-3.088	3.380	7.793	343
2-*E*-C_B	-1563.615145	7.30	-6.380	-3.136	3.244	8.749	366

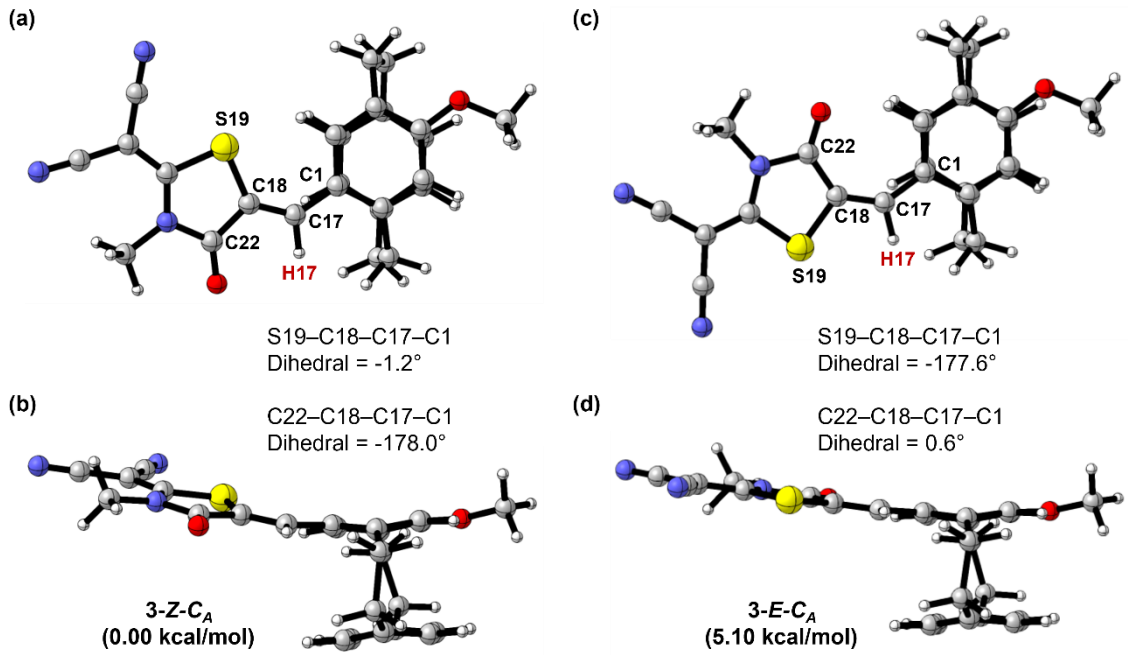

Figure S91. DFT optimized geometries of compounds **(±)-3-*Z*** (a and b) and **(±)-3-*E*** (c and d), adopting Conformation A (C_A), calculated in the gas-phase at the B3LYP/6-31+G(d) level of theory. To be noted, the olefin proton (H17, marked in red) is pointing towards the nearest bridge.

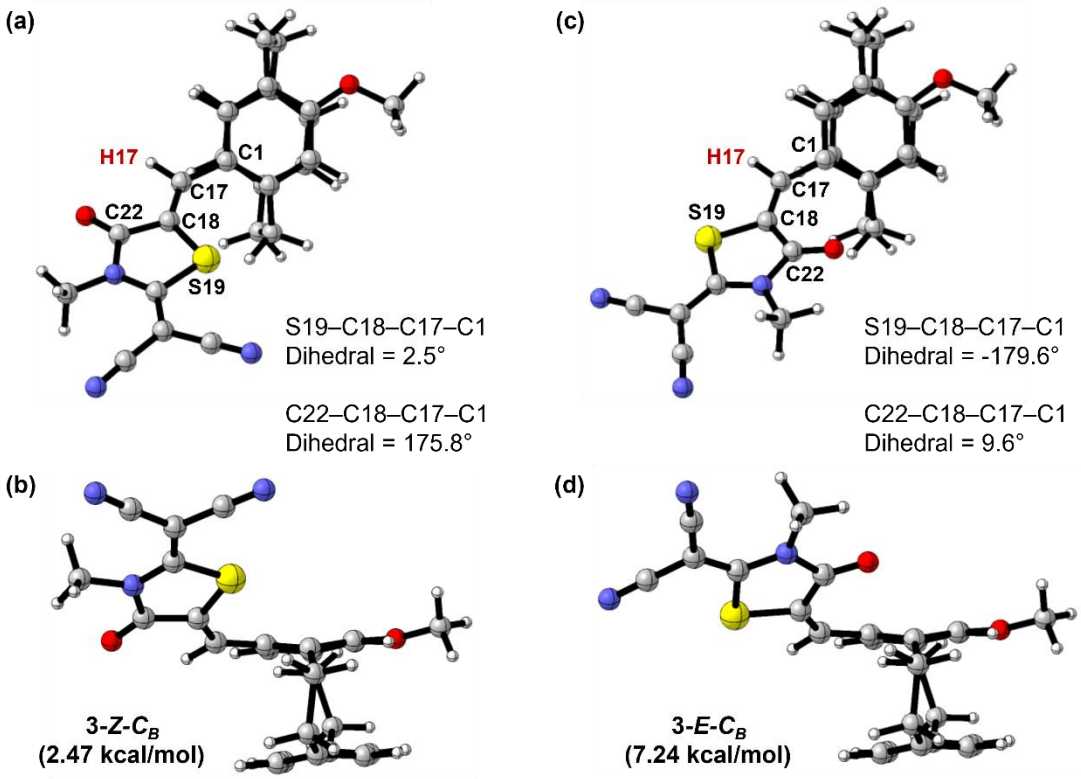

Figure S92. DFT optimized geometries of compounds **(±)-3-*Z*** (a and b) and **(±)-3-*E*** (c and d), adopting Conformation B (**C_B**), calculated in the gas-phase at the B3LYP/6-31+G(d) level of theory. To be noted, the olefin proton (H17, marked in red) is pointing opposite to the nearest bridge.

Table S3. DFT and TD-DFT data summary for compounds **(±)-3-*Z*** and **(±)-3-*E*** in Conformation A (**C_B**), and B (**C_B**), calculated in the gas-phase at the CAM-B3LYP/cc-pVDZ level of theory.

Compound	Energy (in Hartree)	Relative energy (kcal/mol)	HOMO (in eV)	LUMO (in eV)	Δ*E*g (in eV)	Dipole moment (D)	λ_{max} TDDFT (nm)
3-*Z*-C_A	-1678.1575561	0.00	-6.081	-2.933	3.148	10.591	371
3-*E*-C_A	-1678.1494332	5.10	-6.022	-2.980	3.042	11.725	389
3-*Z*-C_B	-1678.1536232	2.47	-6.148	-2.937	3.211	8.485	365
3-*E*-C_B	-1678.1460134	7.24	-6.051	-2.973	3.078	10.607	392

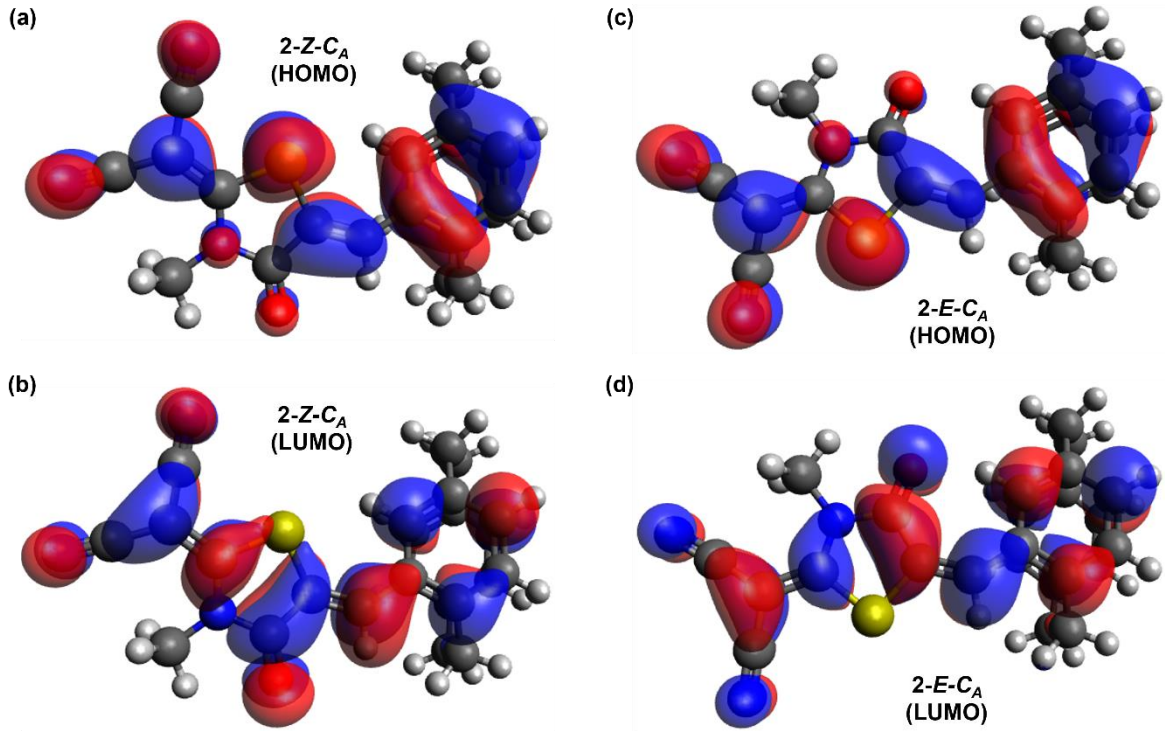

Figure S93. Frontier molecular orbital distributions for compounds **(±)-2-*Z*** (a and b) and **(±)-2-*E*** (c and d), adopting Conformation A (**C_A**), calculated in the gas-phase at the B3LYP/6-31+G(d) level of theory.

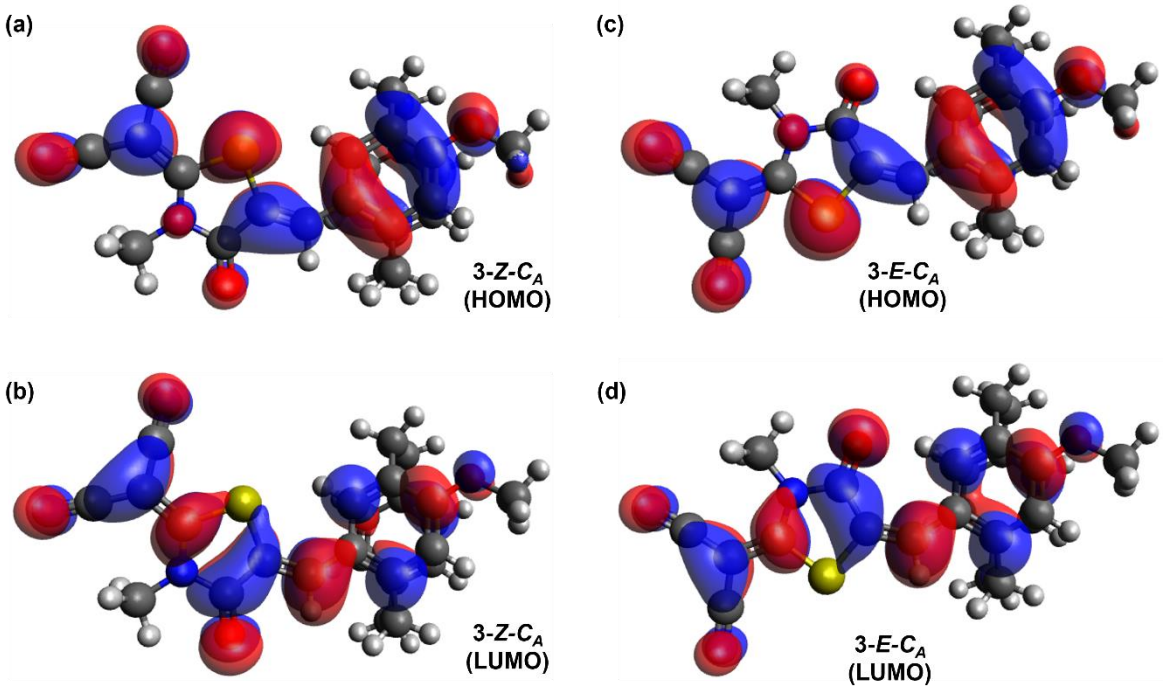

Figure S94. Frontier molecular orbital distributions for compounds **(±)-3-*Z*** (a and b) and **(±)-3-*E*** (c and d), adopting Conformation A ($\mathbf{C_A}$), calculated in the gas-phase at the B3LYP/6-31+G(d) level of theory.

Table S4. Frontier molecular orbital (MO) numbering scheme for compound **(±)-3-*Z*** determined in the gas-phase at the B3LYP/6-31+G(d) level of theory showing predicted numbering for HOMO-3–HOMO, LUMO–LUMO+2 molecular orbitals.

Molecular Orbital	Numbering Scheme
LUMO+2	115
LUMO+1	114
LUMO	113
HOMO	112
HOMO-1	111
HOMO-2	110
HOMO-3	109

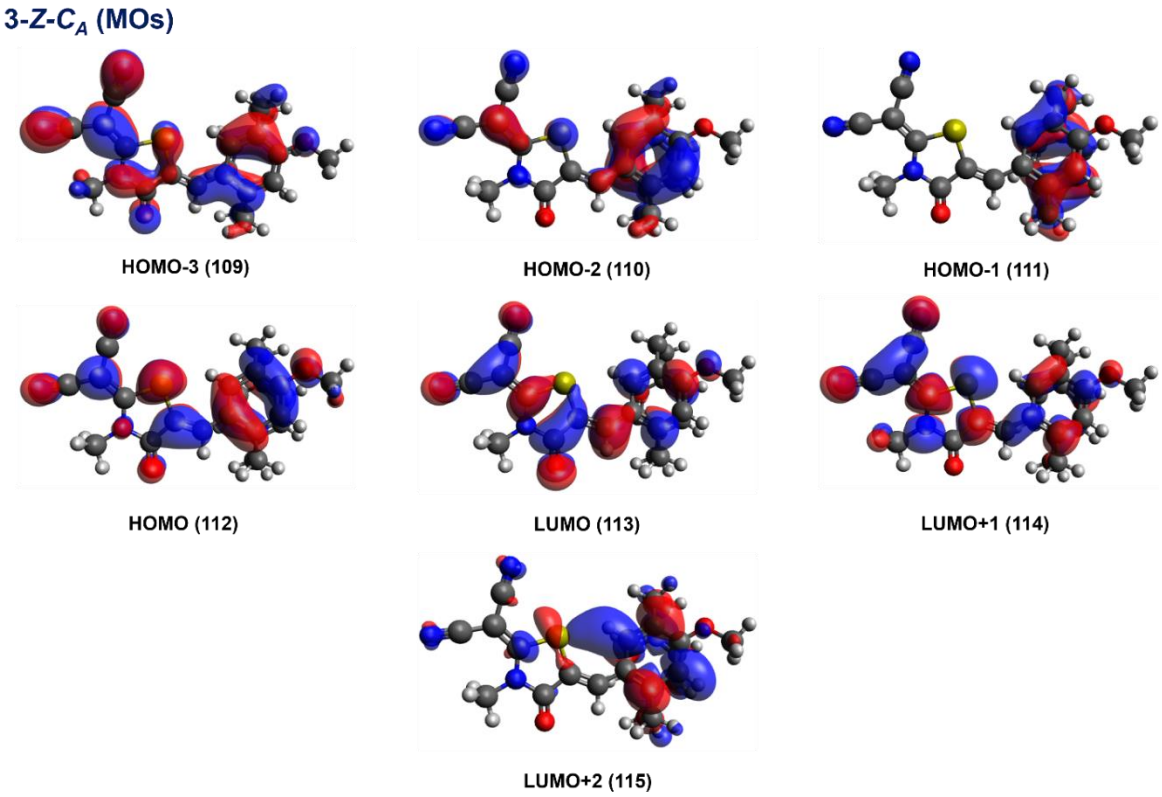

Figure S95. Frontier molecular orbital distributions for compounds **(±)-3-*Z*** adopting Conformation A ($\mathbf{C_A}$), calculated in the gas-phase at the B3LYP/6-31+G(d) level of theory.

Table S5. Time-dependent density functional theory (TD-DFT) excited state data summary showing high contribution orbital transitions for compound **(±)-3-*Z*** adopting Conformation A ($\mathbf{C_A}$), calculated in the gas-phase at the CAM-B3LYP/cc-pVDZ level of theory.

Excited State	FMO Transition	CI Coefficient	Energy (eV)	Wavelength (nm)	Oscillator Strength (*f*)
1	112 → 113	0.69297	3.3399	371.22	0.9077
3	109 → 113	0.21131	4.3015	288.23	0.0342
	109 → 114	-0.10183			
	110 → 113	0.41733			
	111 → 113	0.43873			
	111 → 114	-0.11362			
	112 → 114	-0.10184			
	112 → 115	-0.11345			
4	109 → 113	0.48637	4.5346	273.42	0.1769
	110 → 113	-0.39358			
	111 → 113	0.12437			
	112 → 114	0.20989			

Table S6. Frontier molecular orbital (MO) numbering scheme for compound **(±)-3-*E*** determined in the gas-phase at the B3LYP/6-31+G(d) level of theory showing predicted numbering for HOMO-6–HOMO, LUMO–LUMO+1 molecular orbitals.

Molecular Orbital	Numbering Scheme
LUMO+1	114
LUMO	113
HOMO	112
HOMO-1	111
HOMO-2	110
HOMO-3	109
HOMO-4	108
HOMO-5	107
HOMO-6	106

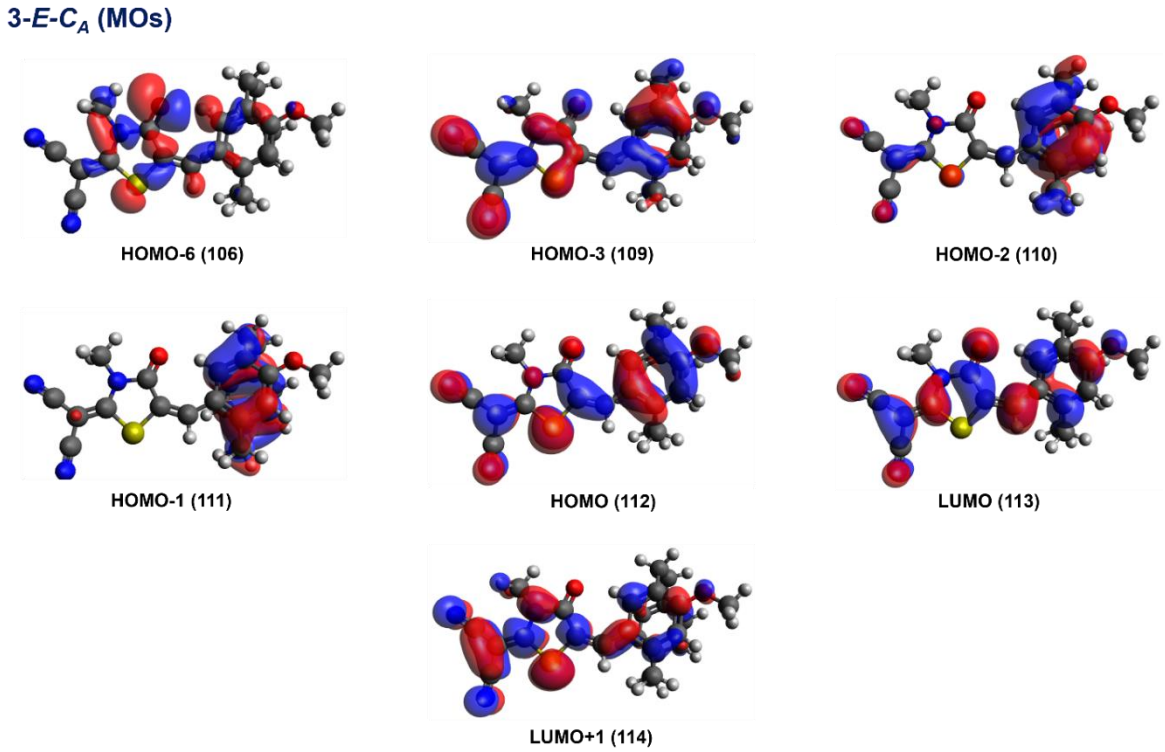

Figure S96. Frontier molecular orbital distributions for compounds **(±)-3-*E*** adopting Conformation A ($\mathbf{C_A}$), calculated in the gas-phase at the B3LYP/6-31+G(d) level of theory.

Table S7. Time-dependent density functional theory (TD-DFT) excited state data summary showing high contribution orbital transitions for compound **(±)-3-*E*** adopting Conformation A ($\mathbf{C_A}$), calculated in the gas-phase at the CAM-B3LYP/cc-pVDZ level of theory.

Excited State	FMO Transition	CI Coefficient	Energy (eV)	Wavelength (nm)	Oscillator Strength (*f*)
1	112 → 113	0.69479	3.1901	388.66	0.9879
3	109 → 113	0.22790	4.1852	296.24	0.0280
	110 → 113	0.46333			
	111 → 113	0.42469			
4	106 → 113	0.10180	4.4342	279.61	0.0857
	109 → 113	0.55960			
	110 → 113	-0.33189			
	112 → 114	0.17545			

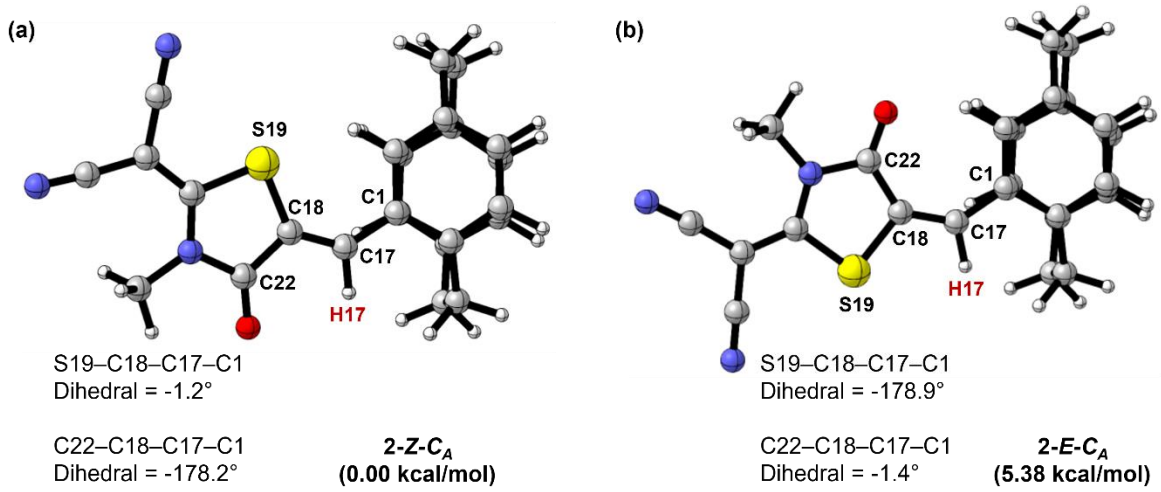

Figure S97. DFT optimized geometries of compounds (a) **(±)-2-*Z***, and (b) **(±)-2-*E***, adopting Conformation A ($\mathbf{C_A}$), calculated using IEFPCM solvent model (solvent: chloroform) at the B3LYP/6-31+G(d) level of theory. To be noted, the olefin proton (H17, marked in red) is pointing towards the nearest bridge.

Table S8. DFT and TD-DFT data summary for compounds **(±)-2-*Z*** and **(±)-2-*E*** in Conformation A ($\mathbf{C_A}$), calculated using IEFPCM solvent model (solvent: chloroform) at CAM-B3LYP/cc-pVDZ level of theory.

Compound	Energy (in Hartree)	Relative energy (kcal/mol)	HOMO (in eV)	LUMO (in eV)	Δ*E*g (in eV)	Dipole moment (D)	λ_{max} TDDFT (nm)
2-*Z*	-1563.6406506	0	-6.249	-3.042	3.207	10.206	373
2-*E*	-1563.6320729	5.38	-6.191	-3.057	3.134	11.707	389

X-RAY CRYSTALLOGRAPHIC STUDIES (CCDC Number: 2480804)

General Information

An intense yellow, needle-shaped specimen of $C_{26}H_{23}N_3O_2S$, approximate dimensions 0.08×0.115×0.495 mm^3, was used for the X-ray crystallographic analysis. The X-ray intensity data of **(±)-3-*Z*** were measured on a BRUKER D8 Venture with PHOTON III four-circle diffractometer system equipped with a micro-focus X-ray tube (MoK_α radiation, λ = 0.71073 Å) and a HELIOS multilayer optics monochromator. The specimen was held at 200(2) K during the measurement with an Oxford Cryostream 800 low temperature device. A total of 2200 frames were collected with APEX5 program.[10] The total exposure time was 4.91 hours. The frames were integrated with the SAINT V8.41 package using a narrow-frame algorithm.[11] The integration of the data using a monoclinic unit cell yielded a total of 45358 reflections to a maximum θ angle of 28.85° (0.74 Å resolution), of which 5608 were independent (average redundancy 8.09, completeness = 99.7%, R_{int} = 5.71%, R_{sig} = 3.21%) and 4856 (86.6%) were greater than 2σ(F^2). The final cell constants of a = 7.9115(3) Å, b = 26.5924(9) Å, c = 10.7186(4) Å, α = 90°, β = 108.1250(10)°, γ = 90°, V = 2143.15(14) Å^3, are based upon the refinement of the XYZ-centroids of 9926 reflections above 20 σ(I) with 5.04° < 2θ < 57.70°. Data were corrected for absorption effects using the Multi-Scan method in SADABS 2016/2.[12] The ratio of minimum to maximum apparent transmission yields 0.790. The calculated minimum and maximum transmission coefficients (based on crystal size) are 0.589 and 0.746.[13] The structure was solved by Intrinsic Phasing methods with SHELXT-2018/2 and refined by full-matrix least-squares methods against F^2 using SHELXL-2018/3 in the space group $P2_1/n$, with Z = 4 for the formula unit $C_{26}H_{23}N_3O_2S$.[14, 15] The final anisotropic full-matrix least-squares refinement on F^2 with 471 variables against 5608 data points and 272 restraints converged at R_1 = 4.04%, for the observed 4856 data with [I≥2σ(I)] and wR_2 = 11.25% for all data. The goodness-of-fit on F^2 was 1.02. The largest peak in the final difference electron density synthesis was 0.32 e$^-$/Å^3 and the deepest hole was −0.28 e$^-$/Å^3 with an RMS deviation of 0.044 e$^-$/Å^3. On the basis of the final model, the calculated density was 1.37 g/cm^3 and F(000), 928 e$^-$. Crystal data and refined structure parameters are presented in **Table S9**.

Disorder Description

The structure is disordered and contains the molecule located at three possible sites with refined occupancy ratio yielding 0.721(2): 0.232(2): 0.0467(11). The fragment with the paracyclophane unit is common for two possible orientation and refined occupation of this moiety is equal 0.9533(11). The disorder of the molecule is presented in **Figure S98**. To preserve reasonable geometry of the disorder molecular fragments a number of distance and angle restraints were used together with restraints for atomic displacement parameters.

Structure Refinement Details

All main component disordered (occupancy > 50%) non-hydrogen atoms were refined with anisotropic displacement parameters. All hydrogen atoms were refined isotropic on calculated positions using a riding model with their U_{iso} values constrained to 1.5 times the U_{eq} of their pivot atoms for terminal sp^3 carbon atoms and 1.2 times for all other carbon atoms.

For the model building and the structure refinement the ShelXle graphical user interface was employed.[16] This report was generated using FinalCif.[17]

Molecular graphics were prepared using program Mercury 2024.3.0.[18] Thermal ellipsoids parameters are presented at 50% probability level in **Figure S99**, whereas packing diagrams are displayed in **Figure S100**. Geometry of major (isomer ***Z***, combination of green and blue colored moieties from Figure S98) and minor (isomer ***E***, red colored moiety from Figure S98) components of the crystal **(±)-3-*Z*** are presented in **Figures S101** and **S102** respectively.

Table S9. Crystal data and structure refinement for (±)-3-*Z* (CCDC Number: 2480804).

Empirical formula	$C_{26}H_{23}N_3O_2S$
M_x [g·mol^{-1}]	441.53
T [K]	200(2)
Radiation	MoK_α (λ = 0.71073 Å)
Crystal size [mm^3]	0.08×0.115×0.495
Crystal habit	intense yellow needle
Crystal system	monoclinic
Space group (number)	$P2_1/n$ (14)
Unit cell parameters	a = 7.9115(3) Å α = 90° b = 26.5924(9) Å β = 108.1250(10)° c = 10.7186(4) Å γ = 90°
V [Å^3], Z	2143.15(14), 4
D_x [g·cm^{-3}]	1.368
μ [mm^{-1}]	0.181
F(000)	928
$2\theta_{min}$, $2\theta_{max}$	4.28°, 57.70° (0.74 Å resolution)
Index ranges	−10 ≤ h ≤ 10 −36 ≤ k ≤ 36 −14 ≤ l ≤ 14
Reflections collected/ independent	45358 / 5608 (R_{int} = 0.0571, R_{sig} = 0.0321)
Completeness to $2\theta_{max}$ = 57.70°	99.7%
Absorption correction	Multi-Scan
T_{min}, T_{max}	0.589, 0.746
Refinement method	full-matrix LSQ on F^2
Data / Restraints / Parameters	5608 / 272 / 471
GOF on F^2	1.023
Final R indexes	4856 data R_1 = 0.0404, wR_2 = 0.1058 all data R_1 = 0.0475, wR_2 = 0.1125
$\Delta\rho_{max}$, $\Delta\rho_{min}$	0.32 e/Å^{-3}, −0.28 e/Å^{-3}

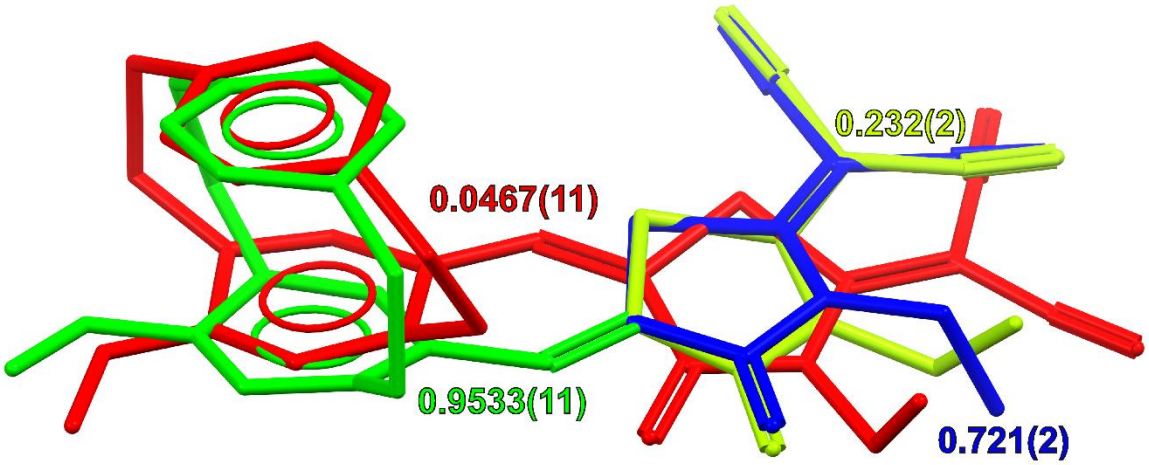

Figure S98. View of the structure of **(±)-3-*Z*** with given occupancies of disordered moieties. Hydrogen atoms omitted.

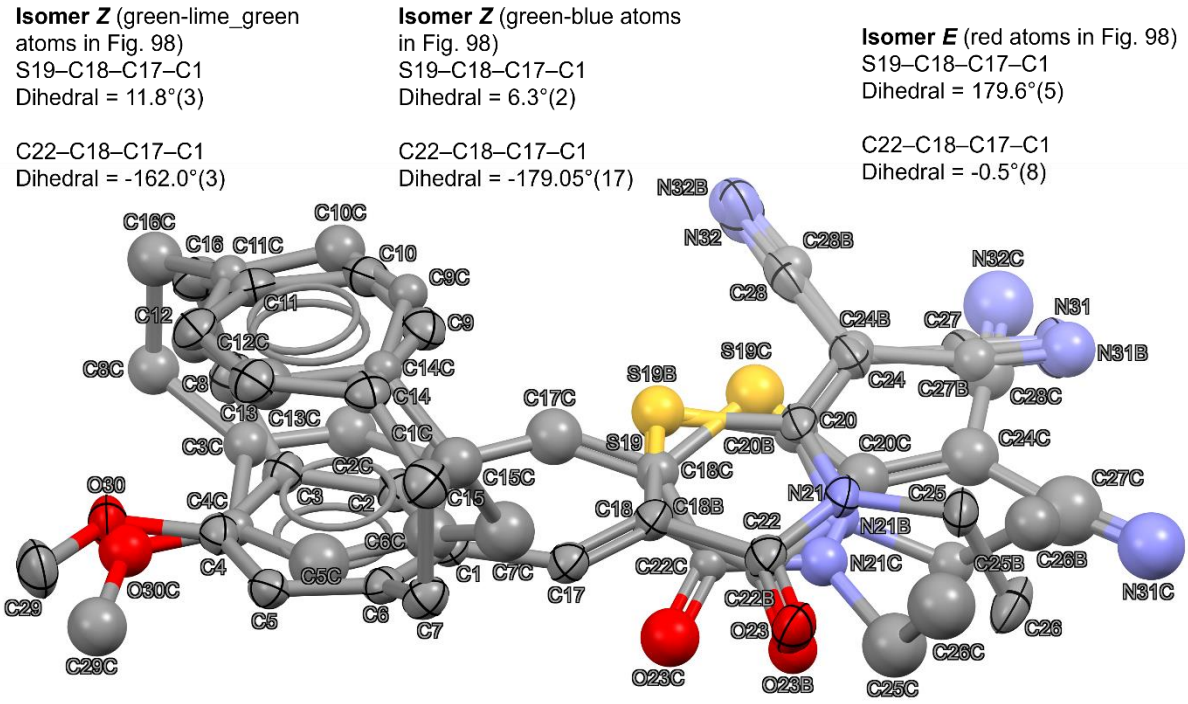

Figure S99. Thermal ellipsoid plot for **(±)-3-*Z*** at the 50% probability level. Hydrogen atoms omitted. The torsional angles are calculated for the three structures with estimated standard deviation (esd) values.

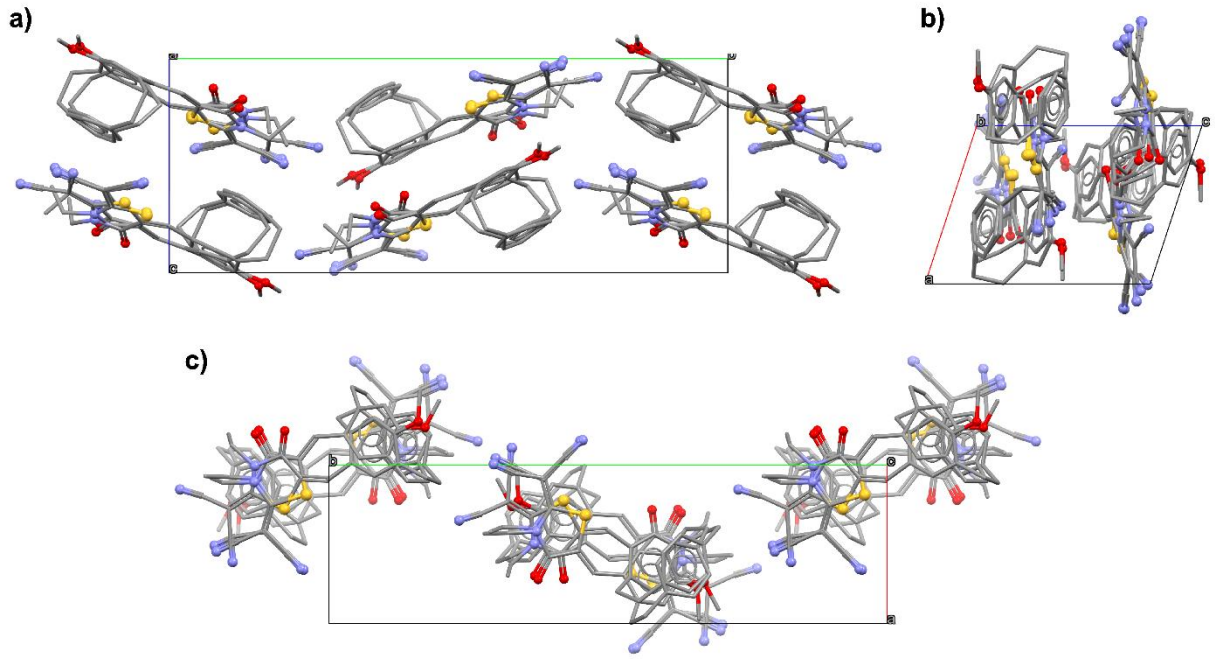

Figure S100. Packing diagram for **(±)-3-*Z***, view along [100] (a), [010] (b) and [001] (c). Hydrogen atoms omitted.

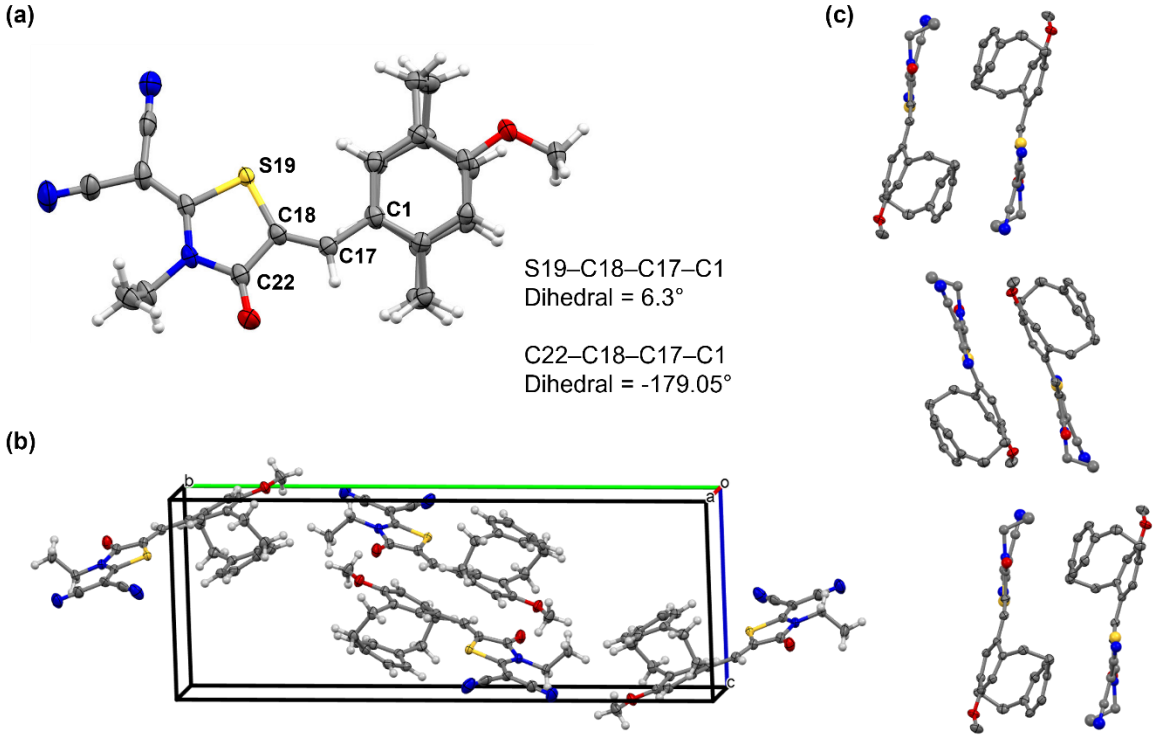

Figure S101. Presentation of the major component of **(±)-3-*Z***– isomer *Z*. (a) Thermal ellipsoid plot at 50% probability level, face-on view. (b) Unit cell view. (c) Long-range packing in the solid state.

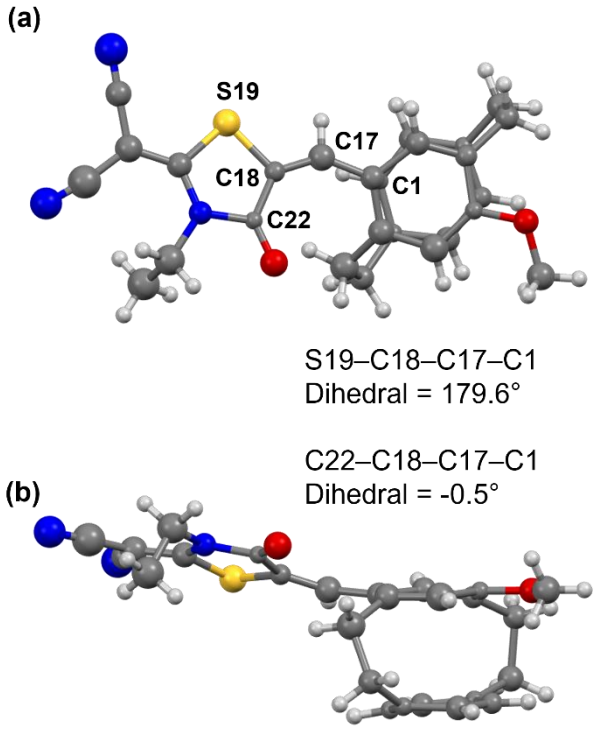

Figure S102. Presentation of the minor component of **(±)-3-*Z*–** isomer *E* with isotropic displacement parameters at 50% probability level. (a) Face-on view. (b) Edge-on view.

REFERENCES

(1) Kornman, C. T.; Li, L.; Weldeab, A. O.; Ghiviriga, I.; Abboud, K. A.; Castellano, R. K. Photoisomerization of dicyanorhodanine-functionalized thiophenes. *Chemical Science* **2020**, *11* (37), 10190-10197, 10.1039/D0SC04409A. DOI: 10.1039/D0SC04409A.

(2) Das, P.; Grinalds, N. J.; Ghiviriga, I.; Abboud, K. A.; Dobrzycki, Ł.; Xue, J.; Castellano, R. K. Dicyanorhodanine-Pyrrole Conjugates for Visible Light-Driven Quantitative Photoswitching in Solution and the Solid State. *J. Am. Chem. Soc.* **2024**, *146* (17), 11932-11943. DOI: 10.1021/jacs.4c00983.

(3) Friedmann, C. J.; Ay, S.; Bräse, S. Improved Synthesis of Enantiopure 4-Hydroxy[2.2]paracyclophane. *The Journal of Organic Chemistry* **2010**, *75* (13), 4612-4614. DOI: 10.1021/jo100468s.

(4) Liu, H.; Wang, W.; Zhou, Y.; Li, Z. a. A ring-locking strategy to enhance the chemical and photochemical stability of A–D–A-type non-fullerene acceptors. *Journal of Materials Chemistry A* **2021**, *9* (2), 1080-1088, 10.1039/D0TA09924D. DOI: 10.1039/D0TA09924D.

(5) Delcourt, M.-L.; Reynaud, C.; Turcaud, S.; Favereau, L.; Crassous, J.; Micouin, L.; Benedetti, E. 3D Coumarin Systems Based on [2.2]Paracyclophane: Synthesis, Spectroscopic Characterization, and Chiroptical Properties. *The Journal of Organic Chemistry* **2019**, *84* (2), 888-899. DOI: 10.1021/acs.joc.8b02773.

(6) Rozenberg, V.; Danilova, T. y.; Sergeeva, E.; Vorontsov, E.; Starikova, Z.; Korlyukov, A.; Hopf, H. Resolution and Novel Reactions of 4-Hydroxy[2.2]paracyclophane. *European Journal of Organic Chemistry* **2002**, *2002* (3), 468-477. DOI: https://doi.org/10.1002/1099-0690(20022)2002:3<468::AID-EJOC468>3.0.CO;2-3 (acccessed 2025/03/11).

(7) Sergeeva, E. V.; Rozenberg, V. I.; Antonov, D. Y.; Vorontsov, E. V.; Starikova, Z. A.; Fedyanin, I. V.; Hopf, H. Novel Multichiral Diols and Diamines by Highly Stereoselective Pinacol Coupling of Planar

Chiral [2.2]Paracyclophane Derivatives. *Chemistry – A European Journal* **2005**, *11* (23), 6944-6961. DOI: https://doi.org/10.1002/chem.200500413 (acccessed 2025/03/11).
(8) Polat, E.; Turbedaroglu, O.; Cakici, M. Synthesis of bis(benzoxazole) frameworks chiralized by planar chiral [2.2]Paracyclophane. *Tetrahedron Letters* **2021**, *67*, 152871. DOI: https://doi.org/10.1016/j.tetlet.2021.152871.
(9) Gaussian 09, Revision D.01, M. J. Frisch, G. W. Trucks, H. B. Schlegel, G. E. Scuseria, M. A. Robb, J. R. Cheeseman, G. Scalmani, V. Barone, B. Mennucci, G. A. Petersson, H. Nakatsuji, M. Caricato, X. Li, H. P. Hratchian, A. F. Izmaylov, J. Bloino, G. Zheng, J. L. Sonnenberg, M. Hada, M. Ehara, K. Toyota, R. Fukuda, J. Hasegawa, M. Ishida, T. Nakajima, Y. Honda, O. Kitao, H. Nakai, T. Vreven, J. A. Montgomery, Jr., J. E. Peralta, F. Ogliaro, M. Bearpark, J. J. Heyd, E. Brothers, K. N. Kudin, V. N. Staroverov, T. Keith, R. Kobayashi, J. Normand, K. Raghavachari, A. Rendell, J. C. Burant, S. S. Iyengar, J. Tomasi, M. Cossi, N. Rega, J. M. Millam, M. Klene, J. E. Knox, J. B. Cross, V. Bakken, C. Adamo, J. Jaramillo, R. Gomperts, R. E. Stratmann, O. Yazyev, A. J. Austin, R. Cammi, C. Pomelli, J. W. Ochterski, R. L. Martin, K. Morokuma, V. G. Zakrzewski, G. A. Voth, P. Salvador, J. J. Dannenberg, S. Dapprich, A. D. Daniels, O. Farkas, J. B. Foresman, J. V. Ortiz, J. Cioslowski, and D. J. Fox, Gaussian, Inc., Wallingford CT, 2013.

(10) Bruker, *APEX5*, *V2023.9-4*, Bruker AXS Inc., Madison, Wisconsin.

(11) Bruker, *SAINT*, *V8.41*, Bruker AXS Inc., Madison, Wisconsin, USA.

(12) Bruker, *SADABS, V2016/2 V8.41*, Bruker AXS Inc., Madison, Wisconsin, USA.

(13) L. Krause, R. Herbst-Irmer, G. M. Sheldrick, D. Stalke, *J. Appl. Cryst.* **2015**, *48*, 3–10, doi:10.1107/S1600576714022985.

(14) G. M. Sheldrick, *Acta Cryst.* **2015**, *A71*, 3–8, doi:10.1107/S2053273314026370.
(15) G. M. Sheldrick, *Acta Cryst.* **2015**, *C71*, 3–8, doi:10.1107/S2053229614024218.

(16) C. B. Hübschle, G. M. Sheldrick, B. Dittrich, *J. Appl. Cryst.* **2011**, *44*, 1281–1284, doi:10.1107/S0021889811043202.

(17) D. Kratzert, *FinalCif*, *(Bruker Edition)*, https://dkratzert.de/finalcif.html.
(18) C. F. Macrae, I. Sovago, S. J. Cottrell, P. T. A. Galek, P. McCabe, E. Pidcock, M. Platings, G. P. Shields, J. S. Stevens, M. Towler and P. A. Wood, "Mercury 4.0: from visualization to analysis, design and prediction", *J. Appl. Cryst.*, **2020**, *53*, 226-235, doi:10.1107/S1600576719014092.